PHOTOACID GENERATORS FOR CATALYTIC DECOMPOSITION OF POLYCARBONATE

A Thesis
Presented to
The Academic Faculty

by

Mark Glenn Cupta

In Partial Fulfillment
of the Requirements for the Degree
Master of Science in the
School of Chemical & Biomolecular Engineering

Georgia Institute of Technology
May 2006

PHOTOACID GENERATORS FOR CATALYTIC DECOMPOSITION OF POLYCARBONATE

Approved by:

Dr. Paul A. Kohl
School of Chemical & Biomolecular Engineering
Georgia Institute of Technology

Dr. Sue Ann Bidstrup Allen
School of Chemical & Biomolecular Engineering
Georgia Institute of Technology

Dr. Dennis W. Hess
School of Chemical & Biomolecular Engineering
Georgia Institute of Technology

Date Approved: January 12, 2006

ACKNOWLEDGEMENTS

I would like to express a considerable amount of gratitude towards my academic advisor, Dr. Paul A. Kohl, who was unswerving in his support for my research and personal academic development. His great intelligence and drive towards innovation is balanced by a consistent jovial attitude, which made my experience in his research group a joyful one. Furthermore, I'd like to show appreciation towards Dr. Paul Jayachandran Joseph, who's vast experience I drew on time and time again. I'd also like to thank Todd Spencer, a group member of mine, for being an outstanding research partner. Together we were able to solve numerous problems that would have been difficult alone. Jason Harry, an undergraduate research student, poured a considerable amount of time and effort into assisting my research and enabled me to place a greater focus on the more inventive aspects of this work. Jassem Abdallah was an excellent experimental resource and provided me with literature that would have taken a significant amount of time to collect. Dr. Dhananja Bhusari was integral in the X-ray Photoelectron Spectroscopy experimentation and analysis. Additionally I'd like to thank Promerus LLC for providing our research group with the necessary polymer and also for the general support and ideas they imparted to me. Dr. William M. Lamanna of the 3M Corporation graciously provided me with samples of the novel photoacid generators he and his team had developed. Finally, I'm grateful for having been part of such a wonderful research group. I wish each person the best of luck in their future endeavors.

TABLE OF CONTENTS

LIST OF TABLES

LIST OF FIGURES

NOMENCLATURE

A	Arrhenius pre-exponential factor
APEX	A positive tone, deep UV, chemically amplified photoresist
BTBPI-BBI	Bis(4-tert-butylphenyl)iodonium bis(perfluorobutanesulfonyl) imide
BTBPI-TF	Bis(4-tert-butylphenyl)iodonium triflate
BTBPI-PTS	Bis(4-tert-butylphenyl)iodonium para-toluenesulfonate
BTBPI-TMM	Bis(4-tert-butylphenyl)iodonium tris(perfluoromethanesulfonyl) methide
C	concentration of the acid
Ciba-263	Non-ionic n-propane sulfonic acid based PAG
C^g	concentration of the acid on the surface of the film in the gaseous state
C^{inf}	concentration of the acid at the edge of the boundary layer and surrounding gas
C^o	initial acid concentration
C^s	concentration of the acid on the surface of the film in the solid
D	overall diffusion coefficient
DPI-DMOS	Diphenyliodomium 9,10-dimethoxyanthracene-2-sulfonate
DPI-NF	Diphenyliodonium perfluoro-1-butanesulfonate
E_a	activation energy
g	weight percent of PAG desired
GBL	γ-butyrolactone
IPOCST	poly(4-isopropyloxycarbonyloxystyrene)

k	reaction rate constant
K	concentration partition coefficient
k_c	mass transfer coefficient
KRS-XE	A positive tone, e-beam, chemically amplified photoresist
l	polymer film thickness
MEMS	microelectricalmechanical systems
n	order of reaction
NHNDC-NF	N-hydroxy-5-norbornene-2,3-dicarboximide perfluoro-1-butanesulfonate
NHN-NF	N-hydroxynaphthalimide perfluoro-1-butanesulfonate
NHN-TF	N-hydroxynaphthalimide triflate
NPOCST	poly(4-neopentyloxycarbonyloxystyrene)
p	mass of polymer
PAG	photoacid generator
PEB	post exposure bake
PPC	poly(propylene carbonate)
r	fluid viscosity correction factor
R	universal gas constant
R^2	proportion of explained variation
Rhordosil-FABA	tetrakis-(pentafluorophenyl)borate-4-methylphenyl[4-(1-methylethyl)phenyl] iodonium
s	mass of solvent
t	time
T	temperature

tBOC	poly(t-butoxycarbonylstyrene)
TBOMDS-TF	tert-(butoxycarbonylmethoxynaphthyl)-diphenylsulfonium triflate
TGA	thermogravimetric analysis
TPS-FABA	triphenylsulfonium tetrakis-(pentafluorophenyl)borate
TTBPS-FABA	tris(4-tert-butylphenyl)sulfonium tetrakis-pentafluorophenyl)borate
TTBPS-NF	tris(4-tert-butylphenyl)sulfonium perfluoro-1-butanesulfonate
T_g	glass transition temperature
UV6	A positive tone, deep UV, chemically amplified photoresist
W	weight percent of polymer desired
x	linear regression variable representing time
XPS	X-ray photoelectron spectroscopy
y	linear regression variable representing film thickness
z	axis of diffusion
α	dimensionless mass fraction
θ	dimensionless concentration, unaccomplished fraction
ω	angular velocity

SUMMARY

It is the goal of this body of work to research an assortment of different photoacid generators (PAGs) and quantify their ability to perform the decomposition of poly(propylene carbonate) (PPC). Adding PAGs to PPC allows for a decreased polymer decomposition temperature, which can in turn be used as a sacrificial polymer for the fabrication of various microelectromechanical and microfluidic devices. A focus will be placed on relating the properties of the PAG such as acid strength, acid volatility, and PAG activation to processing issues like percentage of total film decomposition, amount and composition of film residue, decomposition rate, decomposition temperature, and environmental dependencies. This research discovered that the use of superacid triflic and nonaflic based PAGs were not adequate for the decomposition of PPC due to the high vapor pressure of the acid. Furthermore, the non-fluorinated sulfonic acid based PAGs do not posses the super-acid level acidity needed to sufficiently decompose PPC. Conversely, a perfluorinated methide and a tetrakis(pentafluoropheyl)borate based PAG both demonstrated the capability for high level PPC decomposition. Building on the knowledge gained through experimentation with these individual PAGs, the creation of a novel “Combination PAG” was accomplished. The Combination PAG uses acid groups with different physical properties collectively working to achieve what neither could complete individually.

CHAPTER 1

INTRODUCTION

Sacrificial polymer systems with low decomposition temperatures can be used in the fabrication of a variety of microelectromechanical (MEMS) and microfluidic devices [1-3, 9-10]. For example, these polymers can be used in the packaging of MEMS devices like gyroscopes and resonators. Additionally, they are used to form systems of microchannels to can deliver fluidic cooling to microprocessors, or even to create advanced air-gaps that will provide low dialectic environments for high performance electrical devises [1-3]. One such polymer that has the desired thermal properties for the fabrication of these devices is poly(propylene-carbonate) (PPC). Complete thermal decomposition of PPC occurs at 200ºC to 250ºC; however, this decomposition can be catalyzed in the presence of strong acids, effectively lowering the decomposition temperature into the range of 100ºC to 180ºC. A mechanism for the acid catalyzed decomposition of PPC was proposed by Jayachandran et.al. and is shown in Figure 1.1.

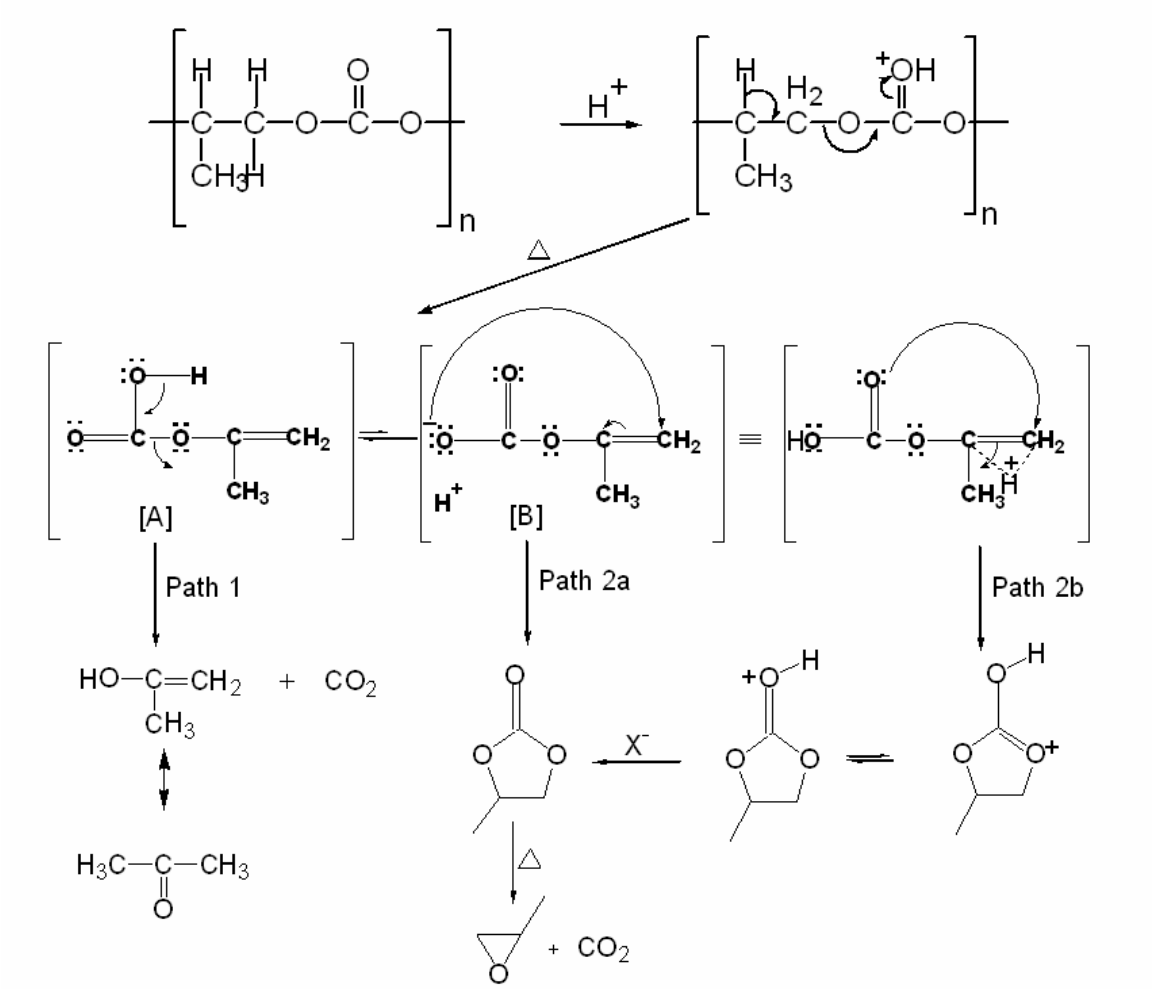

Figure 1.1: Proposed mechanisms for the acid catalyzed decomposition of PPC [2]

The electron donating carbonyl group of the polycarbonate is attacked by the hydrogen ion triggering the catalytic cycle seen in Figure 1.1. This mechanism is considered catalytic because a hydrogen ion is regenerated with each subsequent decomposition reaction. Path 1 is the dominant path, which makes acetone and carbon dioxide the main decomposition products [2]. Paths 2a and 2b both lead to a less prevalent epoxy side product. Both acetone and carbon dioxide are volatile gases at these decomposition temperatures, so during the thermal processing of the PPC, these products evaporate from the film.

Besides a low decomposition temperature, the fabrication of these devices also desires a polymer with photolithographic properties, much like a standard chemically amplified photoresist. In order to make a PPC that can be photo-patterned, the polymer can be combined with a photoacid generator (PAG). Upon irradiation with UV light, a PAG will produce an acid by the following simplified reaction mechanism proposed by Paul Jayachandran Joseph of the Georgia Institute of Technology.

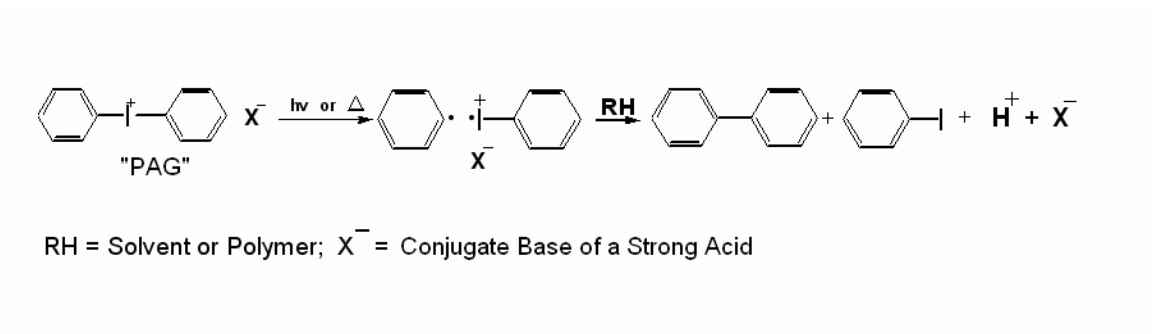

Figure 1.2: Proposed mechanism for the generation of acid by the decomposition of a PAG

The PAG decomposition mechanism seen in Figure 1.2 begins with a diphenyliodonium (DPI) based cation and an anion that could be any conjugate base of a strong acid. Through a combination of heat and/or light, the cation dissociates into two radical species, both stabilized by the presence of benzyl groups. Upon reaction with residual solvent or polymer, there is a release of a hydrogen ion that associates with the conjugate base to form a strong acid. This is the strong acid which catalyzes the decomposition of the PPC. The reaction proceeds at different temperatures depending on the cation activation method, heat or light. Figure 1.3 displays a thermogravimetric analysis (TGA) of a typical PAG, *tetrakis(pentafluorophenyl)borate-4-methylphenyl[4-(1-*

methylethyl)phenyl]iodonium (Rhodorsil-FABA), combined with PPC. The structure of this PAG can be found in Appendix A.

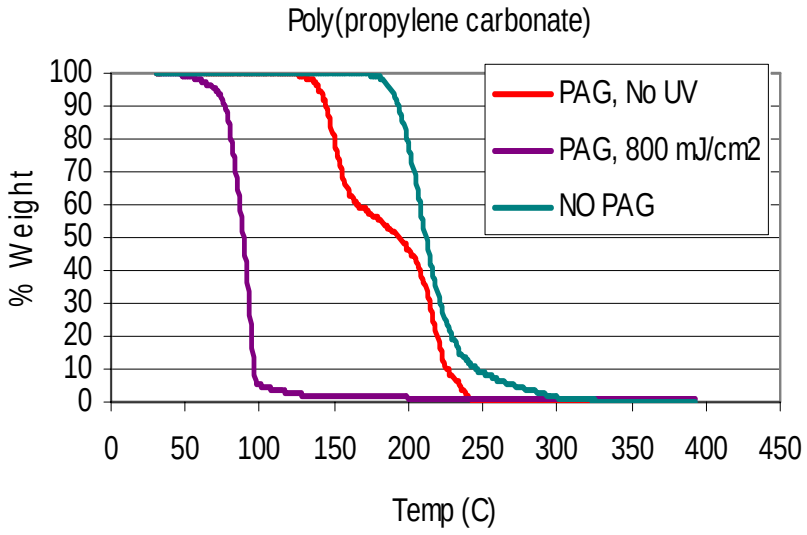

Figure 1.3: Sample TGA for a photoactive PPC system with a temperature ramp rate of 10ºC/min (Courtesy of Paul Jayachandran Joseph)

Figure 1.3 shows that in the absence of a PAG, the decomposition of the PPC occurs between 200ºC and 300ºC. When a PAG is added to the polymer matrix and irradiated with 800 mJ/cm^2 of energy, the acid catalyzes the PPC decomposition so that it now decomposes at 100ºC. However, when the UV irradiation is omitted, the PAG undergoes thermal activation and begins to decompose the polymer at 150ºC. These temperature differences allow a PPC / PAG film to be patterned with typical lithography methods. Figure 1.4 presents a typical PPC sacrificial process flow diagram for the formation of air-gaps.

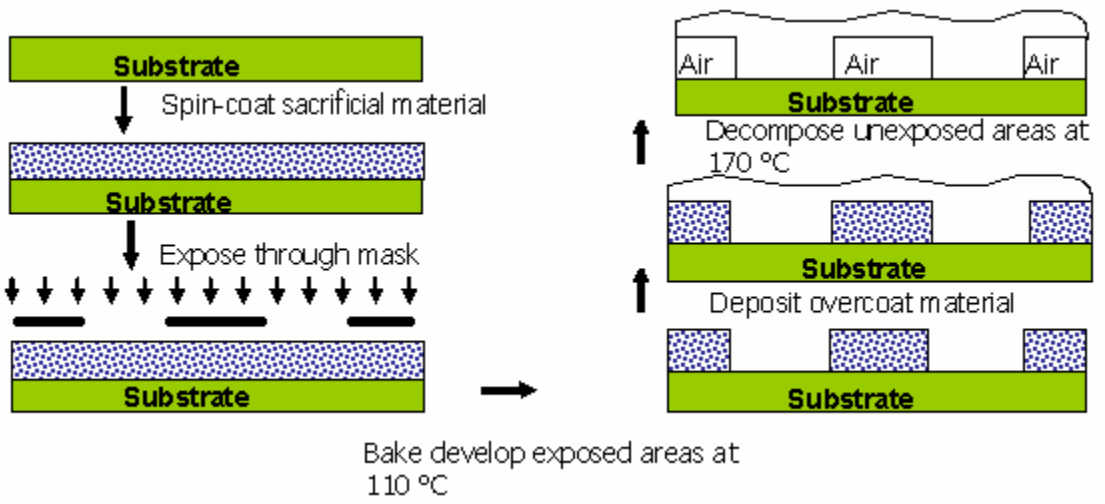

Figure 1.4: Process flow sheet for the formation of air-gaps using sacrificial PPC [2]

The overcoat material described in step four of Figure 1.4 can be any number of materials so long it is thermally stable at and above 170ºC – 180ºC, structurally sound at those temperatures, and permeable to the decomposition products of PPC. Figure 1.5 shows two SEM images taken at steps 4 and 6 in the above process flow sheet, when the overcoat was a high temperature polyimide [1].

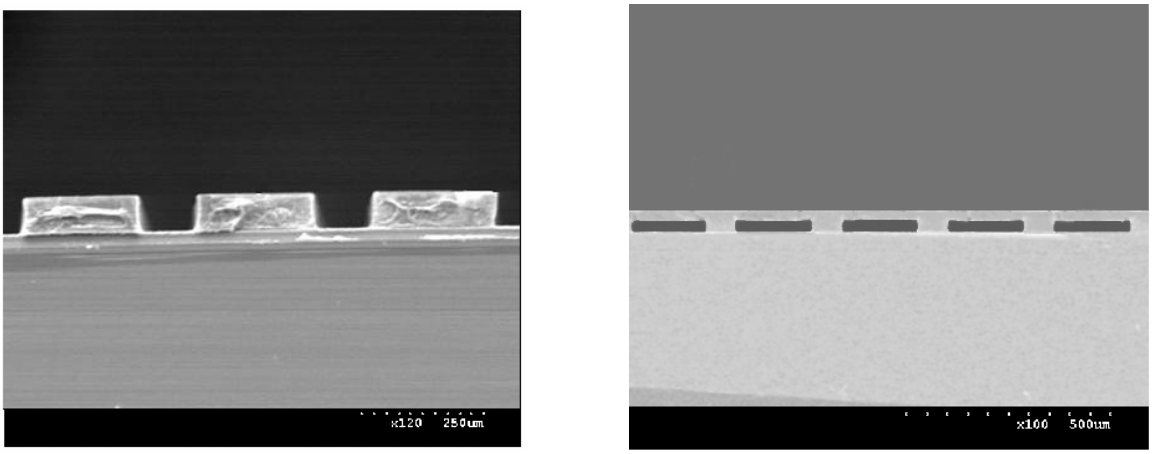

Figure 1.5: Example SEM images of PPC patterning (step 4) and air-gap formation (step 6) [1]

The two images in Figure 1.5 show the effective patterning and formation of simple air-gap structures that mimic the shape of the sacrificial polymer. Similarly, these same air-gap structures can also be used as microchannels for the transportation of fluids. In addition to the simple air-gap and fluid channel designs, more complex designs, like structures that use air-gaps for electrical isolation, as in the diagram in Figure 1.6.

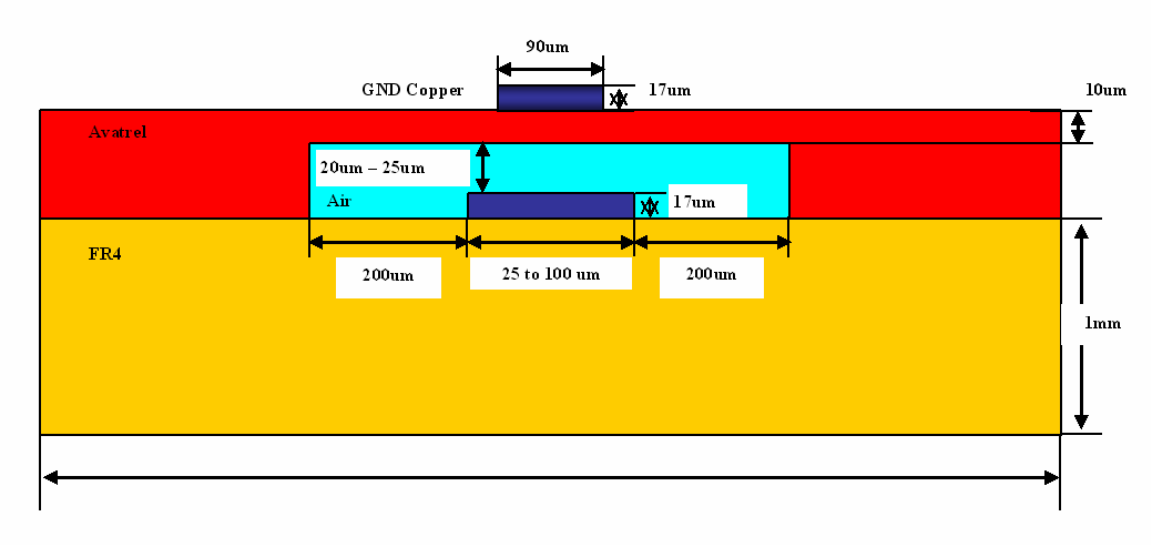

Figure 1.6: Schematic of a micro-strip configuration with air-isolation for a predicted 50% reduction in capacitance (Design courtesy of Tae Hong Kim, Georgia Institute of Technology)

In Figure 1.6, the air-gap was formed from the decomposition of the sacrificial PPC. Upon the removal of the polymer, an air-gap is formed; this theoretically reduces the capacitance between the two copper lines by 50%. The following two figures (1.7 and 1.8) show two SEM images before and after the decomposition of the sacrificial PPC layer, respectively.

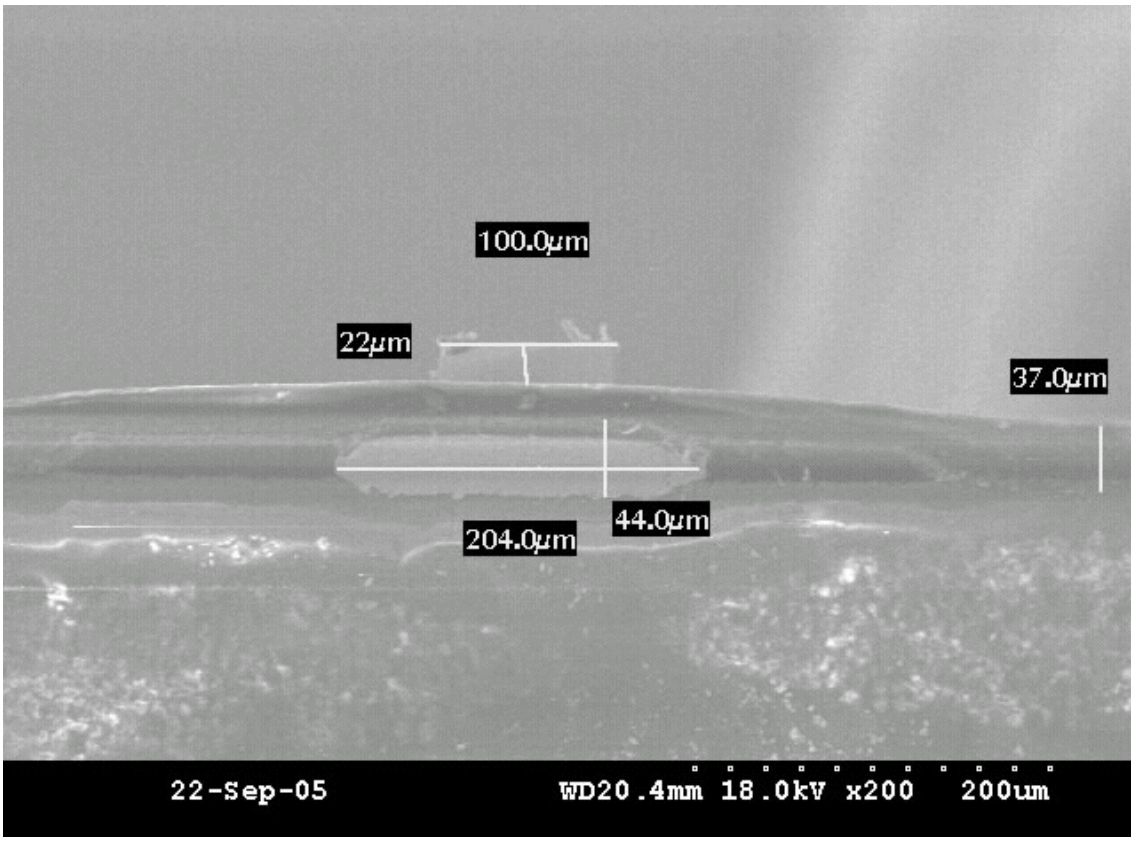

Figure 1.7: SEM of the electrical isolation air-gap device prior to PPC decomposition (Courtesy of Todd Spencer and Paul Jayachandran Joseph, Georgia Institute of Technology)

There are a few points of note in Figure 1.7. First, the copper signal line, which is 44um tall and 204um wide is completely encapsulated in PPC. The copper ground line is above the signal line and is 22um tall and 100um wide. Finally, the overcoat polymer is 37 um tall, on which the ground line rests.

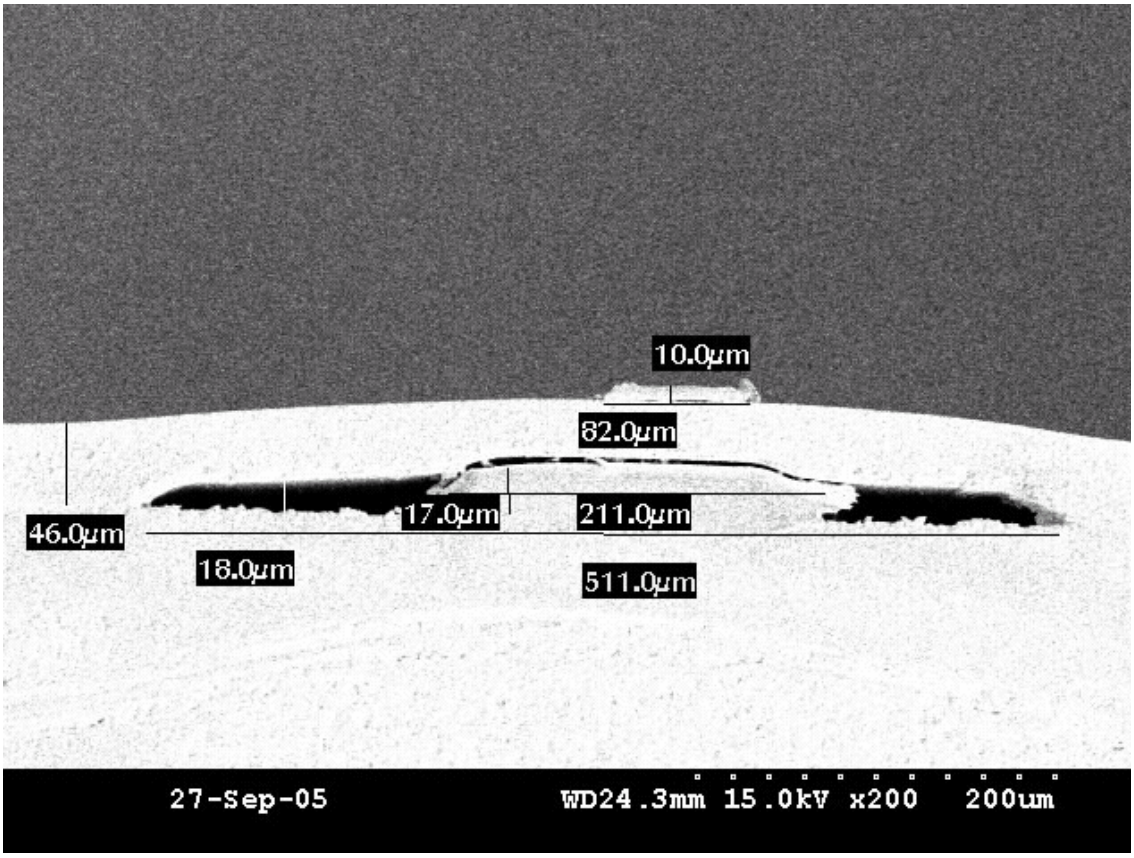

Figure 1.8: SEM of the electrical isolation air-gap device after the PPC decomposition (Courtesy of Todd Spencer and Paul Jayachandran Joseph, Georgia Institute of Technology)

After the decomposition, the structure is the same (dimensions are different because it is a different sample), except for the presence of an air-gap (black region) where the sacrificial polycarbonate used to be.

All of the aforementioned examples of using the PPC for the fabrication of micro-devices share similar processing issues. One of those issues regards the presence of residual matter that is present after the decomposition of PPC. This residual matter can be a result of numerous issues with the polymer system. For example, the polymer is not a 100% pure polycarbonate. During the polymerization process, polyether compounds form with the PPC in low percentages. Acid initiated decomposition of PPC is a catalytic

process; however, when a hydrogen ion attacks an ether group, the ether group forms an alcohol, consuming the acid, effectively acting as a catalyst poison. These polyether groups may be responsible for the post decomposition residue issues. Another possible source is the PAG itself. The PAG used in all of the above examples is Rhodorsil-FABA, shown in Figure 1.9.

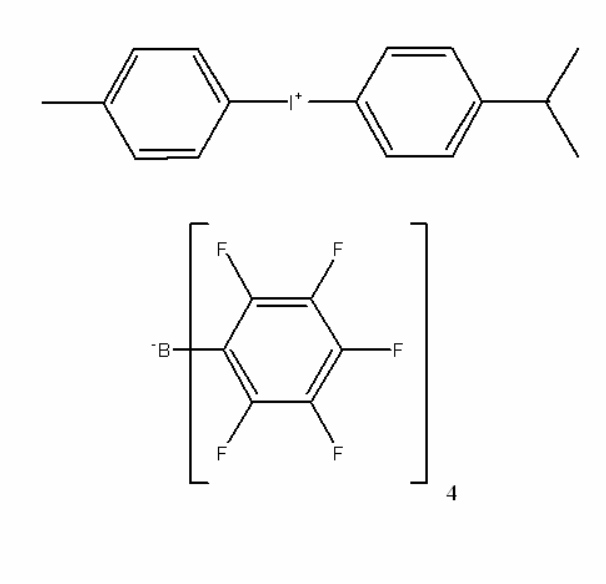

Figure 1.9: Chemical structure of the Rhodorsil-FABA PAG

The above PAG shown in Figure 1.9 has been the dominant active agent for PPC decomposition [1-3]. It is hypothesized that the FABA acid may be responsible for some of the residual issues observed after decomposition [14]. It is the goal of this body of work to not only examine the Rhordosil-FABA PAG, but research an assortment of different PAGs and quantify their ability to perform the decomposition of PPC. A focus will be placed on relating the properties of the PAG like acid strength, acid volatility, and PAG activation to processing issues like percentage of total film decomposition, amount

and composition of film residue, decomposition rate, decomposition temperature, and environmental dependencies.

CHAPTER 2

EXPERIMENTAL

2.1 Materials

The PPC used for all experimentation was obtained from Promerus LLC. The γ-butyrolactone (GBL) solvent was 99+% pure and purchased through Sigma-Aldrich. Also purchased from Sigma-Aldrich was the isopropyl alcohol. The NI PP300 pressurized 99+% pure nitrogen tanks were supplied by Airgas. Silicon wafers were purchased from Polishing Corp of America. The wafers were type P, with one polished surface, 100 mm in diameter, and had a 100 orientation. The glass slides were purchased from Fisher-Scientific. The following table summarizes all of the PAGs used in this study and where they were obtained.

Table 2.1: PAG material list

PAG Chemical Name	Supplier
(tert-butoxycarbonylmethoxynaphthyl)-diphenylsulfonium triflate	Sigma-Aldrich
Bis(4-tert-butylphenyl)iodonium triflate	Sigma-Aldrich
N-hydroxynaphthalimide triflate	Sigma-Aldrich
Diphenyliodonium perfluoro-1-butanesulfonate	Sigma-Aldrich
N-hydroxy-5-norbornene-2,3-dicarboximide perfluoro-1-butanesulfonate	Sigma-Aldrich
Tris(4-tert-butylphenyl)sulfonium perfluoro-1-butanesulfonate	Sigma-Aldrich
N-hydroxynaphthalimide perfluoro-1-butanesulfonate	Midori Kagaku Co.
4-methylphenyl[4-(1-methylethyl)phenyl] iodonium tetrakis(pentafluorophenyl)borate	Rhodia
tris(4-tert-butylphenyl)sulfonium tetrakis-(pentafluorophenyl)borate	Rhodia
triphenylsulfonium tetrakis-(pentafluorophenyl)borate	Rhodia
Bis(4-tert-butylphenyl)iodonium p-toluenesulfonate	Sigma-Aldrich
Diphenyliodomium 9,10-dimethoxyanthracene-2-sulfonate	Sigma-Aldrich
Ciba Non-ionic Photoacid Generator (Ciba 263)	Ciba Specialty Chemicals
Bis(4-tert-butylphenyl)iodonium perfluoro-1-octanesulfonate	Midori Kagaku Co.
Bis(4-tert-butylphenyl)iodonium tris(perfluoromethanesulfonyl)methide	3M Corporation
Bis(4-tert-butylphenyl)iodonium bis(perfluorobutanesulfonyl)imide	3M Corporation

All materials were used unaltered as purchased from the supplier.

2.2 Equipment

All PPC films were deposited and baked using a spin coater / hotplate combination apparatus purchased from Cost Effective Equipment (Division of Brewer Science, Model #2031050). The UV exposure equipment (3 parts) was all manufactured by ThermoOrion Instruments. The lamp was Model #92521-1000. The controller was Model #68945. The power supply was Model #69920. The tube furnace and controller are Lindburg equipment, Model #55322-3 and #58114-P, respectively. The profiling tool was a Sloan Dektak 3. For weight measurements the scale was a Mettler AE 200.

2.3 Procedures

For casting thin (~10um) PPC films, a 30 second final spin with a speed of 4000rpm and a ramp rate of 500rpm/s was used. For the medium (~25um) films, a 30 second final spin with a speed of 1900rpm and a 300rpm/s ramp rate was used. For the thick (~50um) films, a 30 second final spin with a speed of 950rpm and a 250rpm/s ramp rate was used. In all cases, the polymer was dynamically applied to the substrate during an initial 500rpm rotation for 10 seconds. Furthermore, all of the aforementioned spin recipes are based on a 30wt% polymer solution with GBL as the solvent. Creation of the photoacid polymer solutions is described in detail in Chapter 3. The solvent removal (soft bake) procedure was film thickness dependent. For thin films, 10 minutes at 120ºC was used. For medium films, 12 minutes at 120ºC was used. For thick films, 15 minutes

at 120ºC was used. All UV exposures were with 248nm light for a period of 3 minutes and 56 seconds, which yields 4000mJ/cm^2 of dosage based on lamp intensity calculations. The tube furnace sample processing was performed under a flow of 2 L/min of nitrogen after a 30 minute system purge and a 3ºC to 7ºC temperature ramp to the desired set point. The individual processing times and temperatures for both the hotplate and furnace testing vary and are described in the relevant sections of this report. Sample thickness profiling was performed at three different locations on the surface of the film. A razor blade was used to remove a square portion of the film at each of these locations for a base thickness. Each measurement involved averaging the film thickness over a length of 2 mm to 3 mm. The location for the measurements was the same for the initial and final profiling. To ensure accurate and reproducible results, at least two samples were processed at each condition, yielding a total of 6 measurements (approximately 15 mm of profiled film thickness). The surface chemical composition was determined by X-ray photoelectron spectroscopy (XPS), taking the integrated area under the photoelectron peak of each element weighted with their individual sensitivity factors (photoelectron emission cross section).

CHAPTER 3

PHOTOACID GENERATOR ANION STUDY

3.1 Introduction and Selection of Experimental Variables

Ionic photoacid generators are composed of two individual elements. The cation portion is responsible for the photo-activation of the PAG through the absorption of radiant energy. Its counter ion, the anion portion, is the conjugate base of a strong acid, which upon proper activation, extracts a hydrogen ion from the cation in order to form the acid. It was shown in Chapter 1 how the acid catalyzes the polymer decomposition reaction. The carbonyl moiety of the polycarbonate is an electron pair donator (i.e. base) and reacts with the photo-generated acid. Studying the physical properties of the acid formed from anion activation is essential to understanding the PAG's ability to catalyze the decomposition of the poly(propylene carbonate) matrix. This chapter will examine several different acid families and investigate the PAG properties (such as vapor pressure, acid strength, solubility) on the acid activation process.

In order to isolate and understand the anionic effects, very similar PAG cations were used. This will eliminate issues regarding specific cation / anion interaction and possible incompatibilities, while insuring a consistent light energy absorption curve associated with each cation. The selection of iodonium based cations was made due to its absorption at deep UV (248nm) irradiation, which has been used in other PPC patterning applications [1-3].

Second, the experiment will consider decomposition time. Previous studies have outlined PPC patterning recipes that use decomposition time periods ranging from 10 to

30 minutes [1-3]; however, different acids may have different decomposition reaction rates. Therefore, a time period of two hours was selected in the screening experiments as the designated decomposition time. This should provide the PAG system with ample time to be activated and achieve maximum polymer decomposition. In Chapter 6 of this report, the validity of the two hour time period selection for PPC decomposition will be analyzed and supported.

Third, the issue of quantum efficiency of the acid activation in the PPC matrix has been addressed. In keeping with the theme of performance optimization, this study has attempted to maximize the level of activated PAG by using an elevated exposure dosage. Using a 248-nm based chemically activated photoresist as a reference; previous studies have shown that a dosage of 4000 mJ/cm^2 will be more than enough energy to confidently say all of the PAG will be activated. In fact, experimentation shows that 200 mJ/cm^2 of energy is necessary for 100% PAG activation [8]. Erring on the side of caution, a dosage of 4000 mJ/cm^2 of 248-nm light was chosen as the energy infusion amount for all analysis completed in this study. Through experimentation with the Rhodorsil-FABA PAG, it was found that 1000 mJ/cm^2 was adequate for complete activation; however, a number four times as large was chosen to be confident. Furthermore, sample patterning was avoided in favor of complete sample exposure, in order to eliminate difficulties associated with acid diffusion and feature stability commonly observed with PPC polymers and their low glass transition temperature (~40ºC) [1-3, 9-10].

Fourth, there is the issue of selecting decomposition temperatures. The TGA in the introduction (Figure 1.3) is specific to Rhodorsil-FABA and different acids may have

alternate decomposition temperatures. A lower decomposition temperature is of interest for patterning the PPC. Therefore, initial screening temperatures of 60ºC, 90ºC, and 120ºC were chosen for this screening experiment. This should allow for the examination of the system's behavior in a suitable temperature range, while keeping the number of experiments for each PAG at a manageable level.

Fifth, this study examines different decomposition conditions and environments. Two of the common methods employ the use of a controlled environment tube furnace and an open-atmosphere hotplate. Both methods have their advantages and disadvantages. With a furnace, it is easier to isolate the sample from the environment and use a controlled temperature ramping scheme; however overall experiment setup and run times can be quite long and tedious. Conversely, using a constant temperature controlled hotplate is a quick and simple method, but may have environmental control issues. For the sake of completeness, both methods have been examined in this study.

Lastly, the parameters for the base polymer were selected to correspond to spin-coating thickness of interest. A series of PPC solutions without PAG were mixed ranging from 20 wt% to 35 wt%. The solvent used to dissolve the PPC was γ-butyrolactone (GBL). The formula that shows the calculations used to generate these solutions is

$$W = \frac{p}{p + s + g * p}, \qquad \text{(Equation 3.1)}$$

where W is the weight percent of polymer desired, p is the mass of polymer, s is the mass of solvent, and g is the weight percent of PAG desired (based on polymer mass not total mass). The higher weight percent of PPC in solution resulted in higher viscosity. In turn,

the solution's viscosity affects the range of possible uniform film thickness that can be created by standard spincoating methods. The following equation shows the relationship between sample film thickness and the angular velocity of the spincoating apparatus:

$$l = \frac{1}{\omega^r}, \qquad \text{(Equation 3.2)}$$

where l is the film thickness, ω is the angular velocity, and r is a correction factor based on the properties of the fluid (i.e. viscosity). To properly choose a polymer loading weight, a set of samples were made with each solution using several different spincoating angular velocities. Figure 3.1 shows the result of this analysis.

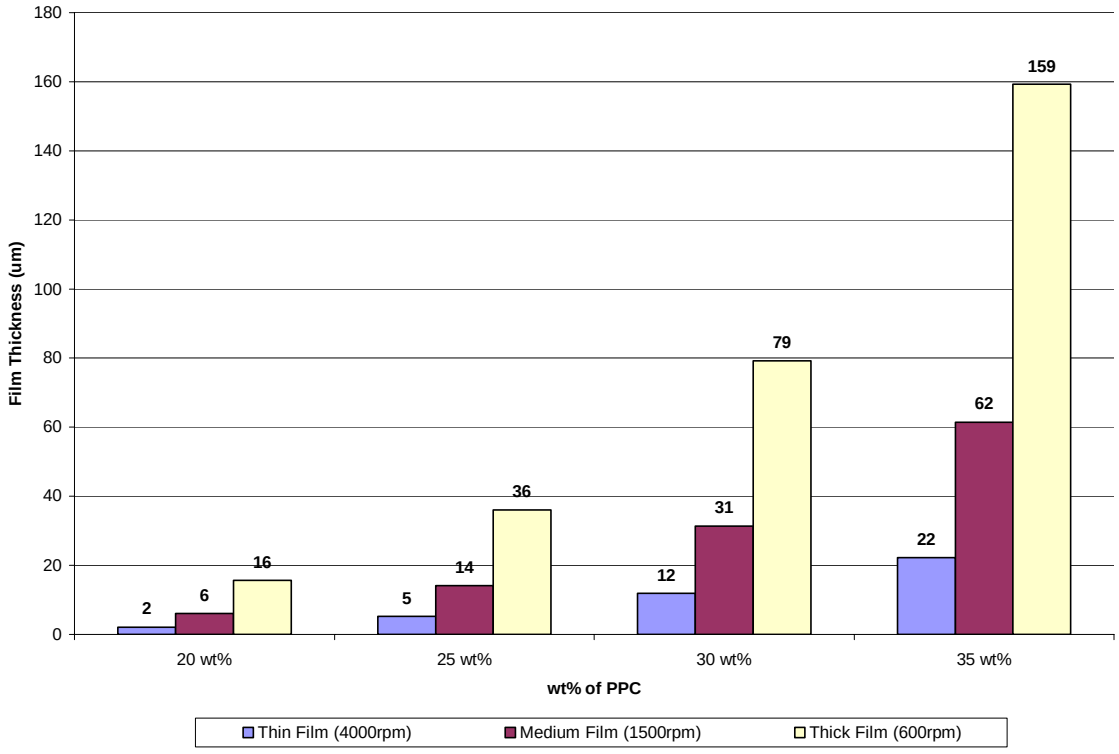

Figure 3.1: Solution thickness curves for the PPC / GBL solutions

The 30wt% PPC loading solution was chosen as the basis for all of the experiments. The second solution parameter is the amount of PAG loading. Since different PAGs will have different molecular weights, selecting an overall molar basis rather than a weight basis is the appropriate way to set this parameter. Seeing as the Rhodorsil-FABA PAG has had prior success with patterning PPC films, it was chosen as the standard. Furthermore, it has also been shown that 3 to 5 wt% Rhodorsil-FABA PAG loading based solely on the polymer's mass is adequate for complete decomposition [1-3]. The midpoint value of 4 wt% Rhodorsil-FABA PAG was chosen as the basis, and all other PAG loadings will be made equivalent through a molecular weight ratio. Each polymer solution was mixed for a minimum of seven days using a standard ball mill roller. The following table displays all of the PAGs used in this experiment along with their molecular weights, acronyms, and acid types.

Table 3.1: PAGs used in the anion study

PAG Chemical Name	Acronym	Generic Acid Family Name	Molecular Weight (g/mol)
Bis(4-tert-butylphenyl)iodonium triflate	BTBPI-TF	Triflate	542
Bis(4-tert-butylphenyl)iodonium p-toluenesulfonate	BTBPI-PTS	Sulfonate	565
Diphenyliodonium perfluoro-1-butanesulfonate	DPI-NF	Nonaflate	580
Diphenyliodomium 9,10-dimethoxyanthracene-2-sulfonate	DPI-DMOS	Sulfonate	598
Bis(4-tert-butylphenyl)iodonium perfluoro-1-octanesulfonate	BTBPI-HDF	Heptadecaflate	892
4-methylphenyl[4-(1-methylethyl)phenyl] iodonium tetrakis(pentafluorophenyl)borate	Rhodorsil-FABA	FABA	1016
Bis(4-tert-butylphenyl)iodonium tris(perfluoromethanesulfonyl)methide	BTBPI-TMM	Methide	805
Bis(4-tert-butylphenyl)iodonium bis(perfluorobutanesulfonyl)imide	BTBPI-BBI	Imide	974

Chemical structures of the PAGs listed in Table 3.1 can be found in Appendix A. Using the 30wt% PPC with 4wt% equivalent PAG solutions, films targeted at 10 μm were spuncoat onto glass substrates. A glass substrate was selected so that the experimenter could easily see any sample color change or deformation. The samples were soft baked at 120ºC for 10 minutes to remove any solvent. An initial film thickness was profiled in multiple places on the sample, and then the entire film was exposed to 248-nm light for a period of 3 minutes and 56 seconds (4000 mJ/cm^2). Six samples were made in this fashion for each PAG. The samples were then subjected to a post exposure bake (PEB) at 60ºC, 90ºC, and 120ºC both in a tube furnace and on an open-atmosphere hotplate for a period of two hours. After the PEB, the samples were once again profiled at the same points to determine film thickness. The percentage of film decomposed was then calculated for each situation and PAG. For the purposes of this analysis, the percentage decomposition will define the samples performance. A sample with a small percentage of decomposition will be considered poor, while a sample with 100% decomposition will be considered perfect.

3.2 Results and Discussion

With the establishment of a procedure for measuring the decomposition of different PPC / PAG systems that focuses on the photo-acid while eliminating confounding variables, the next step is to perform experimentation with specific PAGs. Beginning with the BTBPI-PTS sulfonate based PAG; Figure 3.2 shows the results of the experiment outlined in the previous paragraph.

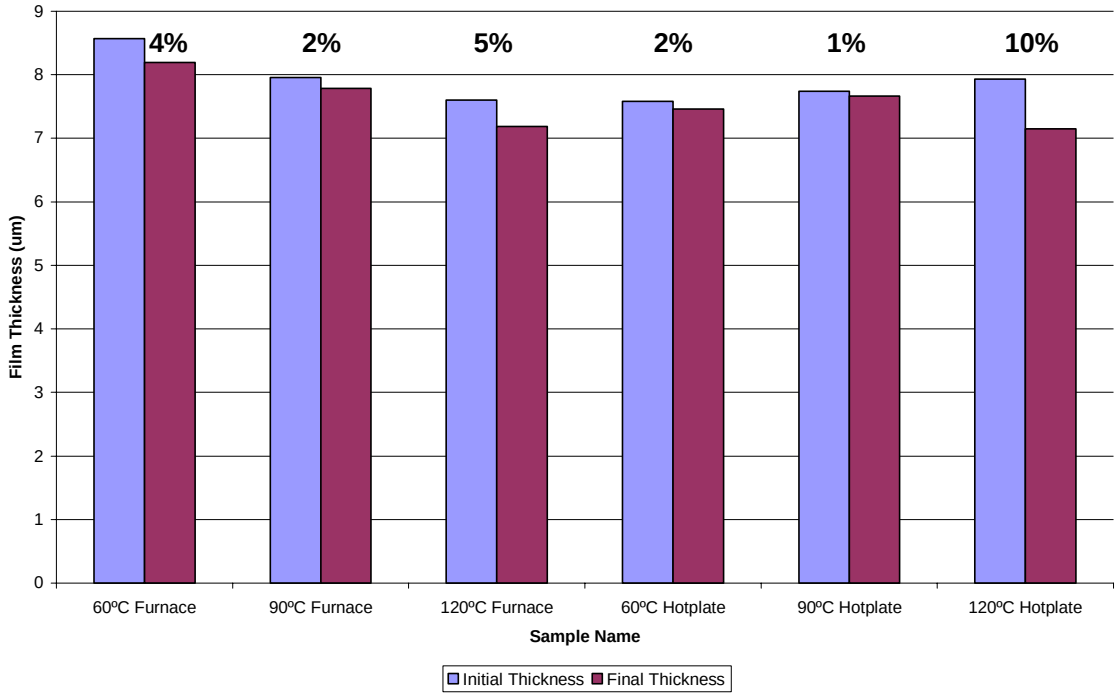

Figure 3.2: BTBPI-PTS PAG decomposition levels

Figure 3.2 relates the film thickness before and after PEB for each set of conditions. The percentages on top of each bar graph show the percent decomposition for that sample. With the best performance at 10% decomposition, BTBPI-PTS is a poor choice for the PPC system. The small decomposition can be explained in two ways. One, the acid formed from this PAG is p-toluene sulfonic acid, which has a pKa value of -4 [15]. Whereas this is acidic, it is not in the super-acid range (pKa < -12) where previous PPC decomposition experimentation showed success [1-3]. Furthermore, the p-toluene sulfonic acid is not a bulky acid, and it has significant vapor pressure at the temperatures involved in the experiment. Therefore, the acid will be evaporating out of the film during decomposition, which will cause a reduction in the acid's concentration. This

combination leads to the poor performance seen is Figure 3.2. Another sulfonate based PAG is DPI-DMOS and its performance is displayed in Figure 3.3.

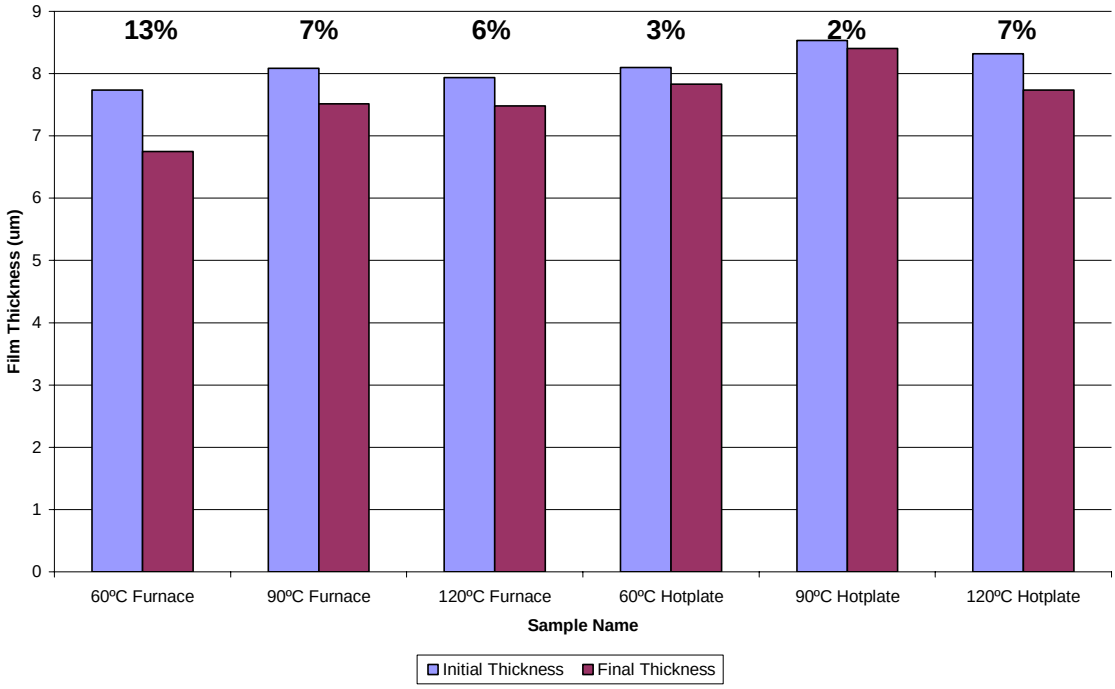

Figure 3.3: DPI-DMOS PAG decomposition levels

As with the BTBPI-PTS, this sulfonate PAG also shows a very poor performance, with a maximum decomposition at 13%. The 9,10-dimethoxyanthracene-2-sulfonic acid is slightly more acidic than p-toluene sulfonic acid because it contains more electron withdrawing groups; however, it still has too low of an acidity function.

The next PAG examined, BTBPI-TF, is in the triflic acid family. Its performance can be observed in Figure 3.4.

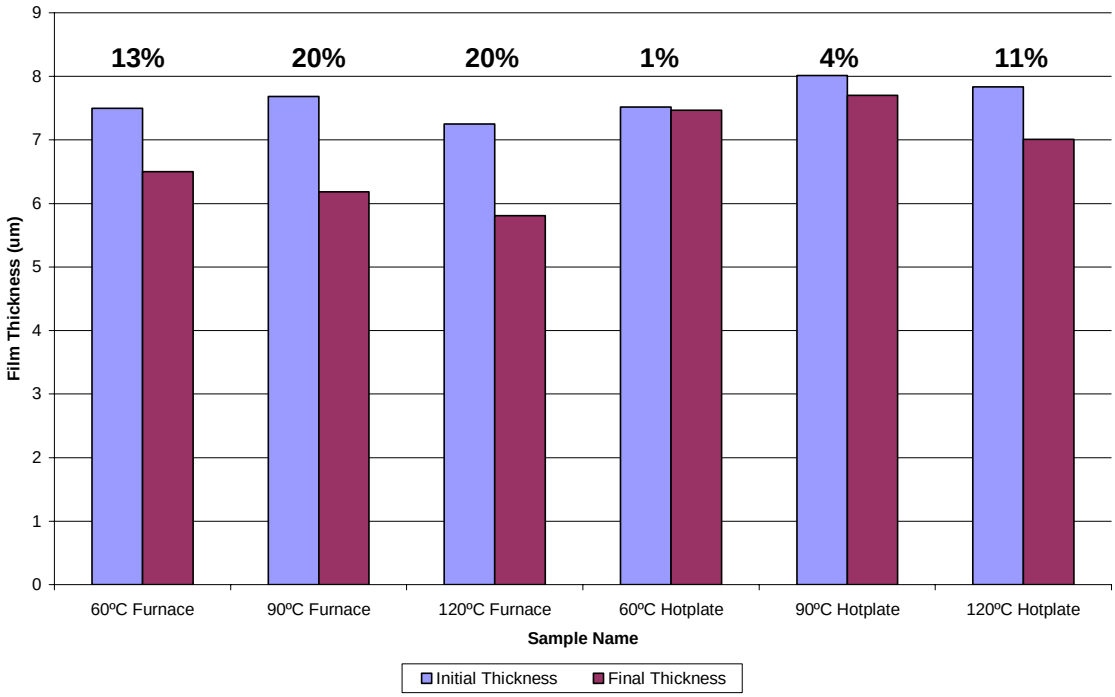

Figure 3.4: BTBPI-TF PAG decomposition levels

There are multiple points of note in Figure 3.4. First, the best performance of this PAG was measured to be at 20% decomposition, which is approximately twice the decomposition of the sulfonic acid PAGs previously mentioned. The performance increase can be accredited to the acidity of triflic acid formed in this system. With a pKa of around -14 to -15, triflic acid meets the criterion of a super-acid [15]. Triflic acid has a relatively high vapor pressure which appears to be responsible for its lower PPC decomposition since it does not remain in a polymer for a sufficient amount of time. The vapor pressure is 200 torr at 120ºC [12]. Another effect of the high vapor pressure can be seen in the difference between tube furnace and hotplate PEB processing. As seen in Figure 3.4, the hotplate samples reach a maximum performance of only 11% decomposition, which is poor when compared to the furnace samples. Several

explanations of this phenomenon like environmental effects and conductive sample heating are explored in Chapter 5. In summary, even with its high acidity, triflic acid PAGs do not appear to be sufficient for PPC film decomposition because of the vapor pressure effect.

The next experimental data set is based on a similar acid, perfluorobutane sulfonic acid (nonaflic acid). Like triflic acid, it has a single perfluorinated carbon chain bonded to a sulfonate group. Nonaflic acid has super-acid level strength; however, its increased molecular weight will lead to a decreased vapor pressure of the acid. Figure 3.5 displays the result of the experimentation.

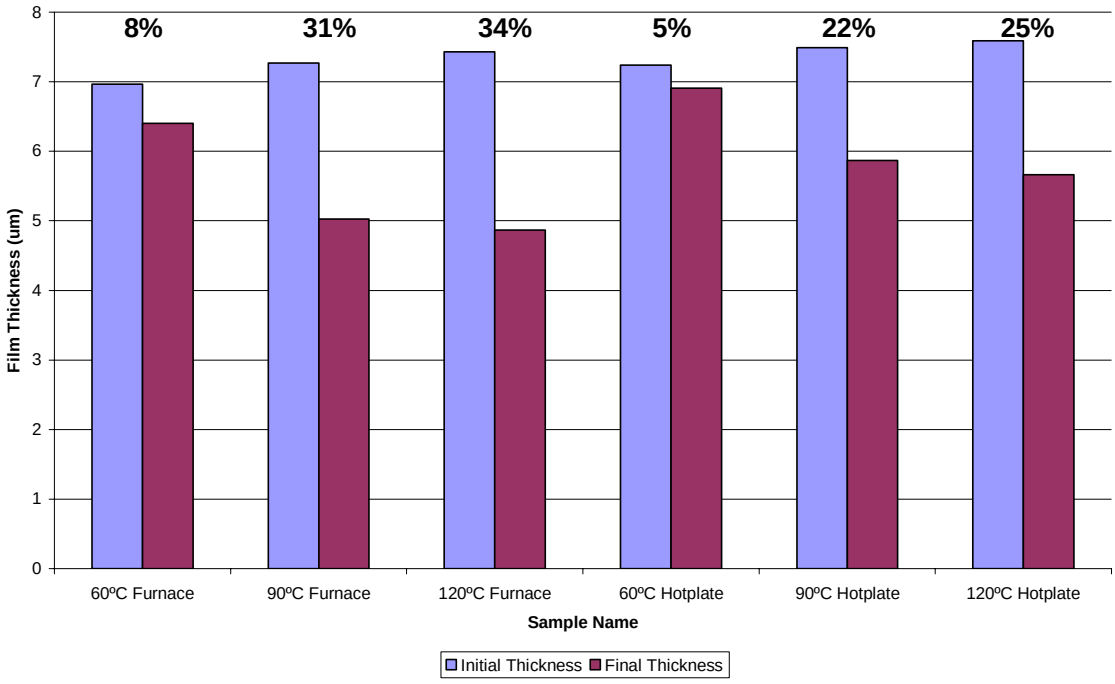

Figure 3.5: DPI-NF PAG decomposition levels

The DPI-NF PAG with an anion based on nonaflic acid performed a higher level of PPC film decomposition when compared to a triflic acid based PAG. Unfortunately, the maximum achievable decomposition peaked at 34%, which is still unacceptable. It appears that nonaflic acid, with a vapor pressure of 30 to 40 torr at 120ºC, is still too volatile for the dry PEB techniques used in the PPC development [12]. Another interesting point seen in Figure 3.5 is the continued trend of reduced performance for hotplate processed samples; however, the effect seems to be less severe for nonaflic acid when compared to triflic acid.

The next perfluorinated sulfonic PAG tested was BTBPI-HDF, with an anion in the heptadecaflate (perfluoro-octane sulfonic acid) family. This acid has an eight carbon chain, which results in a vapor pressure around 5 to 10 torr at 120ºC [12]. The experimental results can be found in Figure 3.6.

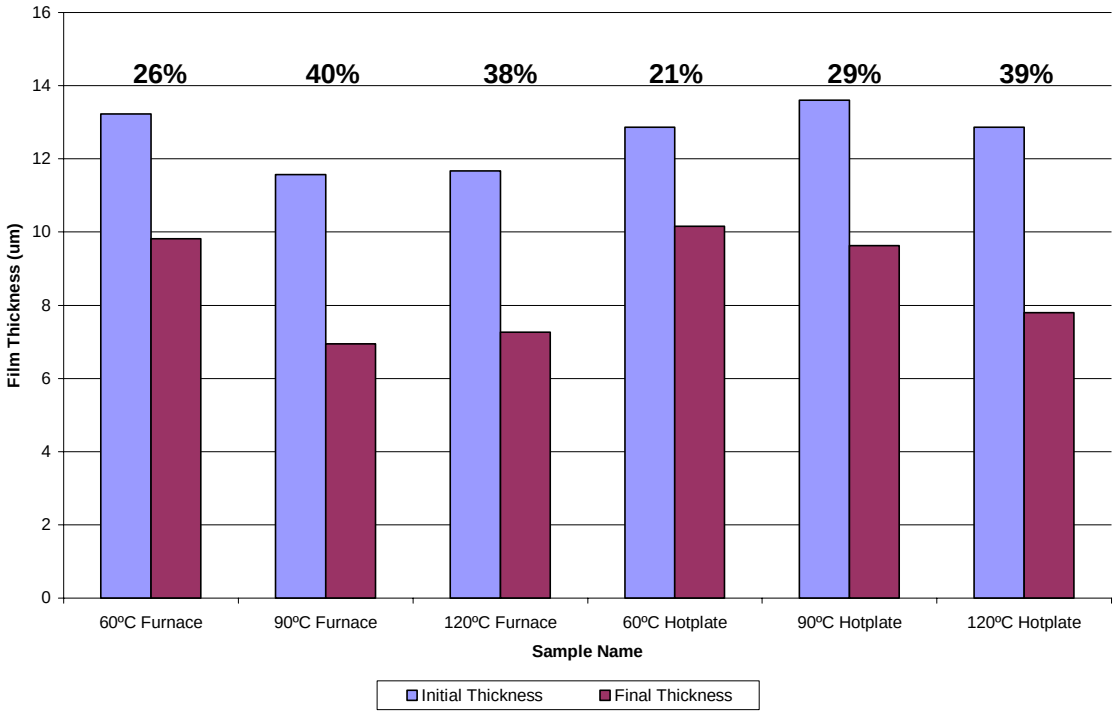

Figure 3.6: BTBPI-HDF PAG decomposition levels

As with the transition from triflic acid to nonaflic acid, the switch to the perfluoro-octane sulfonic acid resulted in a decomposition performance increase; however, the increase was smaller than expected at only 6%. The perfluoro-octane sulfonic acid PAG has the high acidity levels and very low vapor pressure qualities desired for complete PPC decomposition. Unfortunately, the PAG was found unable to fully incorporate within the PPC matrix. The solubility issue was caused by the long perfluorinated carbon chain present on the anion of the PAG. The presence of this fluorophilic chain resulted in the phase separation of the PAG in the PPC film after the soft bake step. The phase separation was visible to the naked eye in the form of white crystals throughout the film. Furthermore, the typically smooth surface of the film becomes rough when profiled also indicating the presence of a crystalline second phase. Since the majority of the PAG is

unable to contact the PPC, the decomposition is restricted from reaching its maximum value. For this reason, perfluoro-octane sulfonic acids do not appear to be good candidates for PPC decomposition.

After the poor performance of the BTBPI-HDF PAG, it is concluded that any length perfluroalkyl chain sulfonic acids is inadequate for these systems. In recent years, a set of new perfluorinated anions have been created by William M. Lamanna, et.al. at the 3M corporation [5, 11-13]. One of these novel PAGs is a perfluorinated methide, BTBPI-TMM. The methide anion contains three triflic acid-like groups, and experimentation with photo-acid reactivity and epoxy curing have shown this anion to be comparable to salts based on one of the most reactive and acidic (pKa ~ -18) anions, SbF_6^- [12]. The results of using BTBPI-TMM with PPC can be found in Figure 3.7.

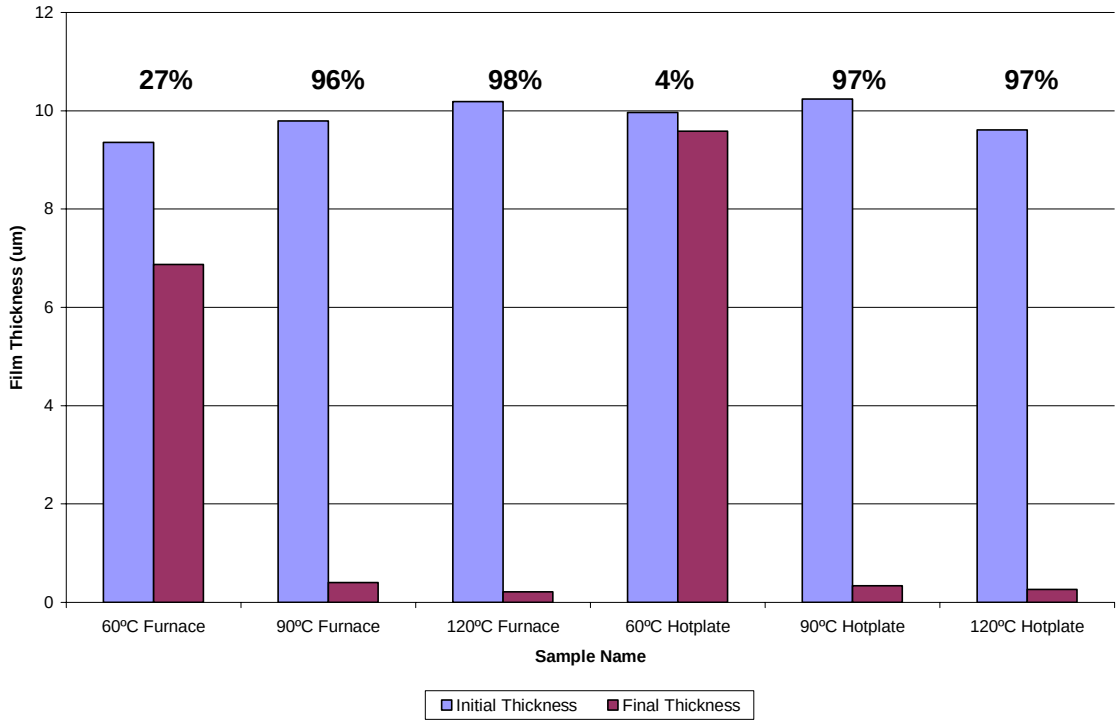

Figure 3.7: BTBPI-TMM decomposition levels

Despite a high vapor pressure of 75 to 80 torr at 120ºC, the BTBPI-TMM PAG reaches decomposition levels of 98%. The remaining 2% on the glass substrate was a light brown, oily residue that does not resemble the initial PPC film. This residue was a product of side reactions taking place within the PPC matrix as well as some PAG remains as seen in the X-ray photoelectron spectroscopy of the residue's surface shown in Figure 3.8.

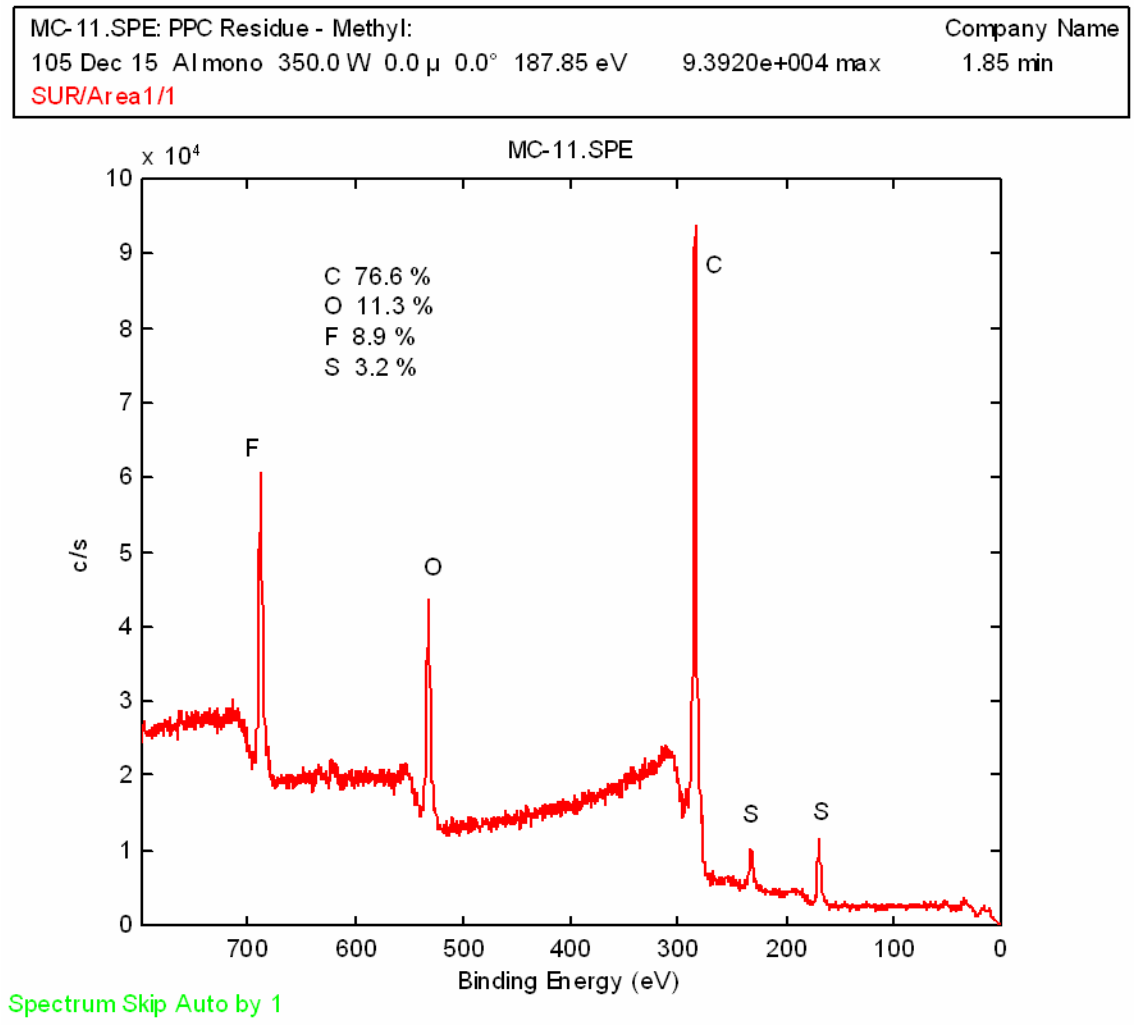

Figure 3.8: X-ray photoelectron spectroscopy (XPS) of BTBPI-TMM residue for the 120ºC sample

The XPS surface analysis shows that there is the presence of carbon, fluorine, oxygen, and sulfur in the residue. This indicates the presence of both PAG and polymer residue. A complete examination of the XPS residue data and its composition can be found in Chapter 8. These results show that the PAG components contribute to the residue even if its vapor pressure is high. It also shows that the contribution to the residue is complex issue because the methide acid has a higher vapor pressure than the nonaflic acid. It is important to remember that the acid vapor pressure is only one property that affects the performance of the PAG, and since the reactivity and acidity of the methide PAG is so high, the decomposition reaction may take place before the acid escapes the system. Support for this explanation can be found in Chapter 6.

The performance of BTBPI-TMM rivals the typical PAG used in these PPC systems, Rhodorsil-FABA PAG. The following figure shows the decomposition performance of the Rhodorsil PAG.

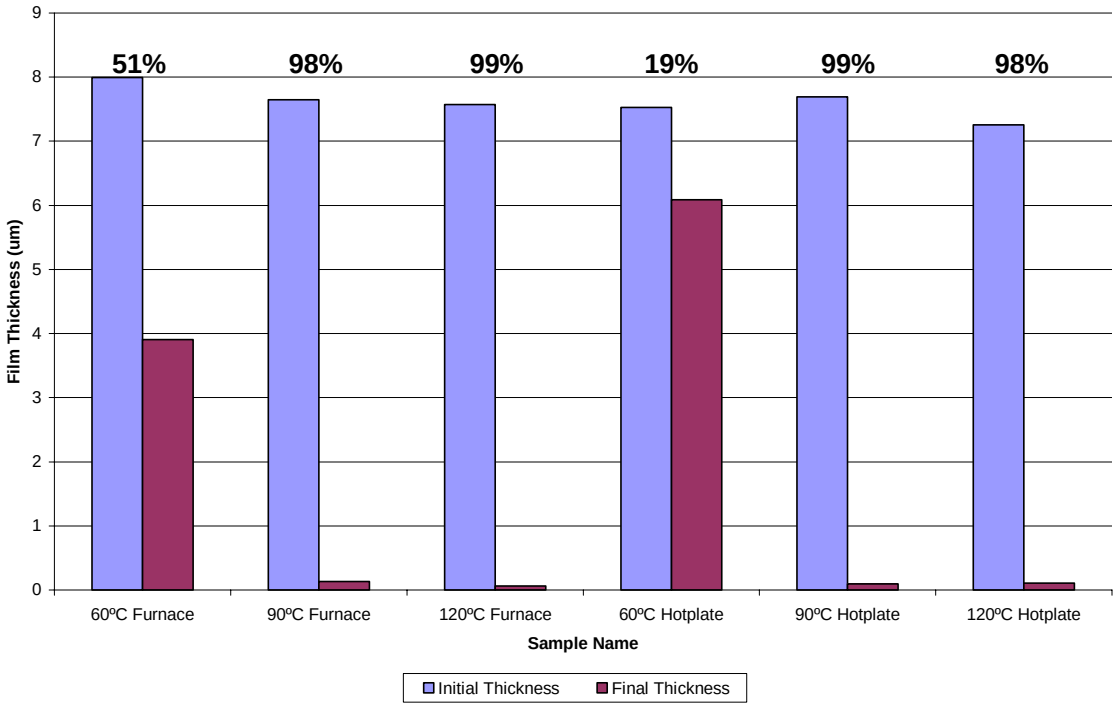

Figure 3.9: Rhodorsil-FABA PAG decomposition levels

Figure 3.9 shows why Rhodorsil-FABA has been the standard for PPC processing with decomposition levels at 99% for both hotplate and furnace PEB. With four fluorinated benzene groups, the FABA acid is bulky and has negligible vapor pressure at these temperatures; however, during activation and decomposition, some of the acid does break down into smaller, more volatile products. Also, the FABA group is considered to be a strong super-acid, unfortunately, a pKa value could not be obtained from a literature search. A knowledgeable estimation would place the pKa value at about -15 to -16. The remaining 1% film residue was analyzed by XPS, and Figure 3.10 shows the results.

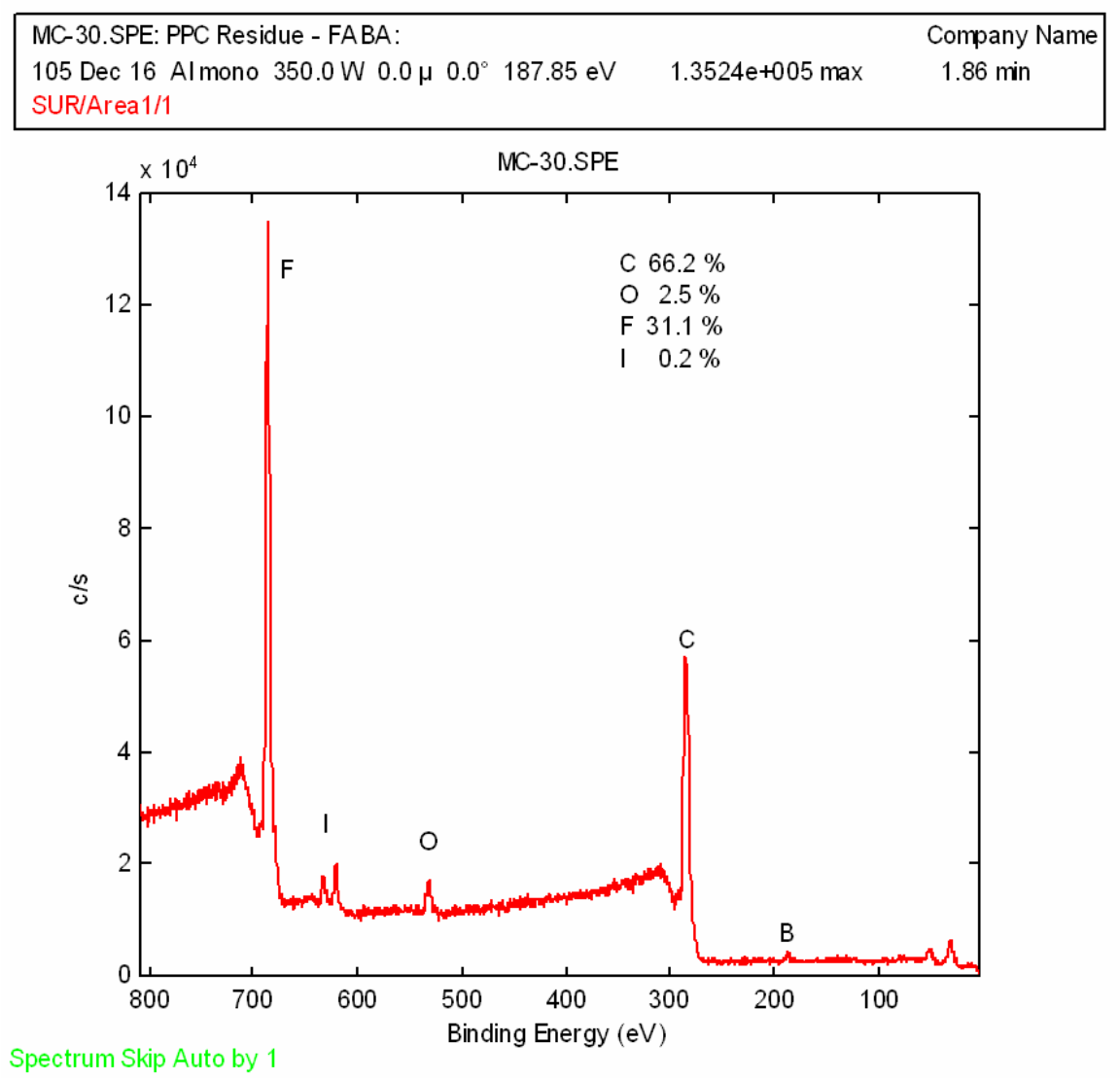

Figure 3.10: X-ray photoelectron spectroscopy (XPS) of Rhodorsil-FABA residue for the 120ºC sample

The FABA XPS data contains carbon, fluorine, oxygen, iodine, and boron (1% to 2% - not shown on graph). There is a significant amount of fluorine in the analysis indicating a high level of PAG based residue, as expected. Also this residue is a dark brown, hard film that is different in appearance from the residue found on the methide samples. The residue appears to be caused by the non-volatile Rhodorsil-FABA salts and side products

of the PPC decomposition. A more complete analysis of the XPS residue data can be found in Chapter 8.

With the success of the methide based PAG when compared to FABA, additional experiments with a perfluorinated imide based PAG (another novel PAG created by Lamanna et.al.) were performed. The PAG selected was BTBPI-BBI, which contains two nonaflic acid like groups bonded to nitrogen. The selection was made based on vapor pressure considerations. BTBPI-BBI has a vapor pressure of around 10 torr at 120ºC, which is essentially identical to the BTBPI-HDF PAG seen earlier in this chapter [12]. The results of processing the BTBPI-BBI PAG can be found in the Figure 3.11.

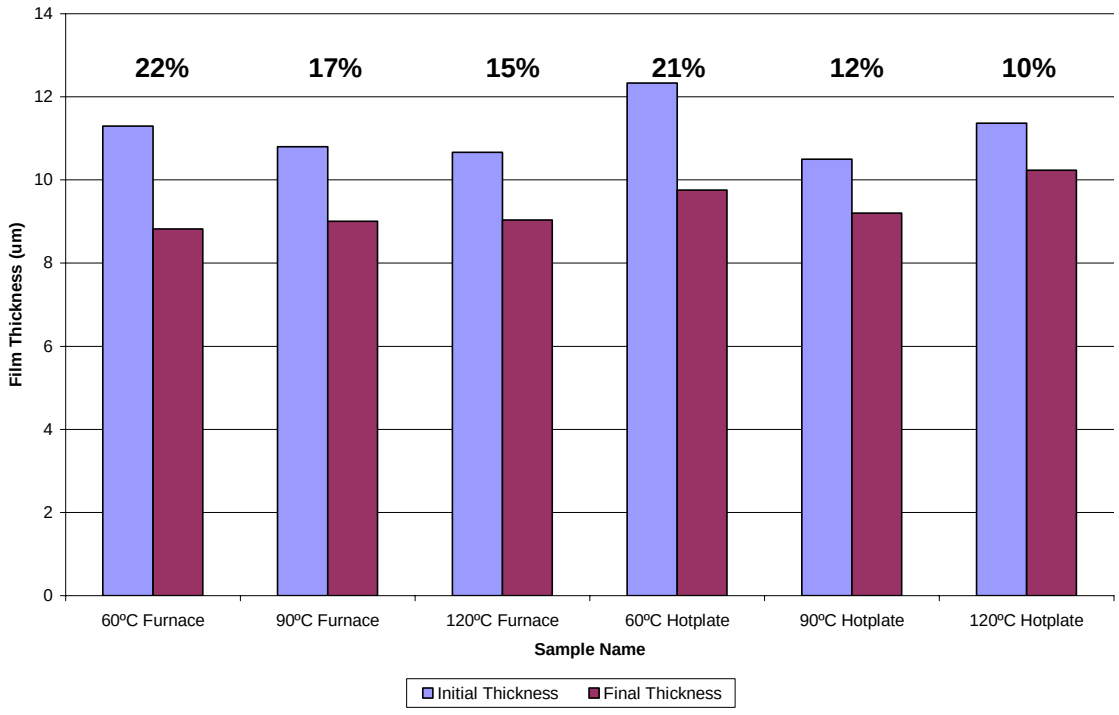

Figure 3.11: BTBPI-BBI PAG decomposition levels

The decomposition performance of the imide based PAG is quite poor as shown in Figure 3.11. The maximum decomposition was 22%. The explanation of these results is similar to the BTBPI-HDF PAG, since there was a phase separation of the PPC and PAG after the solvent removal processing step. The conclusion can be drawn that the presence of multiple long chain perfluorinated carbons is responsible for the separation and ultimately the poor performance. This PAG is not suitable for PPC decomposition.

3.3 Conclusions

Overall, this chapter provides a comprehensive look at a variety of PAG anions and the physical properties that result in the successful decomposition of PPC. An efficient experiment was designed that isolated the PAG anion's performance from that of the cation, quantum acid yield, PEB environment, PEB temperature, PEB time, and PAG loading. The conclusion was drawn that non-fluorinated sulfonic acids do not have the acid strength to catalyze the complete decomposition process. Also, perfluorinated sulfonates like triflic and nonaflic acid have super-acid level pKa's; however, due to their volatility, the acid is unable to remain in the PPC matrix to fully decompose the film. The longest chain perfluorinated sulfonic acid, perfluoro-octane has a very low vapor pressure; however, due to its bulky fluorine chain, it phase separates from the PPC matrix upon removal of the solvent. Thus, its decomposition ability suffered. Similarly, this phase separation phenomenon was present in the long chain perfluorinated imide, which consequently hindered performance. The only two successful anions were the perfluorinated methide and FABA. Despite the methide's moderate vapor pressure, its high reactivity and super-acid strength has been shown to offset this negative effect.

Finally, as expected from surveying literature, the bulky, strong FABA acid completed the decomposition, but left a brown, tar-like residue that requires further examination (See Chapter 8).

CHAPTER 4

CATION AND NON-IONIC PAG STUDY

In Chapter 3, only aromatic based iodonium compounds were used as the energy absorbing cation portion of the PAG. Here, in Chapter 4, an examination of several different cations will be paired with each anion group to determine whether or not the cation portion of the PAG has a significant effect on PPC decomposition performance. Also, this experiment will observe some non-ionic PAGs that covalently bond the "cation" portion to the "anion" portion. For ease of discussion, the energy absorbing portion of non-ionic PAGs will still be referred to as the cation. The majority of the PAGs selected will have significant absorption in the deep UV range, which corresponds to 248 nm wavelength irradiation [16-18]. These PAGs should be fully activated after exposure yielding the highest possible activation and protenation of the anion. PAGs that do not have high absorptions in the 248 nm range may experience performance retardation due to lack of acid activation. Beside absorption and activation, choice of the cation has a large effect on the thermal stability and solvent solubility of the PAG. All of the PAGs found in Chapter 4 are fully soluble in GBL in the necessary concentrations and thermally stable up to at least 120ºC. Therefore, these issues should not present a problem during experimentation. For the sake of consistency and proper comparison, the experimental method for the cation study will be identical to that of the anion study found in Chapter 3.

The first sample set contains non-fluorinated sulfonate acids. The following table summarizes the chemical names and given acronyms of each PAG. PAG structures can be found in Appendix A.

Table 4.1: Sulfonate (non-fluorinated) Acid PAG Group

PAG Chemical Name	Acronyms	Molecular Weight (g/mol)
Bis(4-tert-butylphenyl)iodonium p-toluenesulfonate	BTBPI-PTS	565
Diphenyliodomium 9,10-dimethoxyanthracene-2-sulfonate	DPI-DMOS	598
Ciba Photoacid Generator (1-propane sulfonic acid)	CGI 263	663

The first two PAGs listed in Table 4.1 were studied in Chapter 3, but the third PAG obtained from Ciba Specialty Chemicals is new. The CGI-263 PAG is non-ionic, and it contains two 1-propane sulfonic acid groups per molecule. Figure 4.1 shows the experimental results for the sulfonic acid PAGs.

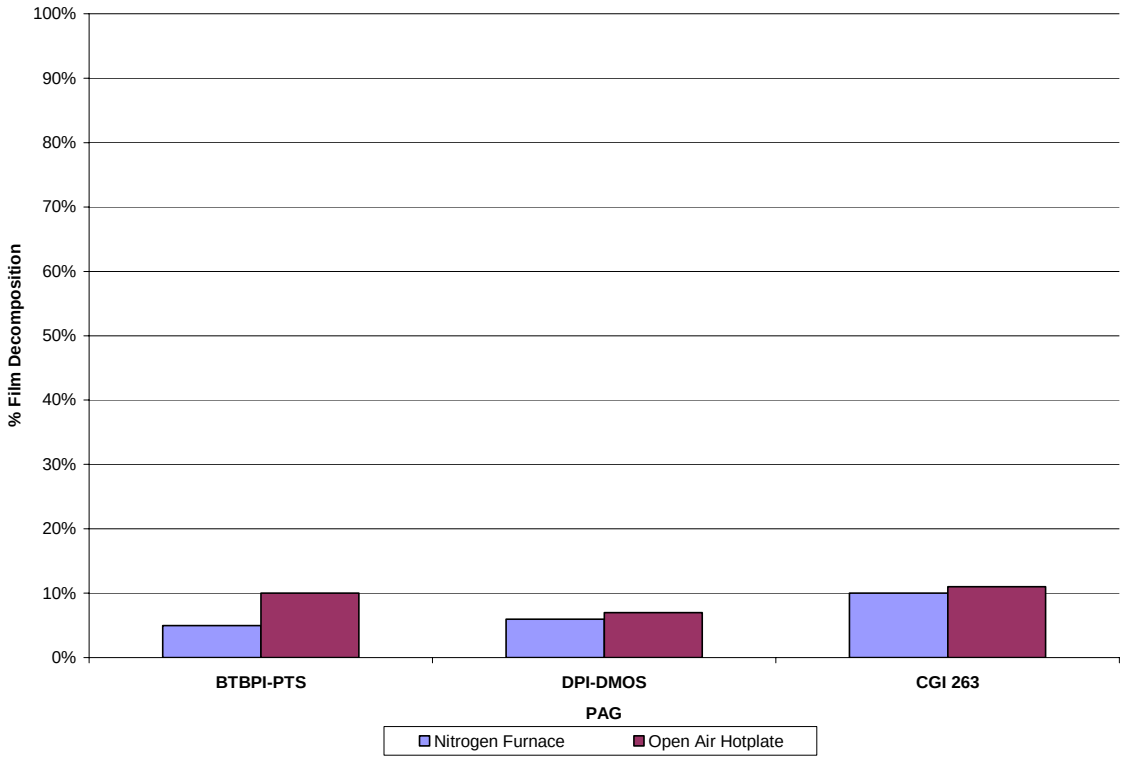

Figure 4.1: Film decomposition study at 120ºC for all sulfonate PAGs

The above figure compares the percentage of PPC film decomposed for each PAG in the nitrogen furnace and open atmosphere environments. Just as in Chapter 3, the higher percentage of decomposition indicates improved performance. To remove graphical clutter, only the 120ºC decomposition data is presented. For trend discussion purposes, the 120ºC data is adequately representative of the entire temperature range. Examining Figure 4.1, the non-fluorinated sulfonate acids show poor decomposition performance, which was also the case in Chapter 3. The newest acid in this group, CGI 263, is no exception. Even though the CGI 263 PAG forms two acid groups for each activated molecule, the acid that it forms is not in the super-acid range (pKa ~ -2 to -4), and for that reason the performance is still low [15].

The next set of PAGs examined is the triflic acid group as shown in Table 4.2 below.

Table 4.2: Triflic Acid PAG Group

PAG Chemical Name	Acronym	Molecular Weight
(tert-butoxycarbonylmethoxynaphthyl)-diphenylsulfonium triflate	TBOMDS-TF	593
Bis(4-tert-butylphenyl)iodonium triflate	BTBPI-TF	542
N-hydroxynaphthalimide triflate	NHN-TF	345

The iodonium based cation PAG, BTBPI-TF was also used in Chapter 3, but the sulfonate based cation PAG, TBOMDS-TF, and the non-ionic PAG, NHN-TF, have not yet been discussed in this body of work. Figure 4.2 displays the results of the triflic acid group experimentation.

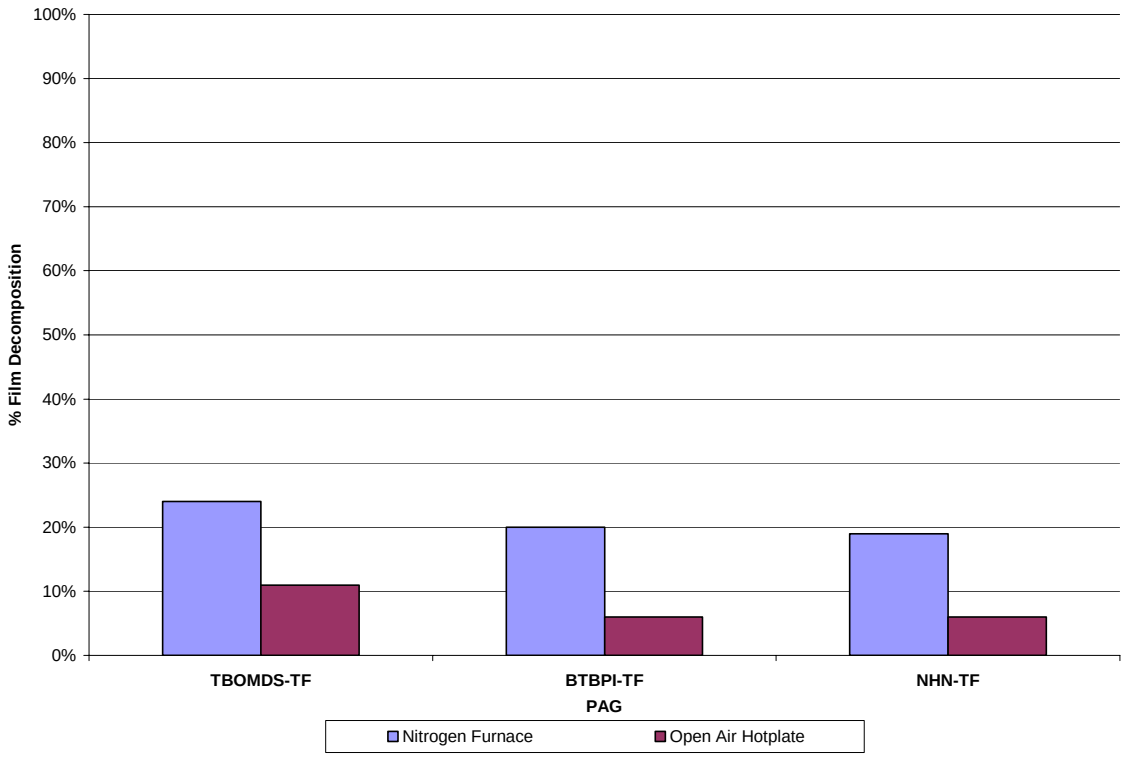

Figure 4.2: Film decomposition study at 120ºC for all triflic acid PAGs

Figure 4.2 above shows that all three triflic acid based PAGs have similar film decomposition levels, with approximately 20% furnace and 5% to 10% hotplate decomposition at 120ºC. The sulfonate cation PAG, TBOMDS-TF, demonstrated the highest performance, if only by a couple percent in both environments. Comparing the hotplate with the furnace environment, there is a trend of decreasing performance with the hotplate samples in all three PAGs. This phenomenon was also mentioned in Chapter 3, and the discussion of possible causes is undertaken in the environmental studies of Chapter 5.

The next group of acids assessed is the nonaflates, and the following table briefly describes the PAGs used.

Table 4.3: Nonaflic Acid PAG Group

PAG Chemical Name	Acronym	Molecular Weight
Diphenyliodonium perfluoro-1-butanesulfonate	DPI-NF	580
N-hydroxy-5-norbornene-2,3-dicarboximide perfluoro-1-butanesulfonate	NHNDC-NF	459
Tris(4-tert-butylphenyl)sulfonium perfluoro-1-butanesulfonate	TTBPS-NF	731
N-hydroxynaphthalimide perfluoro-1-butanesulfonate	NHN-NF	495

The nonaflate PAG, DPI-NF, was utilized in the anion study; however the sulfonium PAG and two other non-ionic PAGs are being introduced here. One of the non-ionic PAGs, NHN-NF, has the exact same energy absorption group as the non-ionic triflic acid PAG. The NHNDC-NF PAG is different from others explored in this study because it has its maximum UV light absorption range at 193-nm rather than 248-nm, where it is only slightly absorbent. The decomposition results of NHNDC-NF and all other nonaflate PAGs can be found in Figure 4.3.

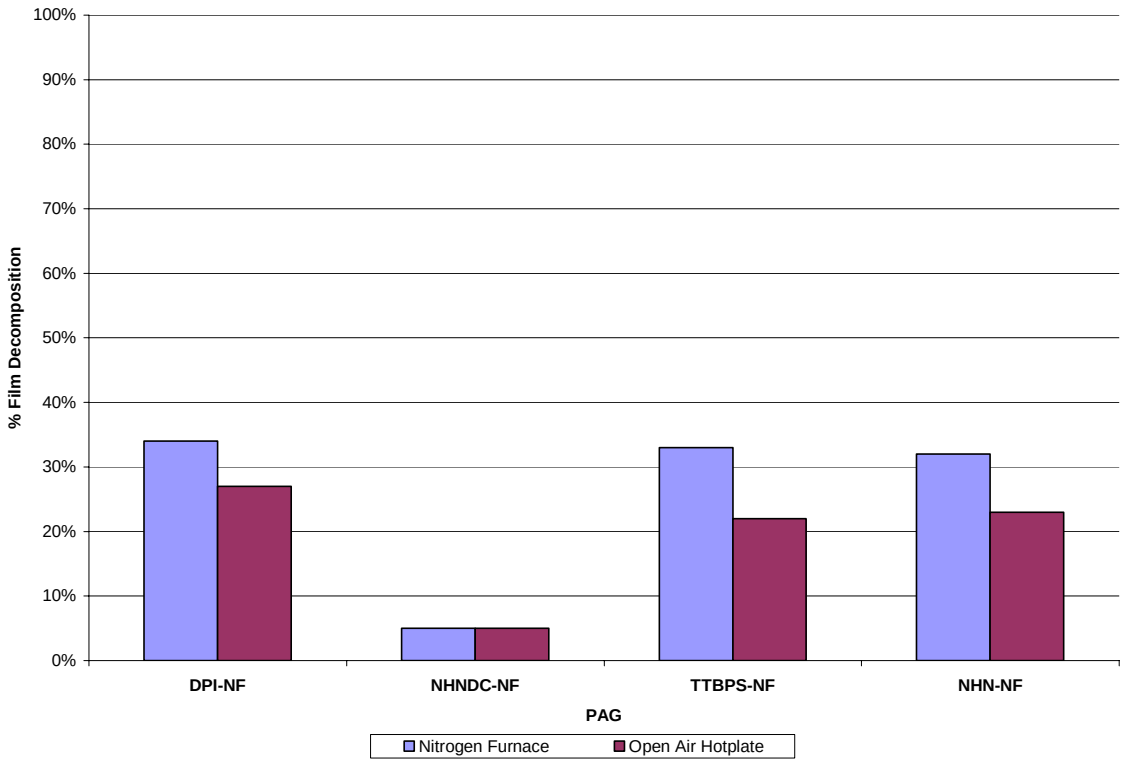

Figure 4.3: Film decomposition study at 120ºC for all nonaflic acid PAGs

Figure 4.3 shows three out of the four PAGs performed the decomposition at similar levels, with the one exception being the NHNDC-NF PAG. With an absorption spectrum not tailored for 248-nm irradiation, it is no surprise that the NHNDC-NF non-ionic PAG performed at extremely low levels. This result illustrates the importance of choosing a cation, or in this case a non-ionic absorption group, that is properly configured for the UV exposure range used in the experiment. When the proper cation is selected, as in the other three nonaflate PAGs, the performance of the acid can consistently reach its pinnacle. In this case the peak performance corresponds to approximately 30% - 35% decomposition in the furnace and 20% - 25% decomposition on the hotplate. As seen in the triflic acid samples, the furnace reliably outperforms the hotplate samples, but the

percentage difference between environments is not as drastic with the triflic acids. Further discussion of this topic will occur in Chapter 5.

The final set of PAG samples are all based on the FABA acid group, and their names and results are displayed in Table 4.4 and Figure 4.4 respectively.

Table 4.4: FABA Acid PAG Group

PAG Chemical Name	Nickname	Molecular Weight
4-methylphenyl[4-(1-methylethyl)phenyl] iodonium tetrakis(pentafluorophenyl)borate	Rhodorsil-FABA	1016
tris(4-tert-butylphenyl)sulfonium tetrakis-(pentafluorophenyl)borate	TTBPS-FABA	1111
triphenylsulfonium tetrakis-(pentafluorophenyl)borate	TPS-FABA	943

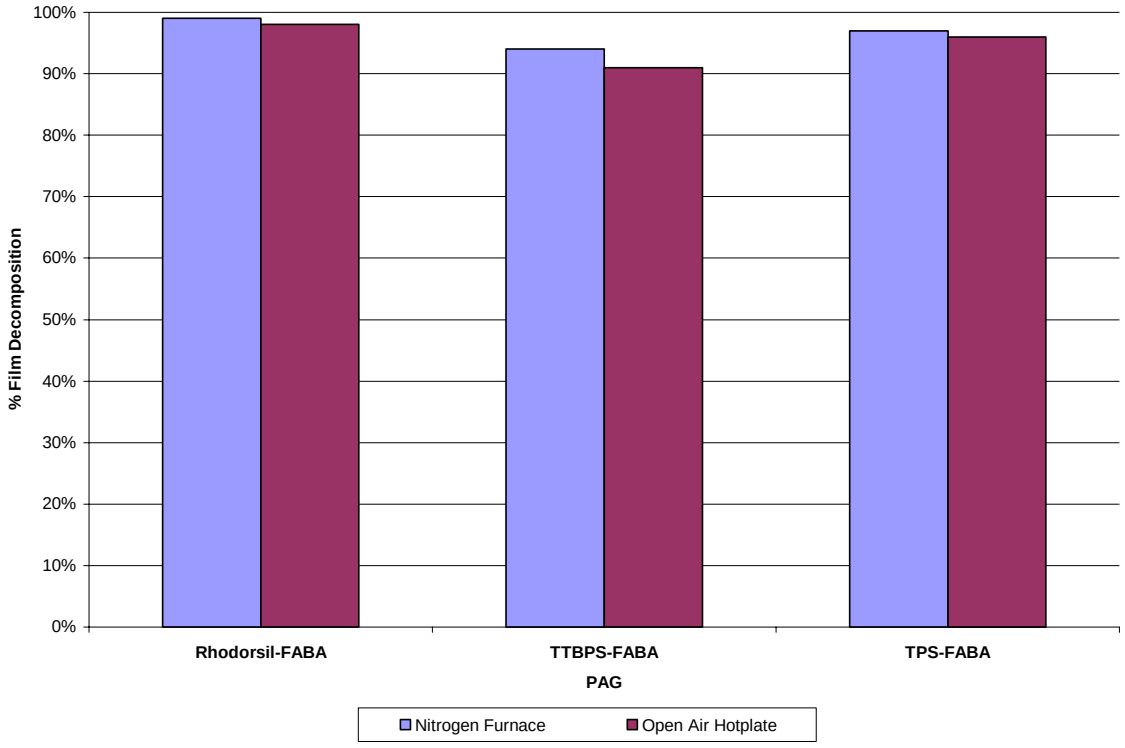

Figure 4.4: Film decomposition study at 120ºC for all FABA acid PAGs

Figure 4.4 exhibits the superior performance of the FABA acid based PAGs when compared to standard non-fluorinated sulfonates, triflates, and nonaflates. All decompositions are 90% and above with the iodonium based PAG, Rhodorsil-FABA, showing the highest level of performance at 98% and above. After decomposition, all three samples exhibited a brownish residue on the substrate. While the sulfonate based PAGs performed quite well, they left slightly thicker residues on the substrate. One possible explanation is the bulky nature of the sulfonium cations causes the increased residue. Another reason may be an improved acid activation of the iodonium based Rhodorsil-FABA that allows for such high levels of decomposition. Never the less, Rhodorsil-FABA has once again shown itself to be an excellent candidate for PPC decomposition.

In summary, the "cation" portion of the PAG whether ionically or covalently bonded (non-ionic) to the "anion" portion is responsible for the energy absorption, acid activation, solvent solubility, and thermal stability of the molecule. From the results in this section, the conclusion can be drawn that cationic manipulation will not result in significant increases in PPC decomposition performance. It was consistently shown that for a given PEB recipe, PAGs with the same acid group and different cation groups performed at or near statistical equivalence. The differences were minor, on the order of a couple percentage points. On the other hand, an exception occurs when the improper selection of a cation is made based on the qualities listed above, and the result is a severe performance hindrance. For that reason, a well-chosen cation is important to ensure the maximum level of performance of the PAG.

CHAPTER 5

ENVIRONMENTAL INFLUENCE STUDY

5.1 Introduction and Experimental Setup

Some mention has already been made in the previous chapters regarding the effect of the PEB environment on the decomposition performance of the PPC matrix. This chapter will attempt to expand the discussion of the aforementioned environmental effects and arrive at conclusions through further experimentation. The environmental effect on the decomposition first arose while observing the results of the triflic and nonaflic acid experimentation. There was a clear disparity between samples processed in a nitrogen controlled tube furnace environment and an open-atmosphere hotplate. At each processing temperature, the nitrogen furnace outperformed the hotplate samples, sometimes showing vast improvements as significant as twice film decomposition. What identifiable circumstances could cause such consistent contrast? One possible explanation is in the atmosphere surrounding the sample. Whereas the furnace is essentially a pure nitrogen environment, the open-atmosphere hotplate is surrounded by not only nitrogen but oxygen carbon dioxide, and a host of additional gases as well. In a body of work by Paul Jayachandran Joseph, a mechanism was proposed where the presence of oxygen interferes with the extraction of a hydrogen ion from the activated cation by reacting with a radical iodine (or sulfur) after the PAG decomposition (see Chapter 1, Figure 1.2). The mechanism is shown in Figure 5.1.

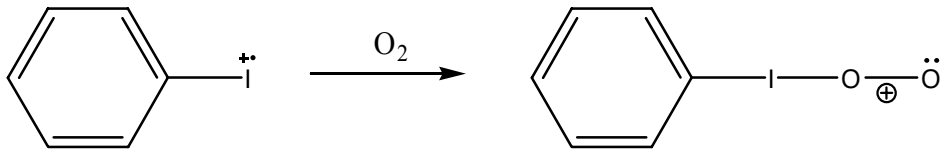

Figure 5.1: Proposed mechanism for the poisoning of PAG hydrogen extraction by the presence of oxygen (Courtesy of Paul Jayachandran Joseph)

Further work needs to be performed in order to verify this mechanism. Besides oxygen, a second gas of interest is water vapor. The incorporation of water into the PPC matrix may have a detrimental effect on the acid catalyzing the polymer decomposition. In the presence of water, the strongest acid that can be formed is the hydronium ion, which will prevent the pH of the system from reaching super-acid levels. Similar ideas were presented in a work by Burns et.al., where the behavior of chemically amplified photoresists in a changing relative humidity environment was undertaken. The results showed that this pH leveling effect was photoresist dependent. Whereas increasing the relative humidity of the PEB environment had a negative effect on the deprotection kinetics of poly(t-butoxycarbonylstyrene) (tBOC) photoresist, it had a positive effect on the reaction rate of KRS-XE photoresist. Moreover, the presence of water in the environment had no effect on APEX or UV6 photoresists [4]. A single unifying conclusion can not be made about the presence of water on the reaction rates in polymeric films, so it is essential to examine the effects specifically on PPC. Since PPC decomposition is highly dependent on acid strength, the hypothesis is that environments saturated with water will have a negative effect of overall decomposition performance.

The second possible cause of the hotplate versus furnace PEB disparity is the heating method. The tube furnace has a programmable controller that allows for a

controlled temperature ramp (~5ºC/min) to the desired set point. For the hotplate experiments, the surface was brought to a desired stable temperature before introducing the sample because of the lack of a programmable controller. Therefore, the temperature ramping of these hotplate samples was high and limited by the thermal conductivity of the substrate, in this case glass. Linked to the ramping effects, the sample processing time might also influence the decomposition performance. This statement does not refer to the two hour time period spent at the temperature set point. Rather, it refers to the approximate half hour the furnace samples get to spend ramping at lower temperatures. Lastly, the method of heat transfer is different for the furnace and hotplate. The hotplate uses pure conduction of heat through the substrate to the film as the heat transfer mechanism while the surrounding air has a cooling effect; however, the furnace samples use convective heating (slight conduction from the sample holder in the furnace), which encapsulates the sample in hot gas until an equilibrium is reached. This difference is inherent to the individual PEB method and cannot be well compensated for. On the other hand, the ramping and increased time at lower temperature effects are examined in this chapter.

Sample preparation for the environmental studies will be identical to the anion and cation studies of Chapter 3 and 4. The necessary experimental changes will be made on the setup of the PEB equipment. For the humidity experimentation, the capability of the furnace will be expanded for it to accept an input from two gas streams. The diagram of the alternate furnace testing setup can be seen in Figure 5.2.

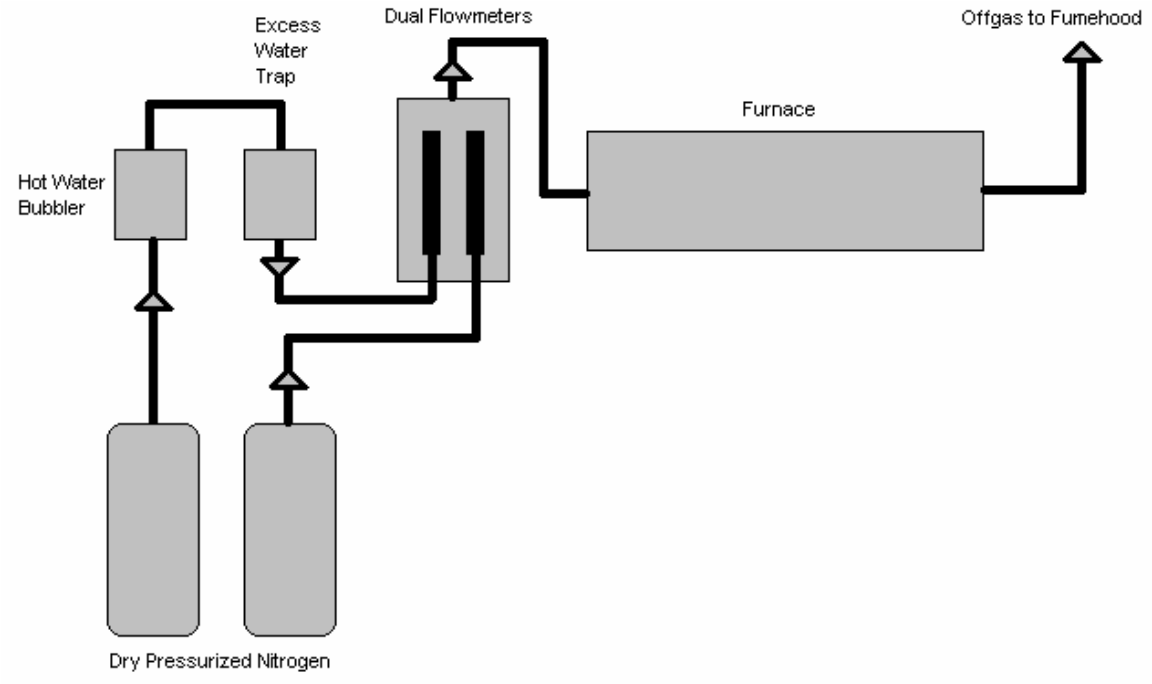

Figure 5.2: Nitrogen tube furnace setup with humidity control capabilities

Looking at Figure 5.2, one of the dry pressurized nitrogen tanks is fed into a hot water bubbler in order to fully saturate the feed before entering the flowmeter. The water temperature in the bubbler is maintained at 60ºC to 65ºC, which is more than adequate to fully saturate the feed as seen in the psychrometric chart below.

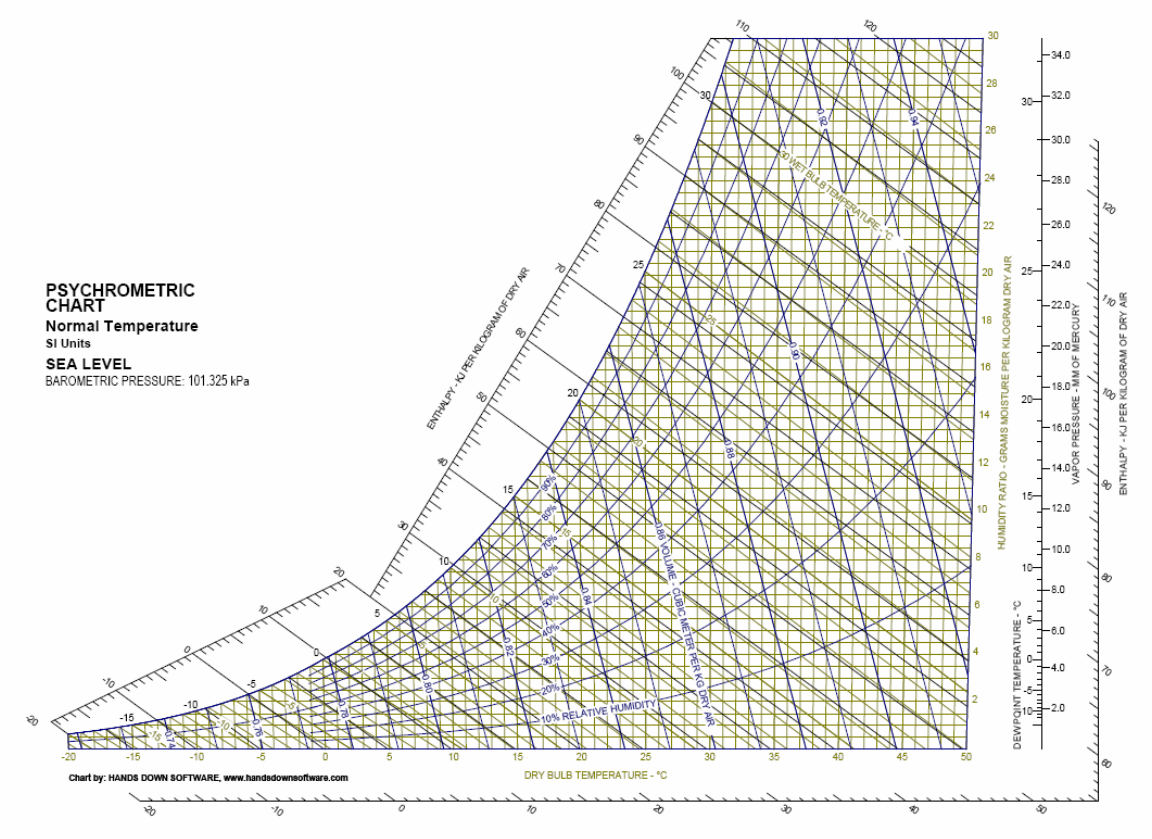

Figure 5.3: Standard psychrometric chart (Courtesy of Nautica Dehumidifiers Inc.)

In fact, the humid nitrogen was supersaturated as it left the hot bubbler environment. To collect the condensate, an excess water trap consisting of plastic tubing coiled in a room temperature water bath needed to be installed prior to the flowmeter. This prevented water droplets from affecting the flowmeter or entering the furnace. The second dry pressurized nitrogen tank was fed directly into the flowmeter. By carefully rationing the two gas streams, the humidity content of the combined stream can be accurately maintained from 0% to 100% saturation at room temperature. All of the relative humidity and water saturation figures presented here are based on room temperature air. When the gas enters the elevated temperatures of the furnace, the relative humidity changes since hot air can hold significantly more water vapor. With the current lab

equipment, there is no way to create a 100% saturated gas environment inside the furnace; however, the setup shown here should be fully capable of providing interesting scenarios that will provide high-quality information.

The second equipment alteration involves the hotplate setup. The temperature ramp rate was measured from ambient conditions to the desired PEB temperature by turning the hotplate setting from off directly to the set-point and measuring the surface temperature. Figure 5.4 shows the plot of hotplate surface temperature versus time for a 120ºC set-point.

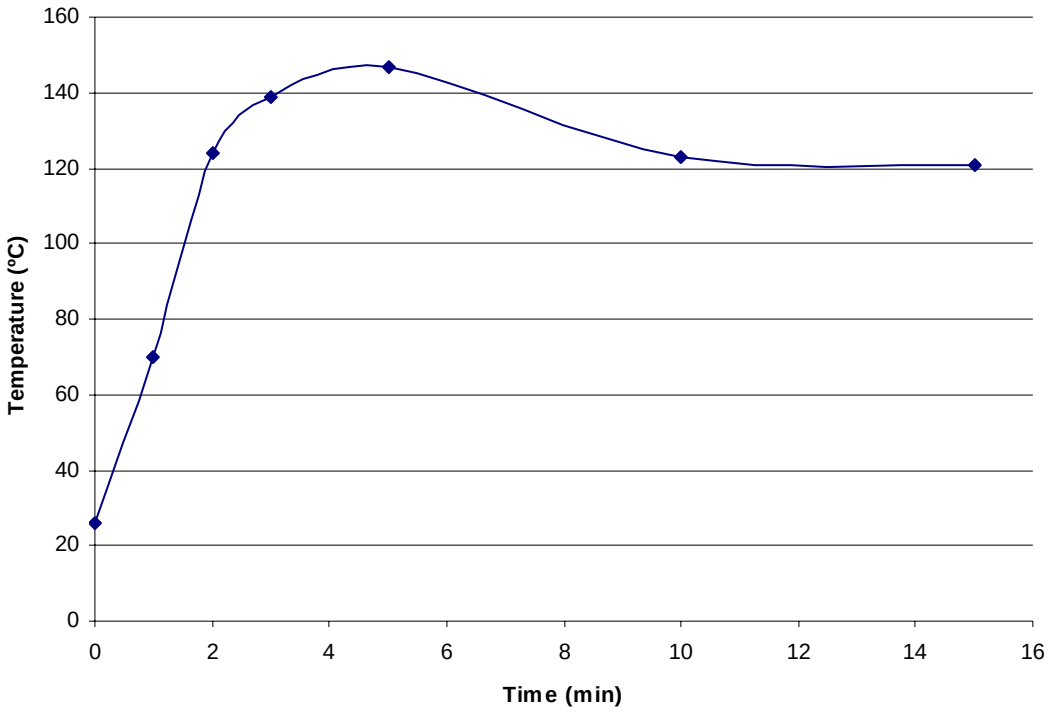

Figure 5.4: Hotplate ramping rate for the temperature measured on the bare hotplate's surface

Observing the above graph, two major issues arrive. First, the set-point temperature of 120ºC is overshot by almost 30ºC. The anion study in Chapter 3 has shown the strong dependence the PAG has with temperature and ultimately PPC decomposition. Therefore, the confidence one can place in a sample processed under these conditions is low. Second, the ramp rate of apparatus in the first three minutes averages almost 40ºC per minute. Since one of the goals of the ramping style hotplate experiment is to simulate the smooth temperature increase of the furnace, this procedure once again falls short of expectations. In order to restrict the rapid heating of the equipment, a solid, 1" thick aluminum block was placed upon the hotplate's surface. Once again the temperature was measured as the hotplate was taken from ambient conditions directly to the desired set-point. Figure 5.5 illustrates the temperature versus time behavior on the surface of the aluminum block.

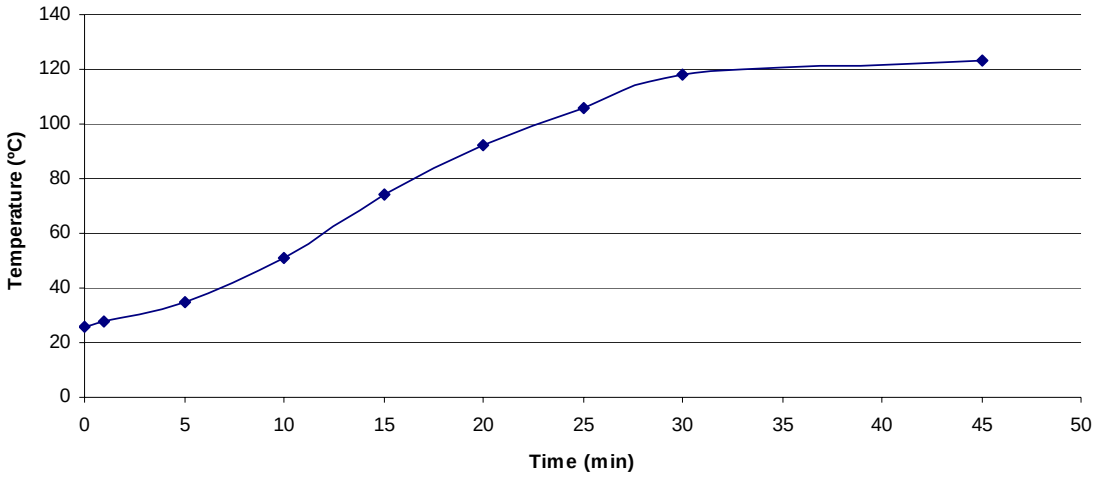

Figure 5.5: Hotplate ramping rate for the temperature measured for the aluminum block's surface

Figure 5.5 shows a more controlled temperature increase over time. Averaged over the first 30 minutes of heating, the ramp rate of the aluminum block was calculated to be 3ºC to 4ºC per minute. This rate is very close to the targeted 5ºC per minute used in the furnace testing. Since a sample processed in this manner would receive a similar amount of time at temperatures below its targeted set-point, another confounding issue is solved. Finally, once the set-point is reached, the targeted temperature is consistently maintained within an acceptable range of a few degrees centigrade.

Before presenting the experimental data, now is an appropriate time to discuss the issue with the complexity of these systems. Each scenario created here attempts to provide a simple, yet fully valid solution to a more complicated overall problem statement involving the complete understanding of the PPC / PAG relationship. Each situation has the possibility for further exploration; however, it is the intent of this author for this report to be a strong starting point for these explorations in future works. Therefore, some discussions may fall short of fully describing specific correlations observed in these results, but this is done to avoid forcing a straightforward conclusion to a very complex system.

Section 5.2: Results and Discussion

The first PAG to be analyzed using the aforementioned PEB equipment modifications is the triflic acid based PAG BTBPI-TF. Recalling the conclusions from Chapter 3, BTBPI-TF is a PAG that is composed of a highly volatile but very strong acid group. At a decomposition temperature of 120ºC, BTBPI-TF showed a very large disparity between experimental PEB environments. Figure 5.6 once again displays the

BTBPI-TF data from the Chapter 3 anion experiment; however, it also includes decomposition data from a range of humidity and the hotplate ramping experiment.

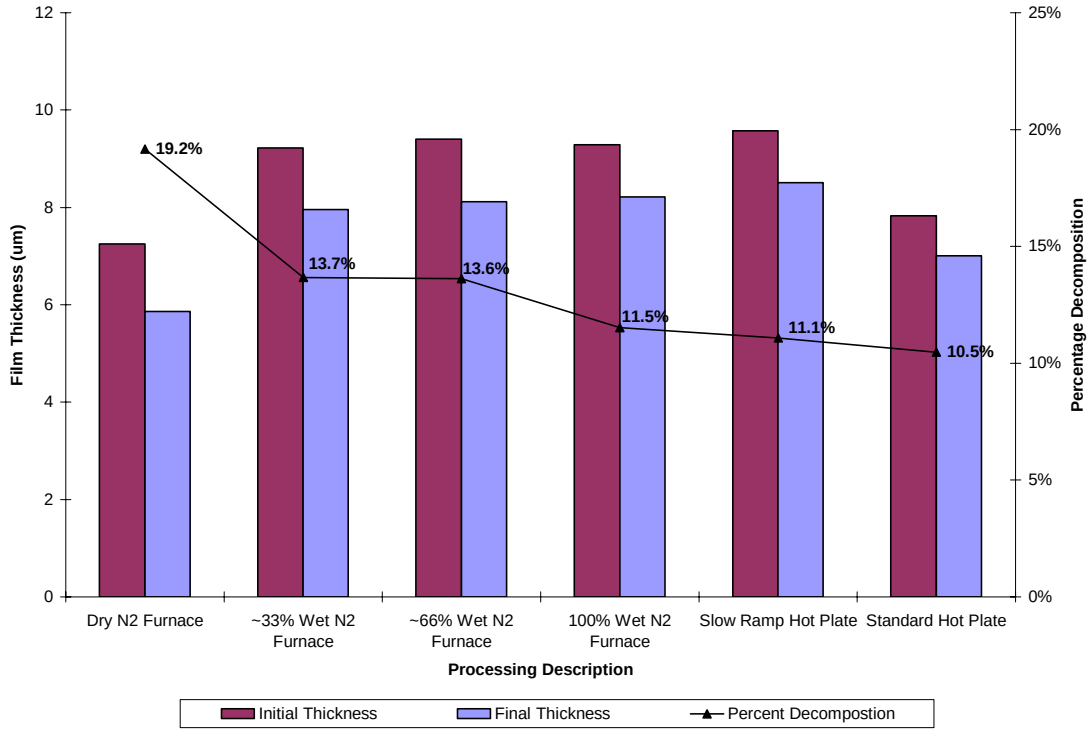

Figure 5.6: BTBPI-TF film decomposition levels at 120ºC for all environmental and ramping studies

There are two pieces of information in this figure. The bar graphs show the average measurements of the initial and final film thicknesses, and they correspond to the y-axis on the left. The line graph with the numerical labels displays the calculated percentage of decomposition, and they correspond to the y-axis on the right. The four leftmost bar graphs in the above figure correspond to the complete range of humidity experimentation. Specifically, these graph shows the BTBPI-TF loaded PPC that was decomposed in a furnace with dry nitrogen, 33% saturated nitrogen, 66% saturated nitrogen, and 100%

saturated nitrogen furnace gas streams (based on room temperature air). No matter what the ratio of wet to dry nitrogen, the total flow rate of gas was held constant at 2 L/min to ensure consistency. The performance of the PAG in the completely saturated nitrogen environment is 40% lower than that of the sample processed in dry nitrogen conditions. Also, the performance of the two samples with both wet and dry nitrogen flows was appropriately found in the middle of both extremes. These results show that the presence of humidity in the surrounding environment has a negative impact on PPC films decomposed with a triflic acid based PAG.

Unfortunately, humidity alone cannot explain the large disparity between hotplate and furnace processed samples. The lab's air conditioned environment keeps the air at around 30% to 40% relative humidity, which would place decomposition around 14% using a linear extrapolation with the furnace data. However, as seen in Chapter 3 and Figure 5.6, the standard hotplate processing results in a decomposition of 10% to 11%. Even the hotplate experiment with the aluminum assisted controlled ramping rate did not make a difference in the decomposition percentage (11%). Therefore, slow ramping and extended time spent at lower temperatures were not found to have an impact on triflic acid based PAG in PPC. The remaining justification for reduced hotplate performance is the inherent heating mechanism of the different PEB equipment. On an open-air hotplate, there will be a temperature gradient through the sample because of the surrounding ambient atmosphere. Therefore the film will not be at a uniform temperature like in a furnace environment. Chapter 3 has shown that lower temperatures hinder the decomposition of PPC, which will be based on the Arrhenius kinetic relationship (see Chapter 6, Equation 6.1). On the other hand, lower temperatures also decrease the vapor pressure of the acid [14]. These effects will counteract one another; however, with the

high vapor pressure of triflic acid, the rate of reaction decrease should be a more significant factor. Further work needs to be done in this area to make a more definitive conclusion. Yet, recalling the specific temperature dependence data, BTBPI-TF did show 13% decomposition in a 60ºC furnace and 20% decomposition in a 120ºC furnace. Consequently, the cooler surface of the film will have a reduced rate of decomposition when compared to the film that is contacting the substrate. This rate reduction will ultimately allow time for more vaporization of the highly volatile triflic acid, thus, lowering the overall decomposition of the sample.

To further solidify the conclusions drawn from the BTBPI-TF PAG, the same set of humidity and ramping experiments were completed with a nonaflic acid PAG, DPI-NF. The results are shown in the figure below.

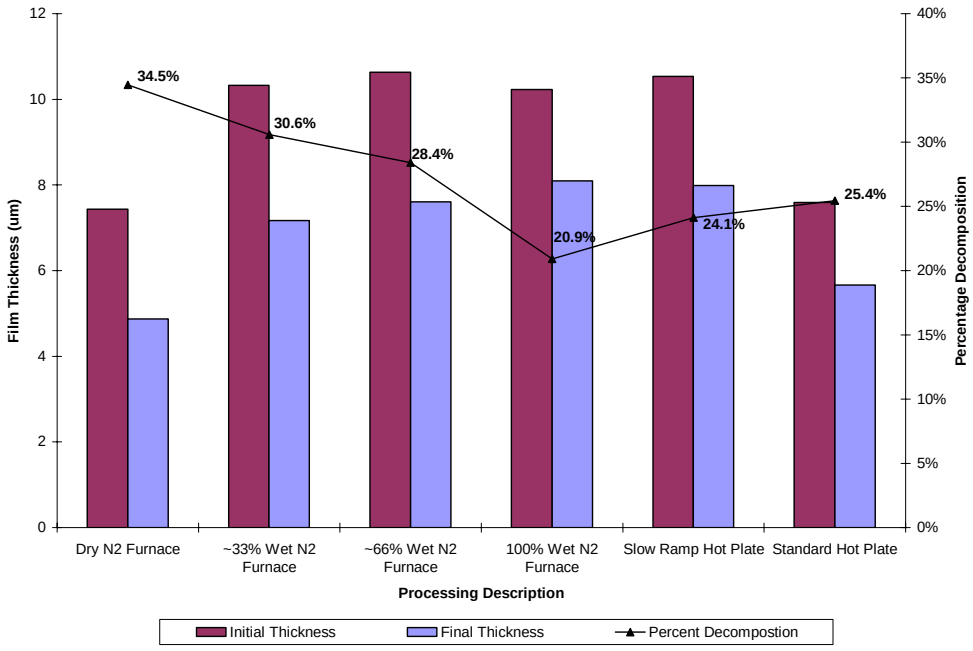

Figure 5.7: DPI-NF film decomposition levels at 120ºC for all environmental and ramping studies

As with the triflic acid environmental study, this graph presents data gathered from two separate experiments. The DPI-NF humidity experiments (four bar graphs from the left) show a decreasing decomposition performance with an increasing level of saturated nitrogen. Specifically, the sample processed with the fully saturated nitrogen stream showed a 40% reduction in performance when compared to the dry nitrogen environment. This information closely supports the results gathered from the BTBPI-TF humidity study, and the conclusion can be made that the introduction of water vapor into the PEB environment will reduce decomposition performance for this system. Moreover, the hotplate ramping study (two bar graphs from the right) once more proves to be ineffective in improving decomposition, again supporting the results found from experimentation with BTBPI-TF. Finally, Figure 5.7 demonstrates that the standard hotplate experiment has inferior performance when compared to nitrogen gas streams saturated at intermediate levels. Thus, this data corroborates the claim that the temperature gradient created in the film during hotplate PEB processing results in reduced decomposition rates and lower performance. One possible way to examine the temperature gradient as a root cause is to use a silicon substrate that will provide more heat flux into the film, reducing the temperature gradient effect. Figure 5.8 shows the decomposition data collected from a DPI-NF sample processed using the standard hotplate methods except the PPC film was deposited on silicon rather than glass.

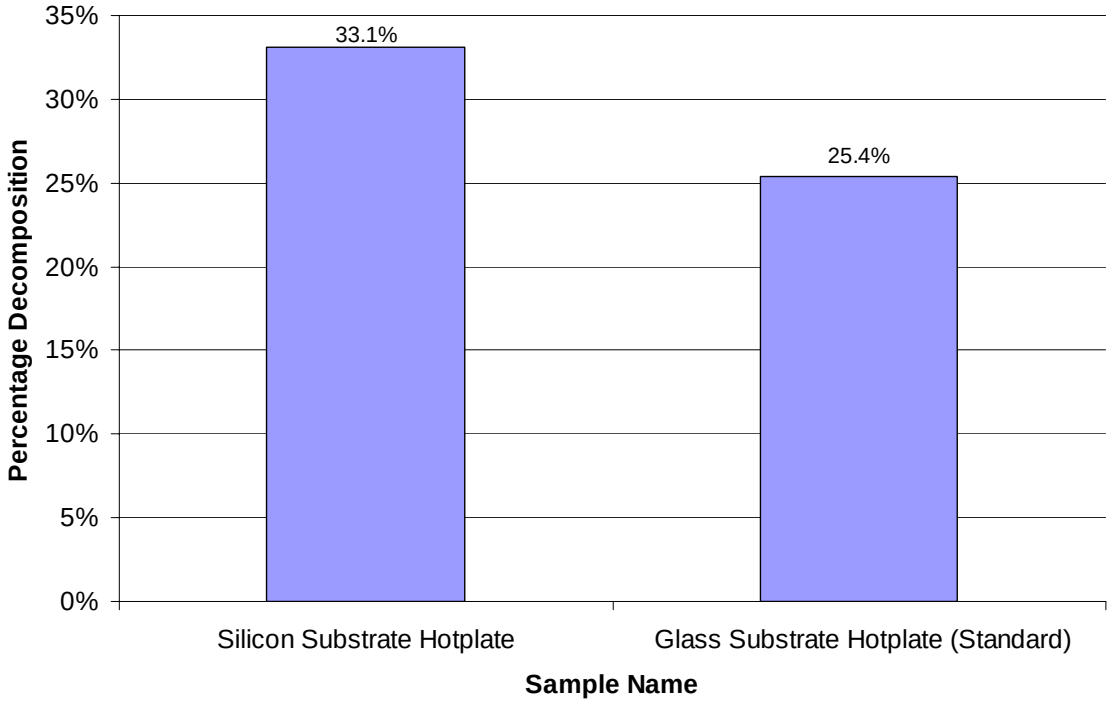

Figure 5.8: Substrate comparisons for the hotplate PEB of a DPI-NF film

Figure 5.8 shows a dramatic increase in hotplate decomposition performance when silicon is used. The 33% decomposition still does not equal the furnace decomposition, but that is to be expected since the open-atmosphere contains water vapor. This result strongly supports the theory that the hotplate samples are strongly tied to the conductive effects.

The effect of environmental influence has been shown for highly volatile and mediocre performing PAGs based on triflic and nonaflic acid. This next section will compare these results with the Rhodorsil-FABA PAG, which has a negligible vapor pressure, high acidity, and a 98-99% decomposition performance. The following figure shows the environmental experimentation results for the Rhodorsil-FABA system.

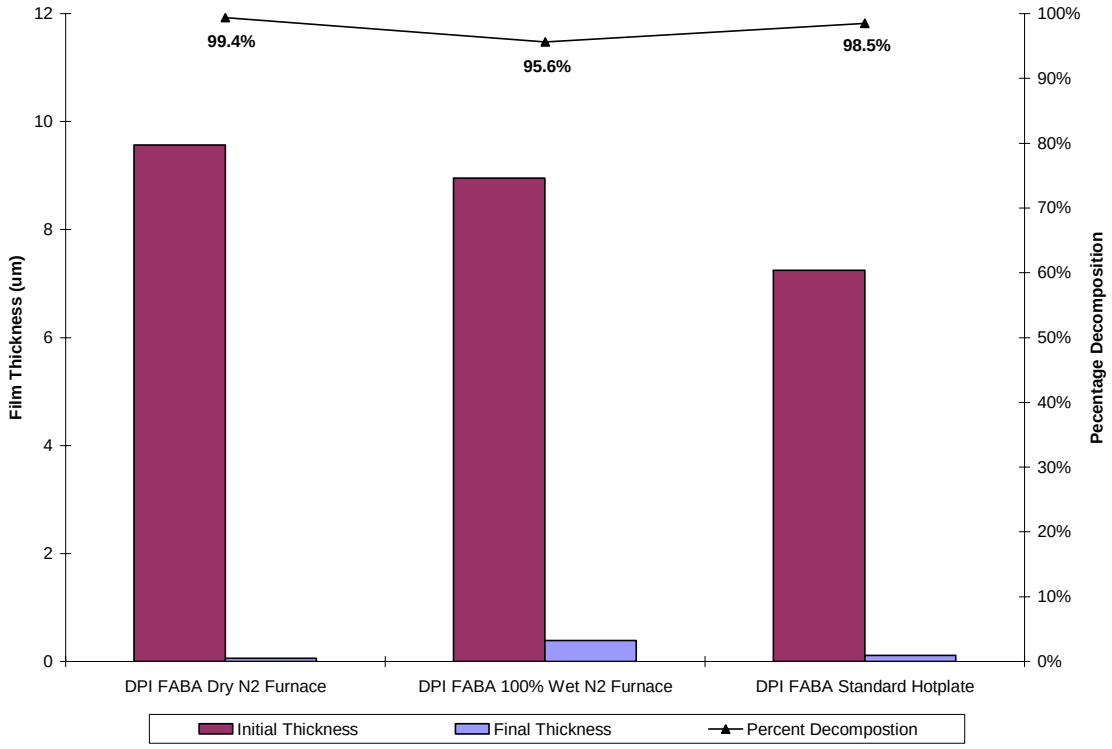

Figure 5.9: Rhodorsil-FABA film decomposition levels at 120ºC for the reduced environmental study

Figure 5.9 has a reduced number of samples when compared to the triflic and nonaflic acid environmental studies. The reduction was made based on the data collected. For example, after performing the 100% saturated nitrogen furnace testing, there was only a 4% reduction in the performance based on the dry conditions. Performing intermediate humidity tests would not have provided much more clarity in the data analysis, so they were omitted. The humidity effect seen in the Rhodorsil-FABA samples is an order of magnitude less significant than the BTBPI-TF and DPI-NF samples. Possibly, the reduced humidity effect could be a product of the negligible vapor pressure and high acidity (high rate of reaction, see Chapter 6) of the FABA acid. As previously stated, the presence of water in the PPC film acts a pH leveler, lowering the acidity of the super-

acids. In turn, this lowers the overall reaction rate of the acid; however, on explanation is that the reactivity of the FABA acid is so high and fast that the majority of the acid is still able to effectively decompose. The remaining 4% to 5% of unreacted film was the portion affected by the reaction quenching presence of high water concentrations. Clearly, this is a complicated problem, and this solution only provides one possible explanation based on knowledge about the FABA acid. Future work would be required to provide further clarity to this phenomenon.

The other environmental experiment that was omitted for the Rhodorsil-FABA PAG is the hotplate ramping study. Besides the fact that past hotplate ramping experimentation showed little difference with standard hotplate procedures, the FABA hotplate sample performed at near equivalent decompositions compared to the dry furnace PEB. For this reason, the experiment was not necessary.

The equivalent decomposition performance of the FABA acid raises an interesting question about whether it is the negligible vapor pressure of the acid, the fast reaction rate, or both that negates the heating mechanism effect. This question may be answered by experimenting with the methide PAG, BTBPI-TMM. Recalling descriptions in Chapter 3, the methide acid has extremely high acidity (pKa ~ -18), and a vapor pressure slightly higher than nonaflic acid. Figure 5.10 shows the results from the shortened listed of environmental experiments.

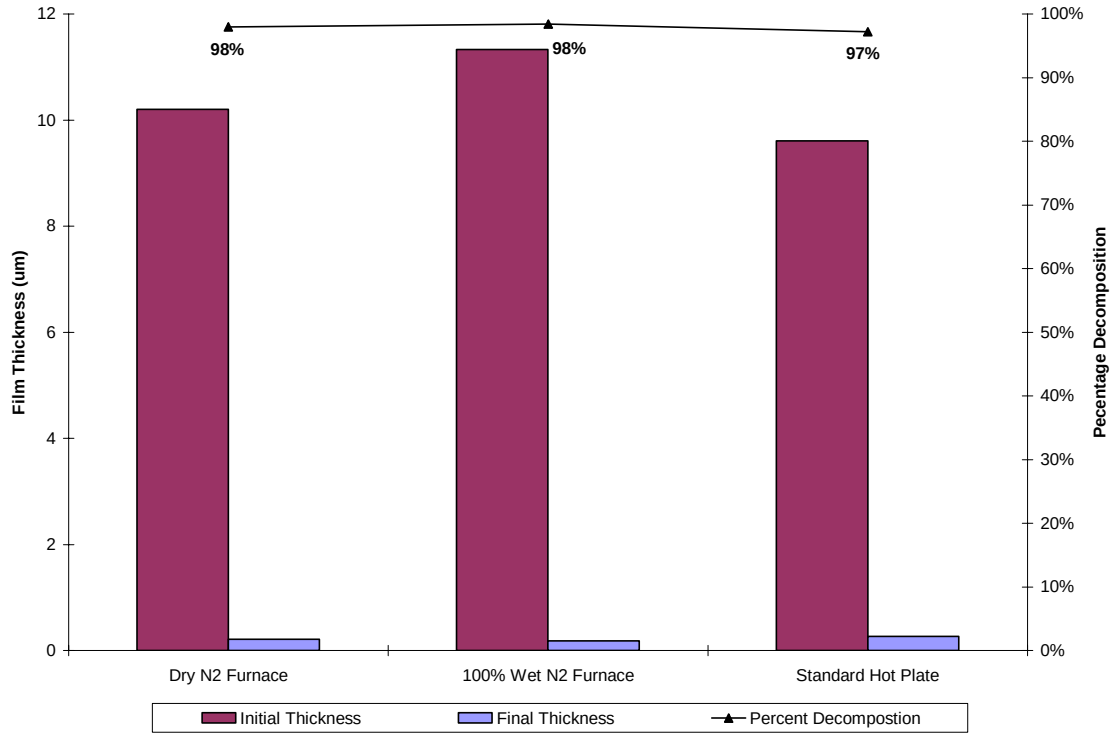

Figure 5.10: BTBPI-TMM film decomposition levels at 120ºC for the reduced environmental study

The data in the above figure is strikingly similar to the aforementioned Rhodorsil-FABA data. For example, both sample sets show very high decomposition percentages (98% and above). Also like the Rhodorsil-FABA, the hotplate processed sample is only 1% less effective than the sample processed in the dry nitrogen tube furnace. Therefore, it seems that the high reactivity of the acid; especially at lower temperatures due to the temperature profile (see Chapter 3 for complete temperature decomposition data set) that dictates similar hotplate and furnace performances. This reactivity at lower temperatures overcomes the temperature profile created by the slow conduction through the glass substrate.

Nevertheless, there is one major difference between the FABA and methide sample sets. The methide based PAG does not appear to be affected by the presence of water. The two furnace samples performed at equivalent levels, specifically, 98% film decomposition. At first, this result may appear to be troubling. It has already been shown that the very volatile triflic and nonaflic acids are affected by the presence of water in the atmosphere. The methide acid has a vapor pressure that falls in between those two acids, so there must be another acid property that is masking the volatility. That property may be the acid strength and resulting high rate of reaction. It will be proven in Chapter 6 that the methide PAG is the fastest reacting PAG tested in this entire report. This demonstrates that the reaction rate of the photoacid is just as, if not more important, than the vapor pressure for samples hindered by environmental effects.

5.3 Conclusions

Overall, a series of experiment were carried out that were able to provide basic explanations to how PAGs are affected by their environment. It was found that humidity and the presence of water vapor does hinder the ability of some PAGs to decompose PPC films. The level of hindrance showed a positive correlation with the PAG's rate of reaction. Basically, the BTBPI-TMM was least affected by the presence of water and also has the fastest reaction rate. On the other hand, BTBPI-TF and DPI-NF have the slowest reaction rates and were also the most affected by the increased relative humidity. Furthermore, it was found that the slow conduction of heat through the glass substrate was one of the principle causes for the poor hotplate performance seen in some of the

PAGs. These simple explanations only begin to explain the behavior of these systems, and further testing that probes deeper into each phenomenon would be beneficial.

CHAPTER 6

RATE OF DECOMPOSITION STUDY

6.1 Introduction and Experimental Setup

The previous three Chapters concentrated on the decomposition performance of the individual PAGs in the polymer matrix. Total decomposition is only one piece of information in the attempt to understand and characterize these sacrificial polymer systems. Designing experimentation in order to observe the rate of film decomposition is equally as important. Previous discussion has introduced the issues associated with the low glass transition temperature of PPC (30ºC to 40ºC). In order to maintain feature integrity for device fabrication, it is desirable to either decompose the PPC at a lower temperature much closer its glass transition or lessen the time required to complete the decomposition. This report has already shown the difficulties of low temperature (60ºC) PEB processing. Therefore, locating a PAG that has the ability to quickly (rate of reaction) and efficiently (total decomposition) process PPC is vital.

Describing the PPC decomposition reaction system is a difficult and complicated task. First of all, each reaction of the catalytic acid with the carbonate group initiates a fissure of the polymer chain through the mechanism described in the introduction. A single cleavage of the polymer chain will not result in the creation of the volatile decomposition products, mostly acetone and carbon dioxide [2]. The number of fissures needed for complete volatilization is function of the molecular weight of the PPC. Therefore, it is difficult to predict actual reaction parameters as a function of film

thickness or weight change, since reactions are occurring that do not alter those measurements.

Building on the concept of reaction rate parameters, it is also complicated to construct a model for PPC decomposition with a PAG. A classic Arrhenius based model for the decomposition of a polymer is expressed as

$$\frac{d\alpha}{dt} = k(1-\alpha)^n = A\exp\left(-\frac{E_a}{RT}\right)(1-\alpha)^n, \qquad \text{(Equation 6.1)}$$

where α is a dimensionless mass fraction, k is the rate constant, n is the order of reaction, A is the Arrhenius pre-exponential factor, E_a is the activation energy, R is the universal gas constant, t is the time, and T is the temperature [6]. A common simplification of this equation is to assume a constant reaction rate for the entirety of the decomposition. This would be a poor assumption since the concentration of acid is always changing for three main reasons. One, the acid may be escaping the system through vaporization. Although this is not true for all PAGs (FABA acids), it is true for the majority of photoacids examined in this body of work. Two, the catalytic regeneration of the acid is being quenched by the presence of polyether impurities in the PPC. At this time, the creation of a 100% pure polycarbonate has not been possible. In fact, test has shown that up to 5% of the polymer purchased from the suppliers is polyether. Whereas the reaction of a hydrogen ion with a carbonate group results in the generation of another hydrogen ion, the reaction of the same hydrogen ion with an ether group results in the creation of an alcohol. This side reaction removes acid from the system lowering the overall concentration. Three, the decomposition reaction changes its environment. As volatile

decomposition products are generated, the mass and thickness of the film are lowered, further concentrating the remaining acid. These three reasons show why the assumption of a constant reaction rate and acid concentration is a poor one.

Despite all of the complications with the system kinetics and reaction rate, an effective method of describing the decomposition rate can still be created. If the change in film thickness is thought of as an etch rate, one can collect film thickness data versus time through similar experimentation as seen in Chapters 3 – 5. A rate experiment was created with similar sample processing steps as prior studies with a few exceptions. First, the PPC film was deposited on a silicon wafer. The wafer can then be diced into as many pieces as desired, and importantly, each wafer piece will have the same initial thickness of film, which will be measured and recorded. The second change has to do with the PEB time. Each wafer division will have a different PEB time from 1 minute to 30 minutes. The only PEB method used is the hotplate at 120ºC. By measuring the remaining film thickness of each sample, the desired plot of the thickness change versus time can be realized. Furthermore, fitting a curve to this plot and taking its derivative will result in an overall decomposition rate for the system. Lastly, the targeted initial thickness will increase from 10 microns to 40-50 microns in order to closer simulate the need for thick PPC films in the fabrication of devices such as micro-fluidic channels.

6.2 Results and Discussion

Using the methods described in Section 6.1, the decomposition rate was calculated for the Rhodorsil-FABA PAG as seen in the figure below.

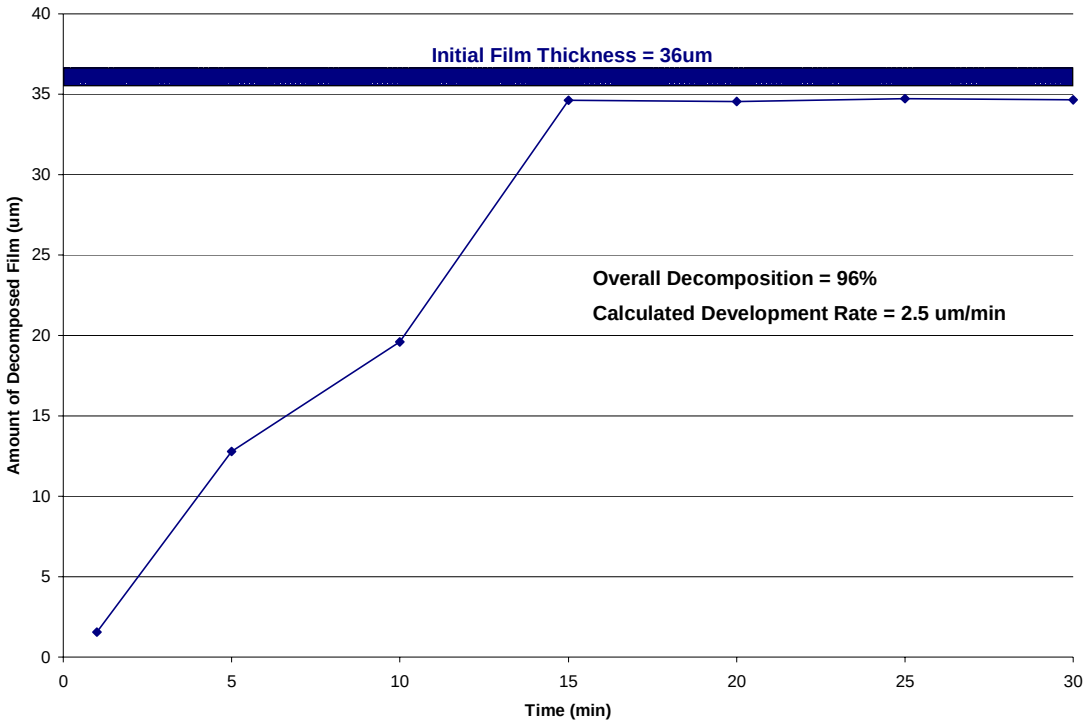

Figure 6.1: Rhodorsil-FABA thickness versus time data at 120ºC PEB for a 36um film

An overall decomposition of 96% was achieved in only 15 minutes. Using linear regression over the first 15 minutes of development time generates an equation in which the slope is the decomposition rate. The following equations show an example of this calculation:

$$y = 2.49x$$
$$R^2 = 0.979, \qquad \text{(Equations 6.2 – 6.4)}$$
$$\frac{dy}{dx} = 2.49$$

where y represents the thickness of the film, R^2 is the proportion of explained variation (calculated by Microsoft Excel), and x represents time. For the Rhodorsil-FABA the development rate was calculated to be approximately 2.5 μm per minute.

This rate calculation is nice for prediction PEB times based on film thickness; however, the greater value lies in comparison with other PAGs. In previous chapters, it has been discussed that the decomposition rate of the perfluorinated methide based PAG, BTBPI-TMM, is quite high. Figure 6.2 shows the decomposition rate analysis for this PAG.

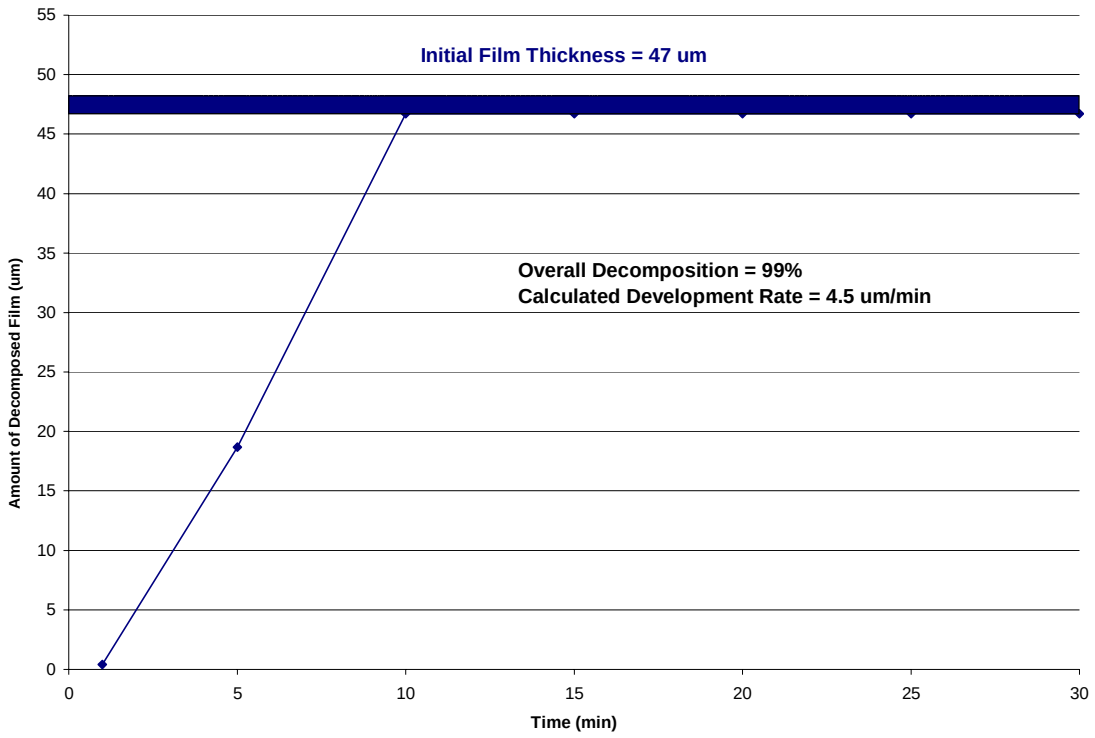

Figure 6.2: BTBPI-TMM thickness versus time data at 120ºC PEB for a 47um film

Figure 6.2 shows that the film was decomposed to approximately 99% of its value in 10 minutes. The 99% decomposition value can only be considered an estimate because of

the residue properties. The residue is extremely oily, and the needle of the profilometer had a difficult time measuring the thickness because the needle cut through rather than traversed over the film. For a better head to head comparison of the FABA and methide residues based on weight percentages, please see Chapter 8. Another important piece of data that can be obtained from Figure 6.5 is the calculated development rate of 4.5 microns per minute. That value for the decomposition rate places the BTBPI-TMM PAG at 80% faster than the FABA based PAG, confirming the claims made in previous chapters and supporting results found by Lamanna et.al.

This study would not be complete without examining the perfluorinated sulfonic acid PAGs, triflate and nonaflate. First, a thick film sample of TBMODS-TF (top performing triflic acid PAG) was decomposed using the same rate determining method. Figure 6.3 presents this data below.

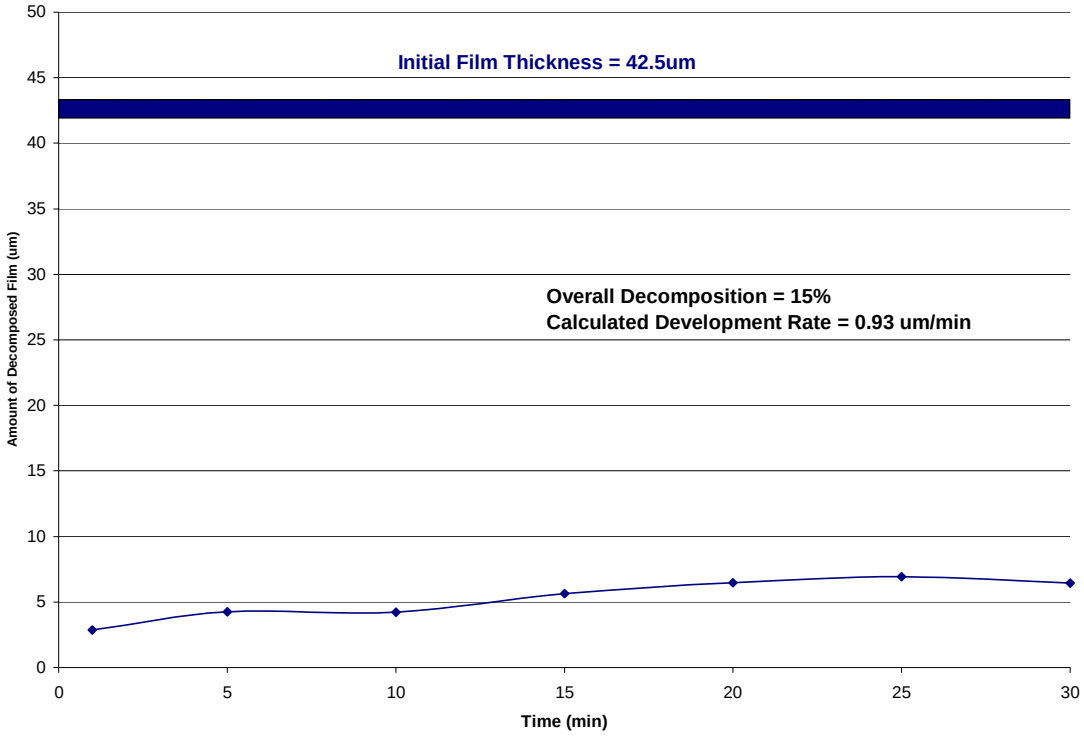

Figure 6.3: TBMODS-TF thickness versus time data at 120ºC PEB for a 42.5um film

As expected from prior experimentation, the TBMODS-TF PAG performs the thick film (42.5um) PPC decomposition quite poorly, peaking at 15% decomposition over the 30 minute time period. About half of the decomposition occurs in the first minute of the PEB, which indicates that the acid is initially strong enough to perform the decomposition. However, due to the vapor pressure effect, the acid concentration is reduced quickly, quenching the reaction. Also, the rate of decomposition reaches a value of zero between 20 and 30 minutes, indicating that a larger time for the PEB would not provide any benefit, supporting the decision of a two hour PEB made in Chapter 3. Furthermore, the calculated development rate is less than 1 μm per minute, much smaller than both the FABA and perfluorinated methide acids.

Moving onto the nonaflic acid PAG, DPI-NF, one might expect similar results to the triflic acid PAG. Figure 6.4 below shows that this is not the case.

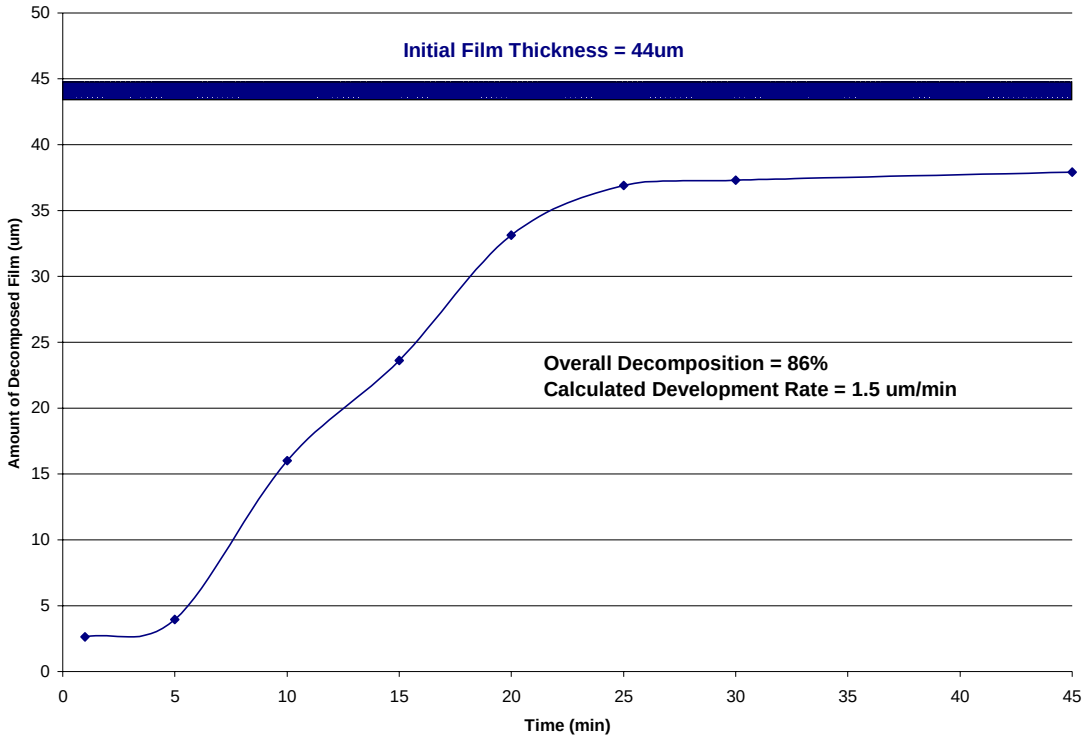

Figure 6.4: DPI-NF thickness versus time data at 120ºC PEB for a 44um film

Contrary to prior experimentation with thinner (~10um) PPC films, this thicker (~44um) PPC film was decomposed at a significantly high value of 86%. Recalling data from Chapter 5, the DPI-NF was only able to achieve 33% decomposition on a 120ºC hotplate with silicon as the substrate. Also seen in Chapter 3 and 5, in the furnace environments, the performance of the DPI-NF similarly reached a decomposition value of approximately 35%. These results suggest that this dramatic performance increase may be a function of the increased film thickness. If the thickness of the PPC film is an important factor, a film with a thickness in between 10um and 44um would result in

decomposition between 33% and 86%. Figure 6.5 demonstrates that the previous statement is in fact true.

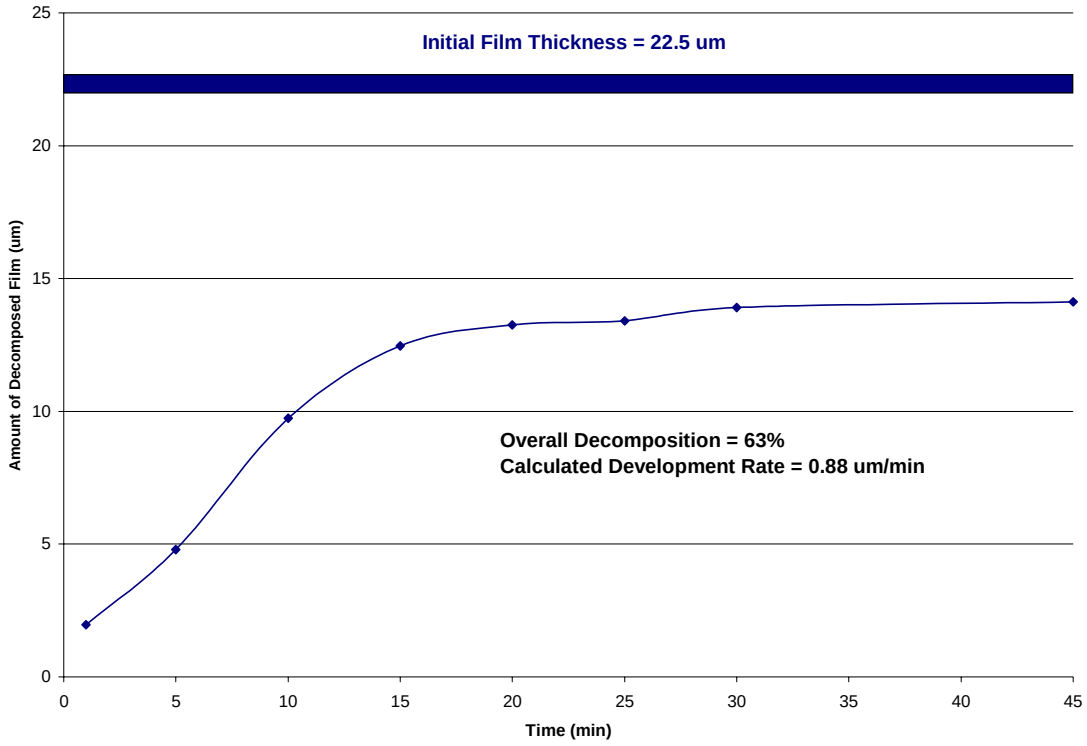

Figure 6.5: DPI-NF thickness versus time data at 120ºC PEB for a 22.5um film

With an overall decomposition performance of 63%, the 22.5 micron film supports the aforementioned hypothesis. Another noteworthy fact derived from the comparison between Figure 6.4 and 6.5 comes from the decrease in the calculated development rate for a thinner film. However, this result is not surprising since the decrease in overall decomposition performance of the thinner films suggests the absence of adequate acid concentrations at a short time into the PEB, thus, slower rates. Both the decomposition rate and percentage as a function of film thickness phenomenon are summarized in the table below.

Table 6.1: Summary of all film thickness change phenomena

	Total Decomposition Percentages		
	Thin Film (~10um)	Medium Film (~25um)	Thick Film (~50um)
Rhodorsil-FABA	98%	-	96%
BTBPI-TMM	97%	-	99%
TBMODS-TF	11%	-	15%
DPI-NF	33%	63%	86%

	Calculated Decomposition Rates (um/min)		
	Thin Film (~10um)	Medium Film (~25um)	Thick Film (~50um)
DPI-NF	0.34	0.88	1.5

Table 6.1 shows for a second time that the fast decomposition rates of FABA and perfluorinated methide based PAGs do not show a strong correlation of overall decomposition with film thickness. Moreover, the triflic acid PAG shows a modest 36% increase (11% to 15%) in performance with the thicker films; however that figure pales in comparison to the 160% increase observed with the nonaflic acid PAG. As mentioned in the previous chapters, this system is quite complex, and simple reasoning may fall short of capturing the complete explanation. Yet, some insight and clarification can be made. The high vapor pressure of the triflic acid combined with the relatively small size of the acid molecule would tend to counteract the effect of a thickness increase. Vaporization and evaporation can only occur at the surface of the film. However, diffusion and reaction can occur throughout the entirety of the film. Therefore, as the thickness of the film increases, the volume where the reaction occurs can increase, where as the two-dimensional surface for vaporization remains constant. As a volatile acid diffuses through the film on a path toward the surface, it continues to participate in decomposition reactions. A longer diffusional path will yield an increased number of reactions and a greater overall decomposition. As previously mentioned, the high vapor pressure of the

triflic acid still causes it to evacuate the system without much more decomposition, but the mediocre (relative to other PAG acids used) vapor pressure of nonaflic acid performs quite differently. These PAG / PPC systems can be approximately modeled by a one-dimensional transient diffusional differential equation. If the reaction effects are neglected, the partial differential equation simplifies to the following:

$$D\frac{\partial^2 C}{\partial z^2} = \frac{\partial C}{\partial t}, \qquad \text{(Equation 6.5)}$$

where D is the overall diffusion coefficient for the acid in PPC, C is the concentration of the acid , z is the axis of diffusion, and t is the time. It is understood that neglecting the reaction term may be a poor assumption; however, it is necessary to generate a useful model. If a reaction is allowed to proceed, not only will it add an additional term to the PDE, but it will also make the thickness of the film a function of time. These complications are not desired for this basic analysis. To proceed with solving the simplified equation, one initial condition and two boundary conditions are required. The initial condition is simply that the concentration of acid in the PPC is uniform at time zero, shown by the following relationship:

$$C = C^o \text{ for all } z, \text{ at } t = 0, \qquad \text{(Equation 6.6)}$$

where C^o is the initial acid concentration. The boundary condition at the base of the film is straightforward since the flux of acid as the surface of the silicon/glass substrate is zero, shown by Equation 6.7,

$$\frac{dC}{dz} = 0 \text{ for all } t > 0, \text{ at } z = 0, \qquad \text{(Equation 6.7)}$$

Unfortunately, the same cannot be said for the boundary condition at the surface of the film. There will be two concentration profiles in this system, one throughout the film itself and one occurring in the boundary layer formed just above the film from the convective flow of the fume hood. If both these concentration profiles are considered, then the following boundary condition arises assuming a linear concentration profile in the boundary layer:

$$-D\frac{dc}{dz} = k_c(C^g - C^{\inf}) \text{ for all } t > 0, \text{ at } z = l, \qquad \text{(Equation 6.8)}$$

where k_c is the mass transfer coefficient, C^g is the concentration of the acid on the surface of the film in the gaseous state, C^{inf} is the concentration of the gas at the edge of the boundary layer and the surrounding gas, and *l* is equal to the thickness of the film. The assumption of a linear profile is appropriate for systems with low concentrations. Also, since the fumehood is cycling in fresh gas, the value of C^{inf} is assumed to be zero. Furthermore, for these low concentrations, the following relationship between the surface of the film and the gas is relevant:

$$C^s = K \cdot C^g, \qquad \text{(Equation 6.9)}$$

where C^s is the concentration of the acid on the surface of the film in the solid and *K* is the partition coefficient relating the two concentrations, basically an equilibrium or Henry's Law type constant. This results in the following equation:

$$\frac{dc}{dz} = -\left(\frac{k_c}{D \cdot K}\right) C^s \text{ for all } t > 0, \text{ at } z = l. \qquad \text{(Equation 6.10)}$$

A literature search yielded no accurate information on the partition coefficient for these systems, so using this boundary condition to create a model would be difficult. However, if another assumption is made that if the mass transfer in the boundary layer of the system is fast, the equation becomes solely diffusion limited and the external boundary layer can be neglected. This assumption simplifies the second boundary condition to the following equation:

$$C = 0 \text{ for all } t > 0, \text{ at } z = l. \qquad \text{(Equation 6.11)}$$

Now, only the overall diffusion coefficient remains as a system parameter. Locating an accurate value for this variable is also a difficult task. A body of work published by Stewart et.al., performed experimentation with nonaflic acid in unreactive photoresist analogues in order to arrive at an overall diffusional coefficient free of reaction based confounds. In order to compare their work on poly(4-isopropyloxycarbonyloxystyrene) (IPOCST) and poly(4-neopentyloxycarbonyloxystyrene) (NPOCST) with the PPC polymer used in this study, a basis of comparison must be created. Common practice for comparing similar polymers is to use their glass transition temperatures (T_g) as a

benchmark of equivalence. Basically, PPC will be a similar diffusional environment to IPOCST and NPOCST when heated to their individual T_g's. The T_g's of IPOCST and NPOCST are 88ºC and 82ºC respectively [7]. A conservative estimate of the T_g of PPC is about 40ºC. The following figure is an estimation of the average nonaflic acid diffusivity of the IPOCST and NPOCST polymers as calculated by Stewart et.al.

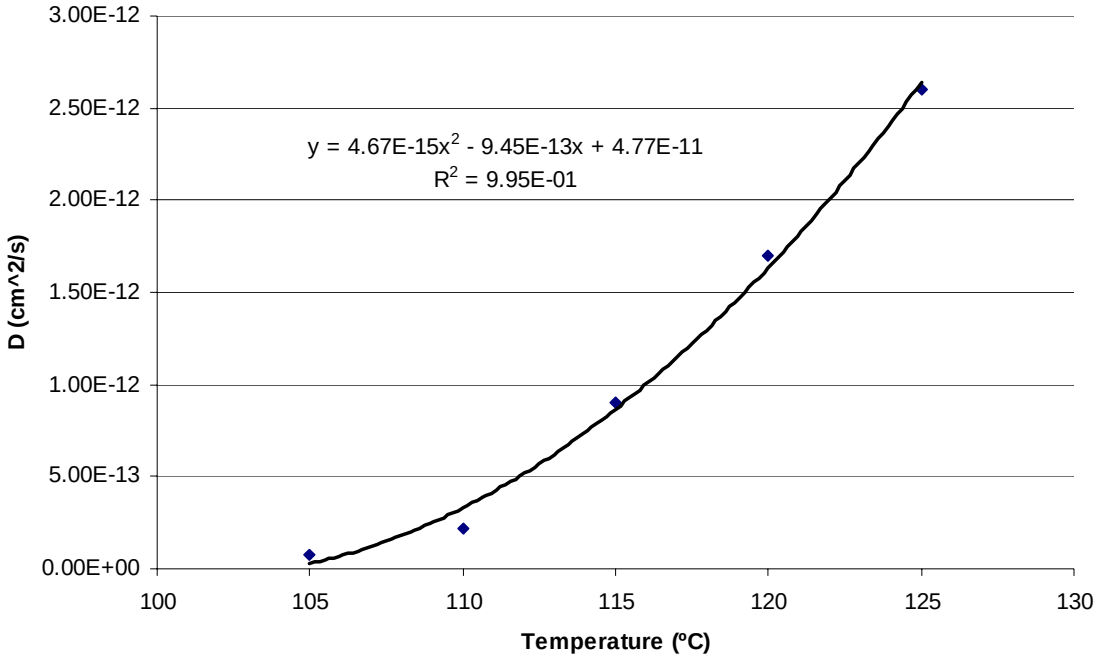

Figure 6.6: Average calculated acid diffusion coefficients for inert polymer systems (Data points provided by Stewart et.al.)

Included in the above figure is a second order polynomial regression equation, which accurately represents the collected data. Since the average T_g of the polymers used by Stewart et.al. is 85ºC, the above data must be extrapolated to 165ºC in order to represent a PPC system at 120ºC. Using the regression equation displayed in Figure 6.6 with a

temperature (x) of 165ºC results in an estimated diffusion coefficient (y) of 1.89×10^{-11} cm^2/s.

Now, by using the estimated value for the diffusion coefficient and the simplified boundary and initial conditions in Equations 6.6, 6.7, and 6.11, the PDE in Equation 6.5 can be solved. Using the computer program, FEMLAB, a numerical solution can be created for a variety of different situations using the nonaflic acid PAG. The following series of curves simulate the diffusion of nonaflic acid out of a 10um film at 120ºC over a time period of 1800 seconds (30 minutes). For ease of analysis, an actual value for concentration as been replaced by a dimensionless term, theta, the unaccomplished fraction. A value of one for theta means 100% of the acid remains in the system.

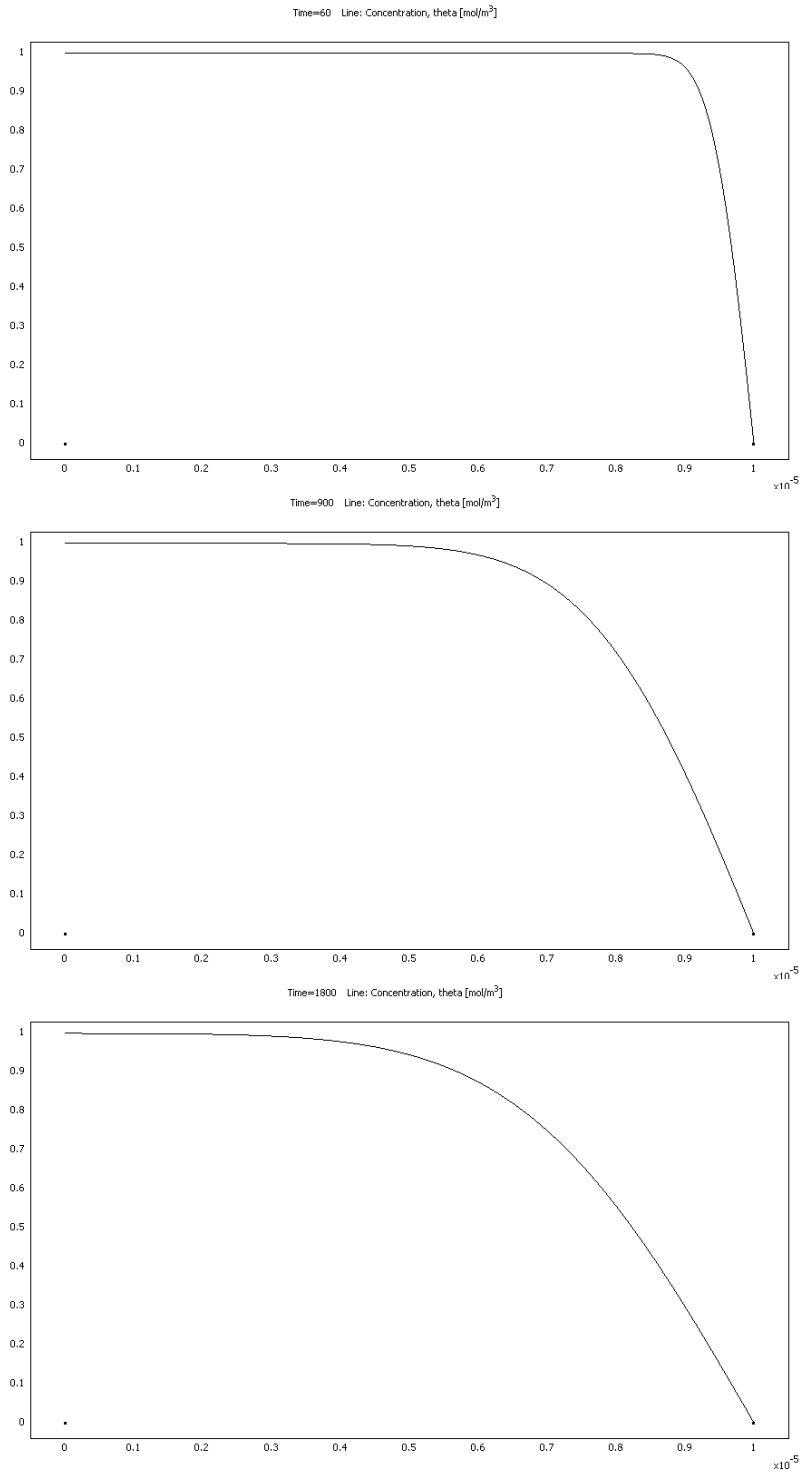

Figure 6.7: Concentration profile model for nonaflic acid in a 10um film over 30 minutes

The concentration curves for 1, 15 and 30 minutes in Figure 6.7 do not show as much acid removal as may be expected from the experimental data collected that shows only 33% decomposition for a 10um thick film. However, this underestimation of the acid diffusion was also found to be true in the work performed by Stewart et.al. It appears that there may be a significant amount of reaction enhanced diffusion taking place in these systems. Specifically for PPC, as the reaction proceeds and volatile products are generated, enhanced diffusional pathways will be created by the increasing amount of gas escaping the film. A more valuable comparison can be seen in Figure 6.8.

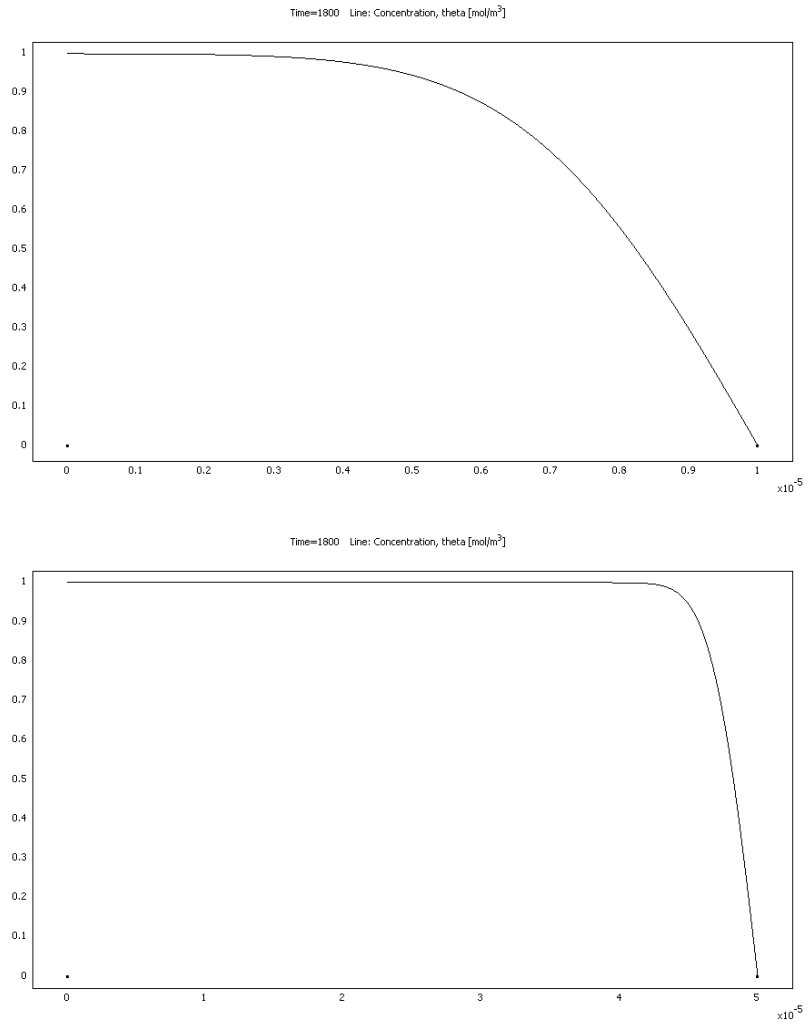

Figure 6.8: Concentration profile model for nonaflic acid for both 10um (top) and 50um (bottom) films at 30 minutes

The curve on the top is the same 10um concentration model as seen in the last curve of Figure 6.7; however, the curve on the bottom is the model for a 50 micron film using the same conditions. Clearly, the 50 um model curve shows the majority of the acid in the film is at its original concentration, which is not the case in the 10 um model. Pulling all this information together, solving the simplified diffusional based PDE resulted in supporting evidence for the correlation between film thickness and overall decomposition percentage for nonaflic acid based PAGs.

6.3 Conclusions

Summarizing important conclusions made in this chapter, first, it was discovered that the perfluorinated methide based PAG did in fact have the fastest decomposition rate at 4.5 um/min for a thick film (~50 um). The FABA based PAG was second with a rate of 2.5um/min. The nonaflate and triflate were the slowest at 1.5 and 0.93 um/min respectively. This result supports conclusions explaining the performance of the BTBPI-TMM PAG despite its high vapor pressure. Furthermore, the decomposition versus time curves also continued to support the hypothesis that the vapor pressure is the limiting factor for PPC decomposition with triflic and nonaflic acid PAGs. Finally, the nonaflic PAG was found to strongly correlate its performance with the thickness of the PPC film. As the film becomes ever thicker (10 um to 50 um), the performance of the DPI-NF PAG increased 160%. A simple diffusional model was generated in order to support the theory that it is the relationship between the two-dimensional surface vaporization versus the three-dimensional reaction occurring in the film that causes this result. Future work improving upon the diffusional based model by accounting for the reaction term, measuring the partition coefficient, *K*, and expanding this analysis to other acids would improve the level of understanding of these systems.

CHAPTER 7

COMBINATION PAG STUDY

A significant amount of knowledge has been gained from the experimentation in the previous four chapters. This chapter describes an attempt to use that knowledge in creating a new photo-active PPC system using multiple PAGs with different desirable properties. The PAGs selected for this analysis are Rhodorsil-FABA and DPI-NF. It has been demonstrated on multiple occasions that the FABA acid has very high decomposition figures, mostly 96% and above. The problematic issue with the FABA acid is the molecular bulkiness. At 120ºC, the majority of the acid does not decompose into more volatile species leaving behind a PAG based residue (see Chapter 8 for the complete residue analysis). The other PAG, DPI-NF, with a mediocre acid vapor pressure has been shown to have moderate levels of decomposition from approximately 35% to 85% based on film thickness (see Chapter 4 and 6). The problematic issue with this PAG is that the acid vaporizes out of the film prior to the completion of the film's decomposition. Looking at the benefits and drawbacks of these two PAGs, one can imagine a situation where their combination would produce a viable decomposition system. By adding a small amount of Rhodorsil-FABA to DPI-NF, the hypothesis is that the nonaflic acid would complete the majority of the decomposition at the beginning of the PEB. As the DPI-NF is reducing the thickness of the film, two things are happening. One, the nonaflic acid is vaporizing from the system, reducing its effectiveness. Two, the small amount of non-volatile Rhodorsil-FABA is becoming more concentrated. As the FABA acid concentrates, it eventually takes over as the major source of catalytic acid and

completes the decomposition. Theoretically, since the sample was initially loaded with a smaller amount of Rhodorsil-FABA, the amount of residue remaining on the sample will decrease when compared to a sample with 100% FABA loading.

For this experiment to have meaning, the amount of Rhodorsil-FABA added to the polymer solution should not be enough to complete the decomposition alone. Only a small amount of FABA acid should be required to decompose the PPC film; however, it has been mentioned both in the Introduction and Chapter 3 that the presence of polyether groups in the polycarbonate poisons the catalytic cycle. Therefore, an excess of PAG is needed to fully complete the decomposition. Using the rate of decomposition experimental method described in Chapter 6, a thick film (~50um) PPC sample set was created with only 1% Rhodorsil-FABA loading and processed on a hotplate at 120ºC. Figure 7.1 shows the result of this experiment.

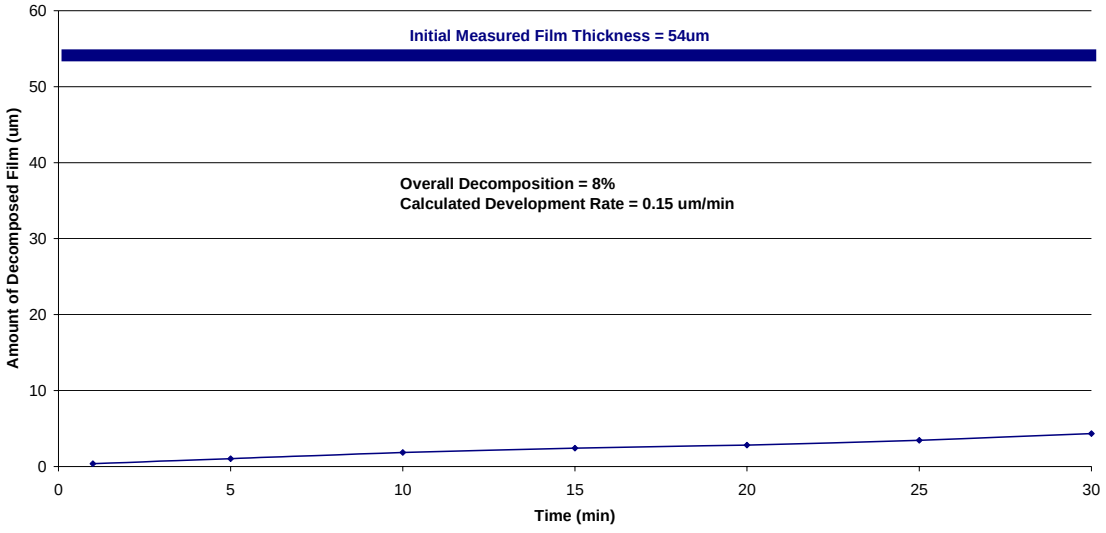

Figure 7.1: Rhodorsil-FABA rate of decomposition experiment with 1% PAG loading

The above figure clearly demonstrates that 30 minutes of PEB at 120ºC with 1% Rhodorsil-FABA loading is inadequate for PPC decomposition. The total decomposition is only 8% and the rate is extremely slow at 0.15 μm per minute.

For a proper comparison, the total PAG loading for this combination PAG study needs to remain at 4% Rhodorsil-FABA molecular weight equivalent (see Chapter 3). Therefore, if the solution is to contain 1% actual Rhodorsil-FABA, it can only contain 3% molar equivalent DPI-NF. Since, 4% DPI-NF loading has been shown on multiple occasions to be inadequate for PPC decomposition, by way of reason, 3% would also be inadequate. By combining the 1% Rhodorsil-FABA and 3% molar equivalent DPI-NF, a system has been created with each individual component lacking the ability to fully decompose a PPC film; however, the hypothesis of the combination PAG states that the sum is greater than its parts, and the two acids working together will be successful. A thick film (~50 um) rate of decomposition study was performed using this solution, and the results are displayed in Figure 7.2.

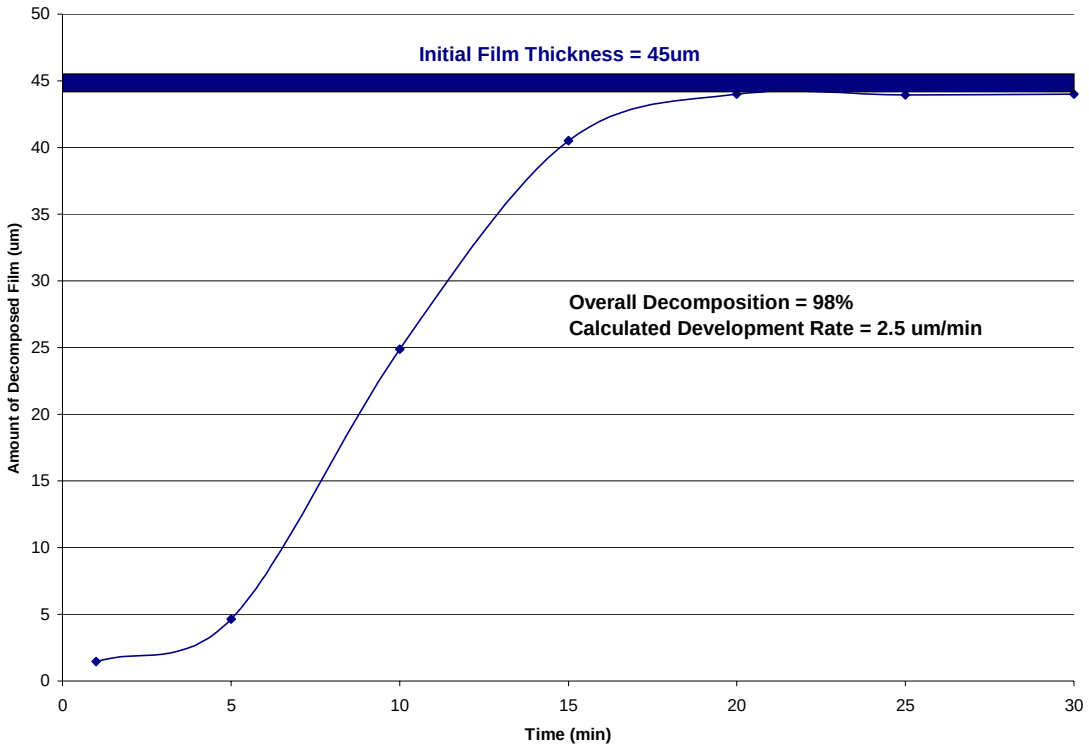

Figure 7.2: Combination PAG rate of decomposition experiment with a 45um initial film

The experiment proved to be a success with an overall decomposition percentage of 98% and a calculated rate of 2.5 um/min, which is 1 um/min better than nonaflic acid alone. The remaining residue on the film was mostly clear, not the dark brown associated with the Rhodorsil-FABA. An XPS performed on the surface of the residue is shown in the following figure.

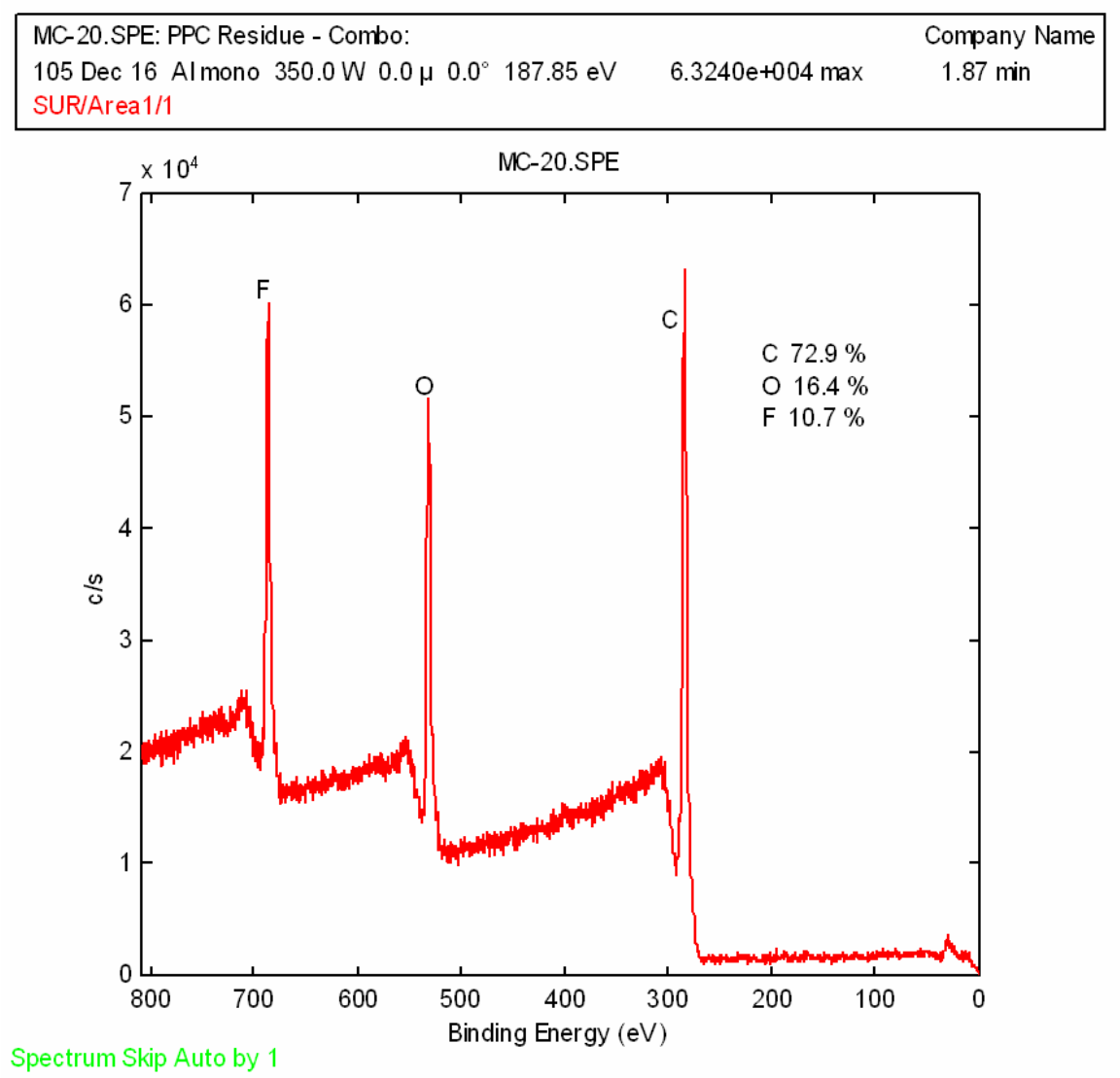

Figure 7.3: XPS analysis of the Combination PAG residue for a PEB at 120ºC

The XPS above shows only the presence of carbon, oxygen and fluorine and no boron, sulfur, or iodine. It is possible that the majority of the residue is composed of unreacted PPC and polyether, masking the small amount of the other elements besides the abundant fluorine. For a more in depth discussion of this residue and the pure FABA and perfluorinated methide PAGs can be found in Chapter 8.

The ability of Combination PAG to perform decomposition of thick PPC films was just presented; however, from Chapter 6, it is evident that the nonaflate based PAG would perform its best under the thick film conditions. To understand whether or not the Combination PAG shared the same positive correlation between performance and film thickness as the DPI-NF PAG, the rate of decomposition experiments were run with both the medium (~25 um) and thin (~10 um) films. The results are shown in the following two figures.

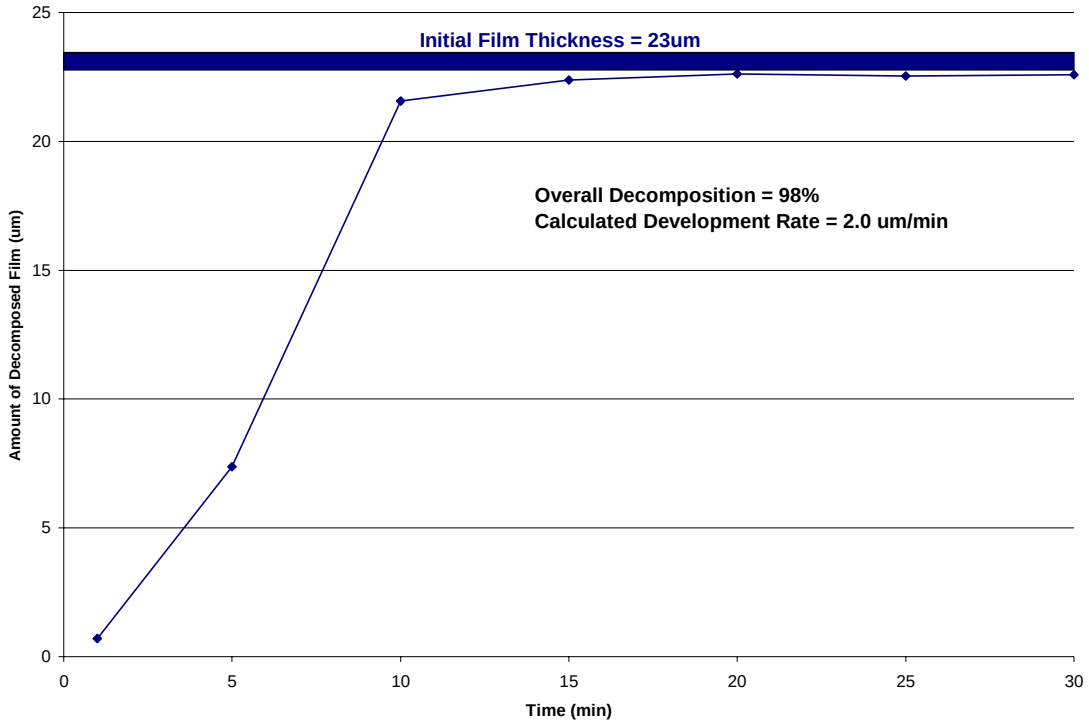

Figure 7.4: Combination PAG rate of decomposition experiment with a 23um initial film

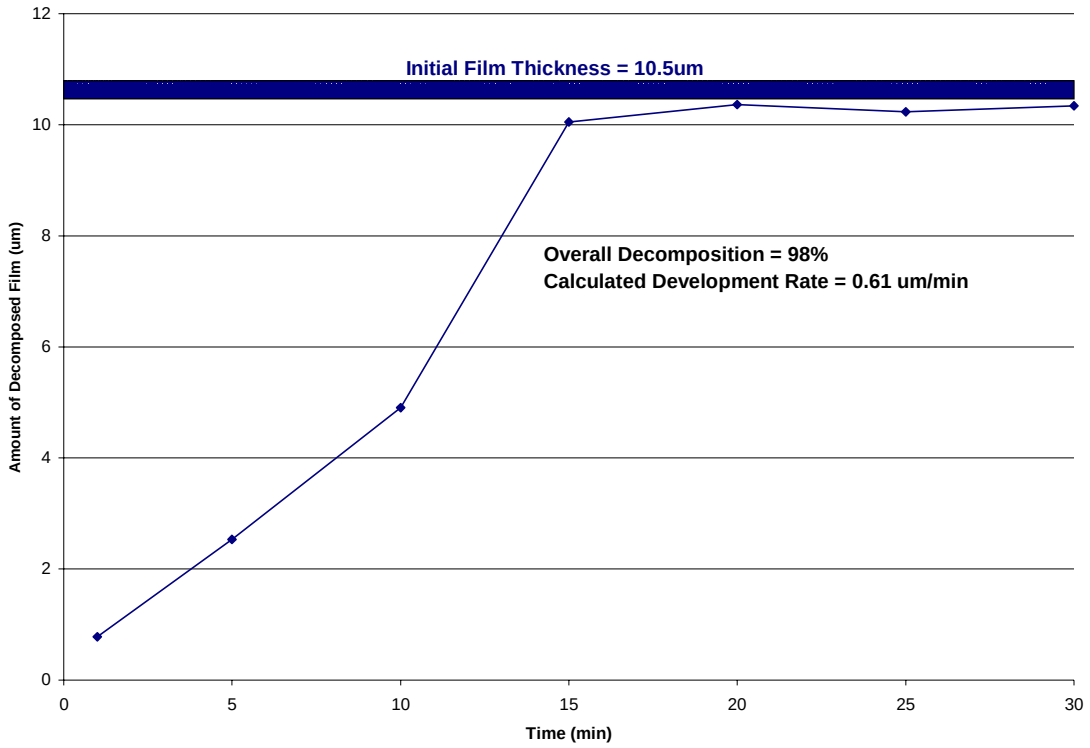

Figure 7.5: Combination PAG rate of decomposition experiment with a 10.5um initial film

In both Figures 7.4 and 7.5, the combination PAG is able to decompose 98% of the film, which counteracts the typical behavior of the DPI-NF. As the film thickness decreases, the calculated development rate also decreases; however, this is a common result seen in all of the PAGs in this body of work, so that result is not alarming.

In summary, the Combination PAG experiment was a success. At a variety of thicknesses it was able to decompose the 98% of the PPC film. Perhaps more significantly, a hypothesis that was generated and upheld based on critical properties of the PAG (i.e. vapor pressure of the acid) identified by this report. It appears that the film remaining on the substrate may contain a majority of unreacted polymer compared to residual PAG, which seems to be contrary to the FABA and methide residues. A full

analysis of the XPS data will take place in the next chapter. Finally, the accomplishments in this chapter warrant further studies with Combination PAGs. Some possible experiments could include altering the PAG percentage loading, using different PAGs (i.e. DPI-NF and BTBPI-TMM), and attempting to combine three PAGs by including triflic acid in the system.

CHAPTER 8

RESIDUE ANALYSIS

Up to this point in the report, despite the numerous polymer solutions created and different types of experimental conditions, a 100% clean decomposition of a PPC film has not yet been achieved. Part of the problem lies in the polyether impurities created during the polymerization of the polycarbonate. The polyether groups not only poison the catalytic cycle of decomposition as described in Chapter 6 and the Introduction, they also do not volatize in the same manner as the polycarbonate groups, thus, leaving a residue behind. The other main contributor to the residue problem is the PAG. During the PEB, not all of the larger cation or anionic groups break apart into smaller more volatile component, also leaving behind a residue. By using a detailed X-ray photoelectron spectroscopy surface analysis, it is possible to determine the elements present in the residue as well as the nature of the bonding between the elements. XPS data was collected on the residue of all the PAGs that completed at least 95% of the film decomposition, which included the perfluorinated methide, FABA, and Combination acid based PAGs. By understanding the compositions of the residues, steps can be taken to help limit their presence, which would be important in the fabrication of microelectronic devices as described in the Introduction.

The first residue that will be examined comes from the BTBPI-TMM (methide based) PAG. For ease of reference, the structure of the PAG is found below.

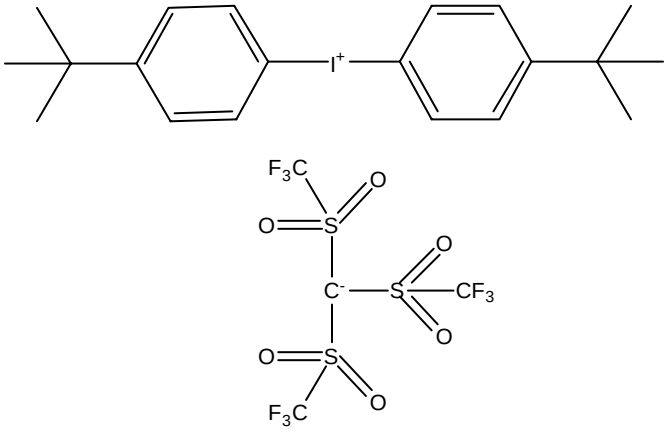

Figure 8.1: Chemical structure of the BTBPI-TMM PAG

The elements (besides hydrogen) found in BTBPI-TMM, as listed in order of decreasing abundance are carbon, fluorine, oxygen, sulfur, and iodine, An XPS of the residue should include these elements as well as additional carbon and oxygen from the polycarbonate and polyether groups. The XPS data below was first presented in Chapter 3; however, to facilitate the discussion, it is displayed again in Figure 8.2.

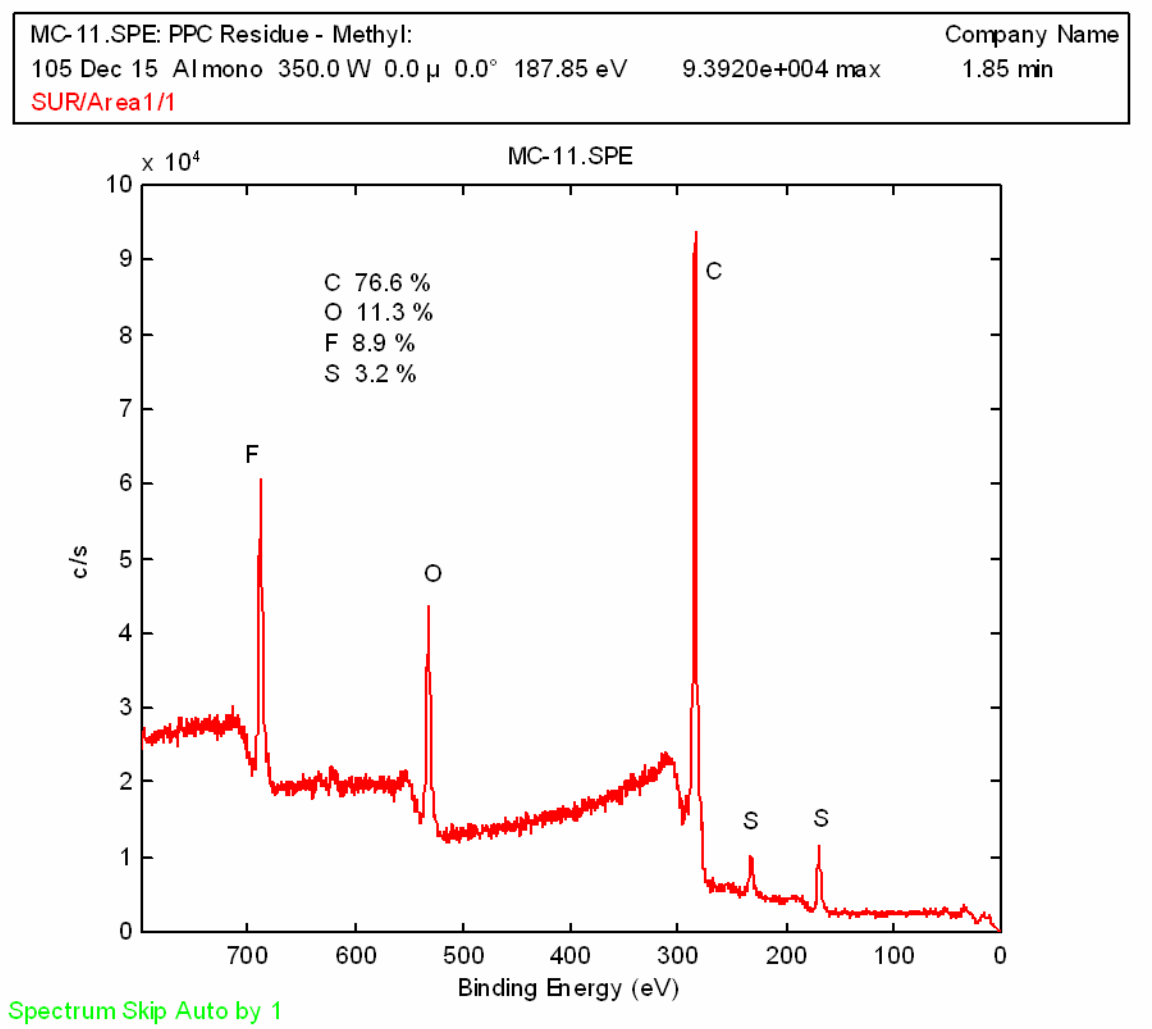

Figure 8.2: X-ray photoelectron spectroscopy (XPS) of BTBPI-TMM residue

All of the elements found in the BTBPI-TMM and the polymer are shown in the XPS data above except iodine. Being the least abundant element on a cation with low thermal stability, the absence of iodine is not surprising. Looking at the percentages of each element in Figure 8.2, they reflect expectations with elemental carbon and oxygen making up a large portion of the residue due to their presence in both the PAG and polymer. The content of fluorine and sulfur is quite small suggesting a low presence of PAG residue, as anticipated from the substantial vapor pressure of the methide acid.

Also, there is three times more fluorine than sulfur, which is expected from looking at the molecular structure in Figure 8.1. Continuing to observe stoichiometric relationships, the oxygen content coming from the PAG would then be 6%, about half of the total amount. The remaining 5% - 6% would come from the polymer groups. The above discussion is important, but just as significant is the analysis of each elemental curve to determine their bonding states. The carbon analysis for BTBPI-TMM is shown below.

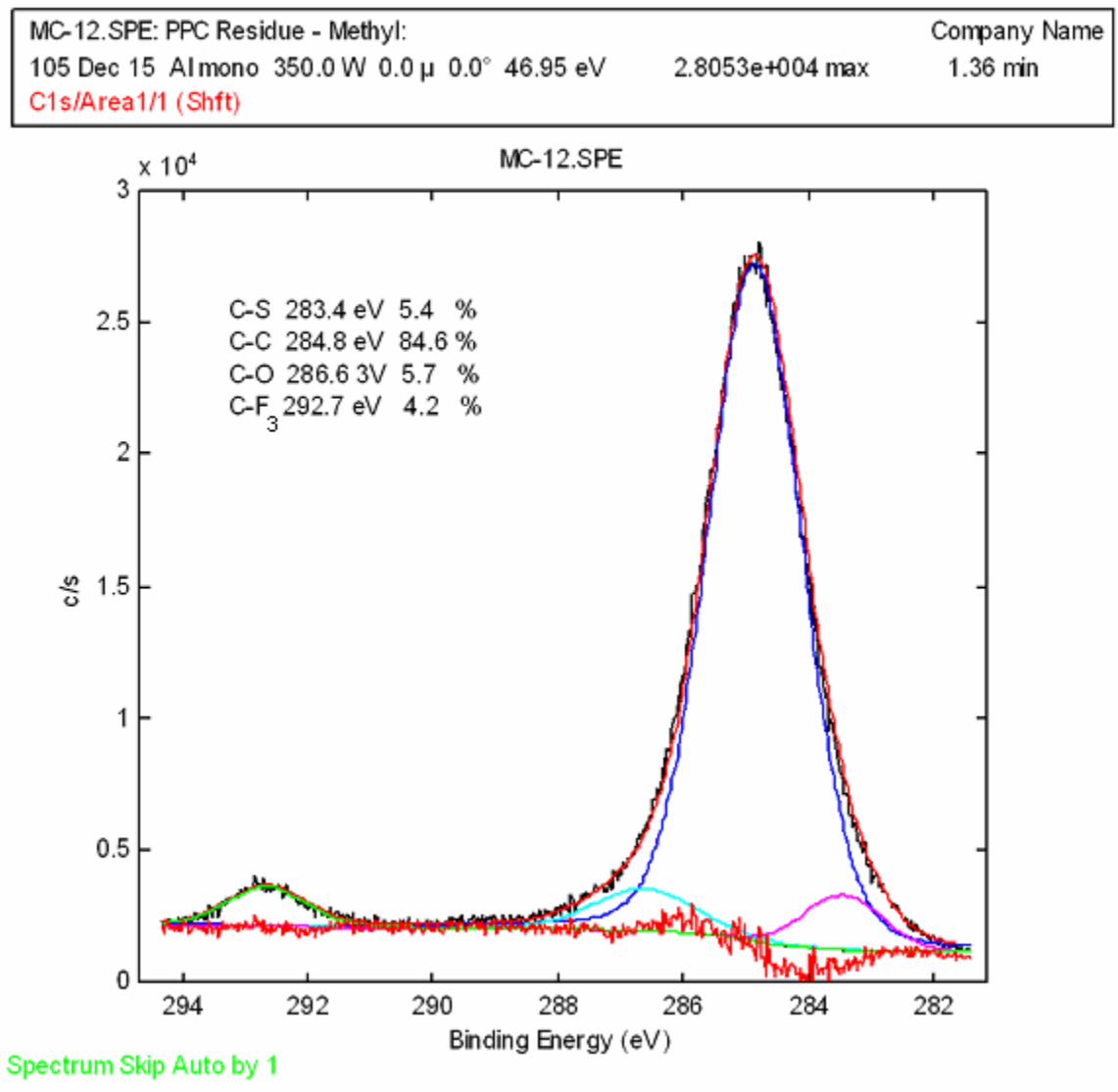

Figure 8.3: XPS analysis of BTBPI-TMM focusing on the carbon bonding data

Over 80% of the carbon in the residue is bonded to other carbon molecules. Since there are no carbon-carbon bonds in the anion of BTBPI-TMM, they must come from either the cation portion of the PAG or the polymer. The cation portion of the PAG dissociates into smaller, more volatile components when releasing a hydrogen molecule; however, the presence of the *tert*-butyl groups on the benzene rings add molecular bulk and may be the reason for the high carbon-carbon bonding content. Other than the bulky cation, residual polyether or unreacted polycarbonate would also add to the carbon-carbon bonding level. Moreover, the polymer groups are the only source carbon-oxygen bonds, which compose about 6% of the residue. Therefore, the presence of carbon-oxygen bonds has a positive correlation with the amount of residual polymer. On the other hand, the only source of carbon-sulfur and carbon-fluorine bonds can be the anion portion of the PAG. With a peak at 292.5eV, the carbon-fluorine bond was correctly analyzed as a CF_3 group, which is the only type of fluorine group in the methide acid. Furthermore, there are three sulfur atoms each bonded to two carbons and three CF_3 groups per anion. Therefore it makes sense that the carbon-sulfur and carbon-fluorine would be similar in percentage with carbon-sulfur being slightly higher. The low percentages of both these bonding groups imply a small amount of residual acid. Moving on to the oxygen analysis, the XPS data is presented in Figure 8.4.

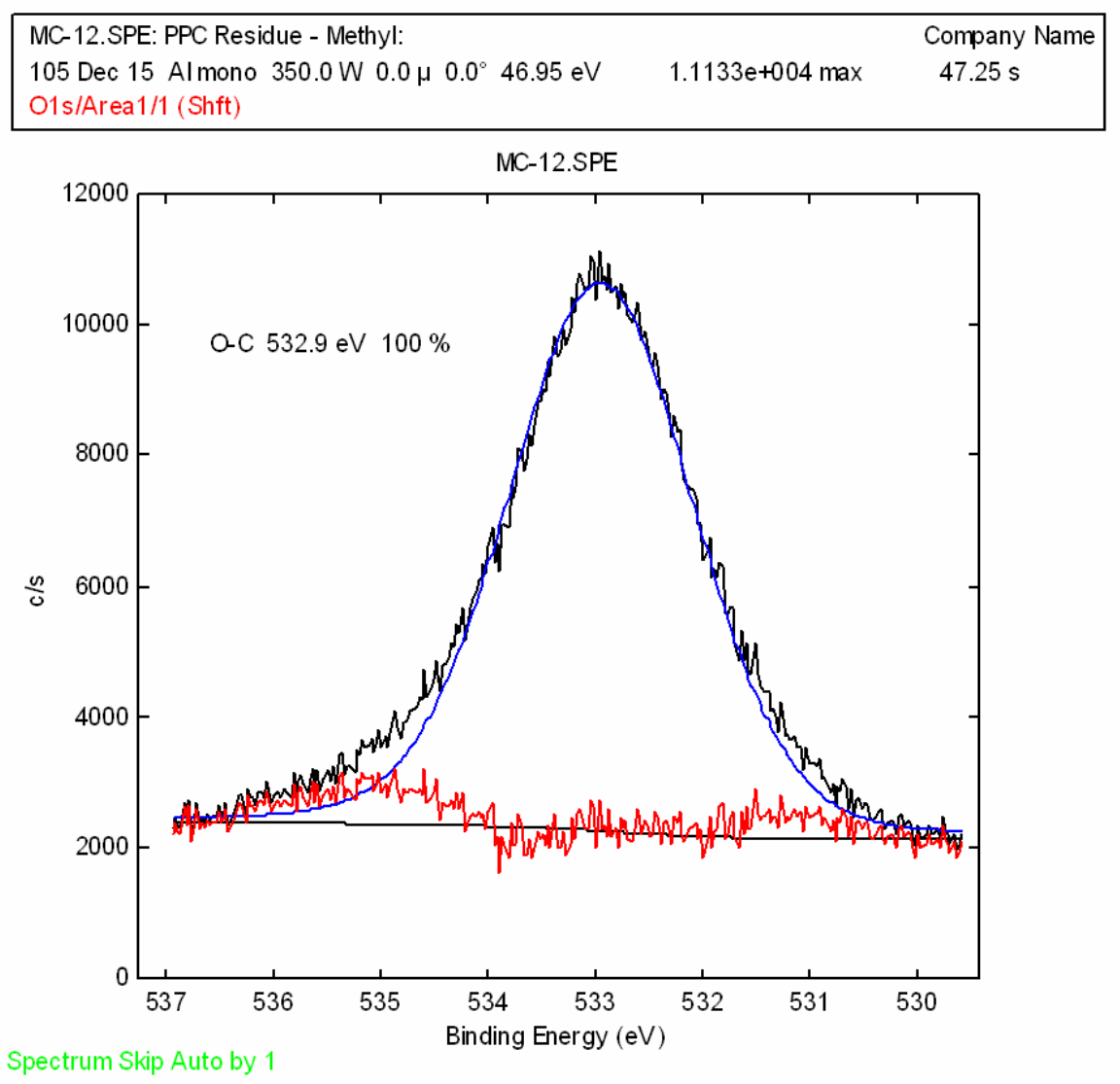

Figure 8.4: XPS analysis of BTBPI-TMM focusing on the oxygen bonding data

The above curve suggests that 100% of the oxygen is bonded to carbon. From the already discovered presence of sulfur and the slight asymmetry of the curve suggests this may not be the case. The hypothesis is that there is also oxygen-sulfur bonds present in the residue, as the structure of the methide acid indicates. To gain more insight into this inquiry, a sulfur bonding analysis was performed and can be found in Figure 8.5.

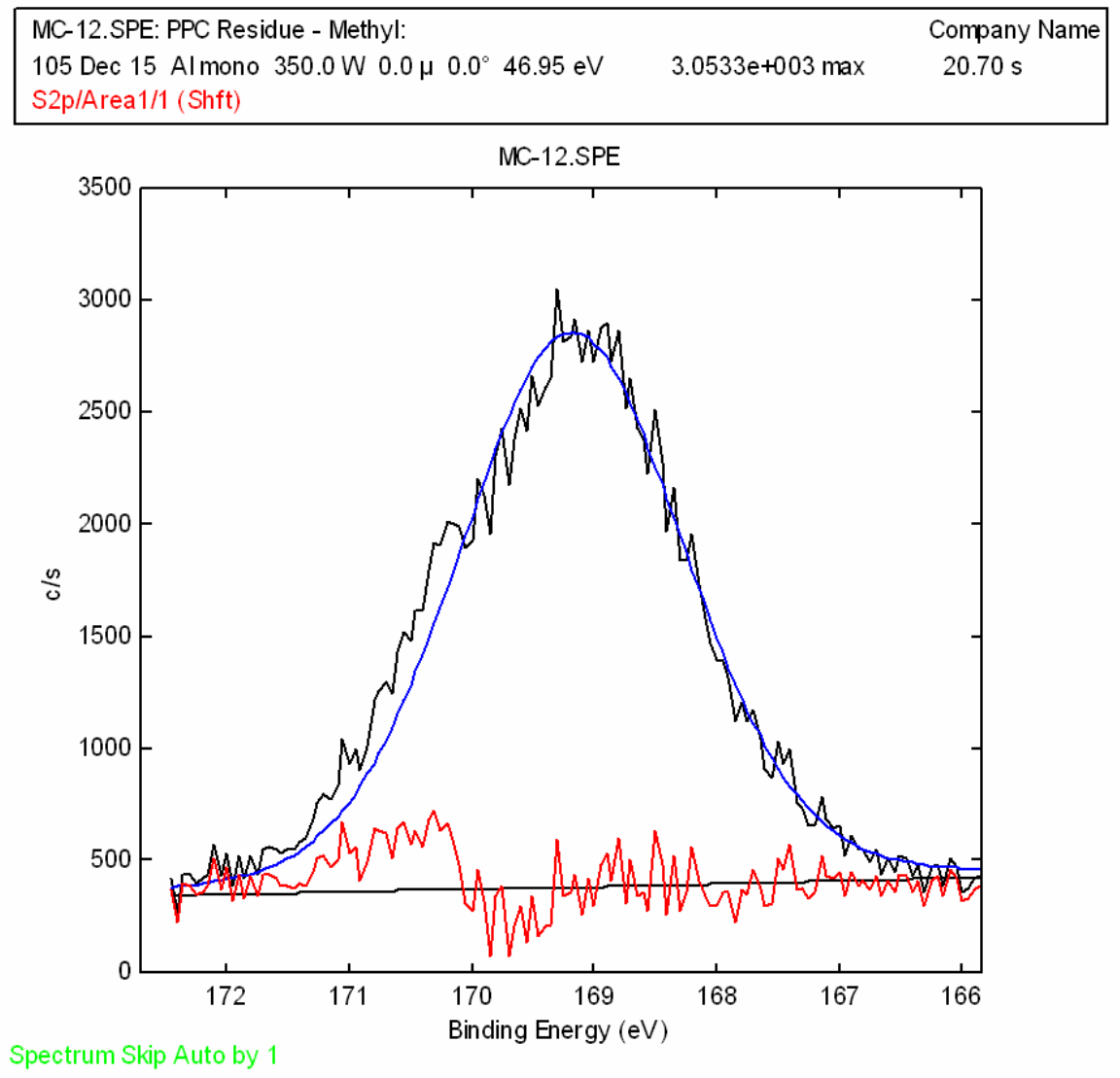

Figure 8.5: XPS analysis of BTBPI-TMM focusing on the sulfur bonding data

With a binding energy at 169.5 eV, Figure 8.5 illustrates that the sulfur bonds are indicative of a sulfate group. The oxidized sulfur groups observed in the structure of the BTBPI-TMM PAG support this data. Progressing to the final elemental analysis, the fluorine data is shown in Figure 8.6.

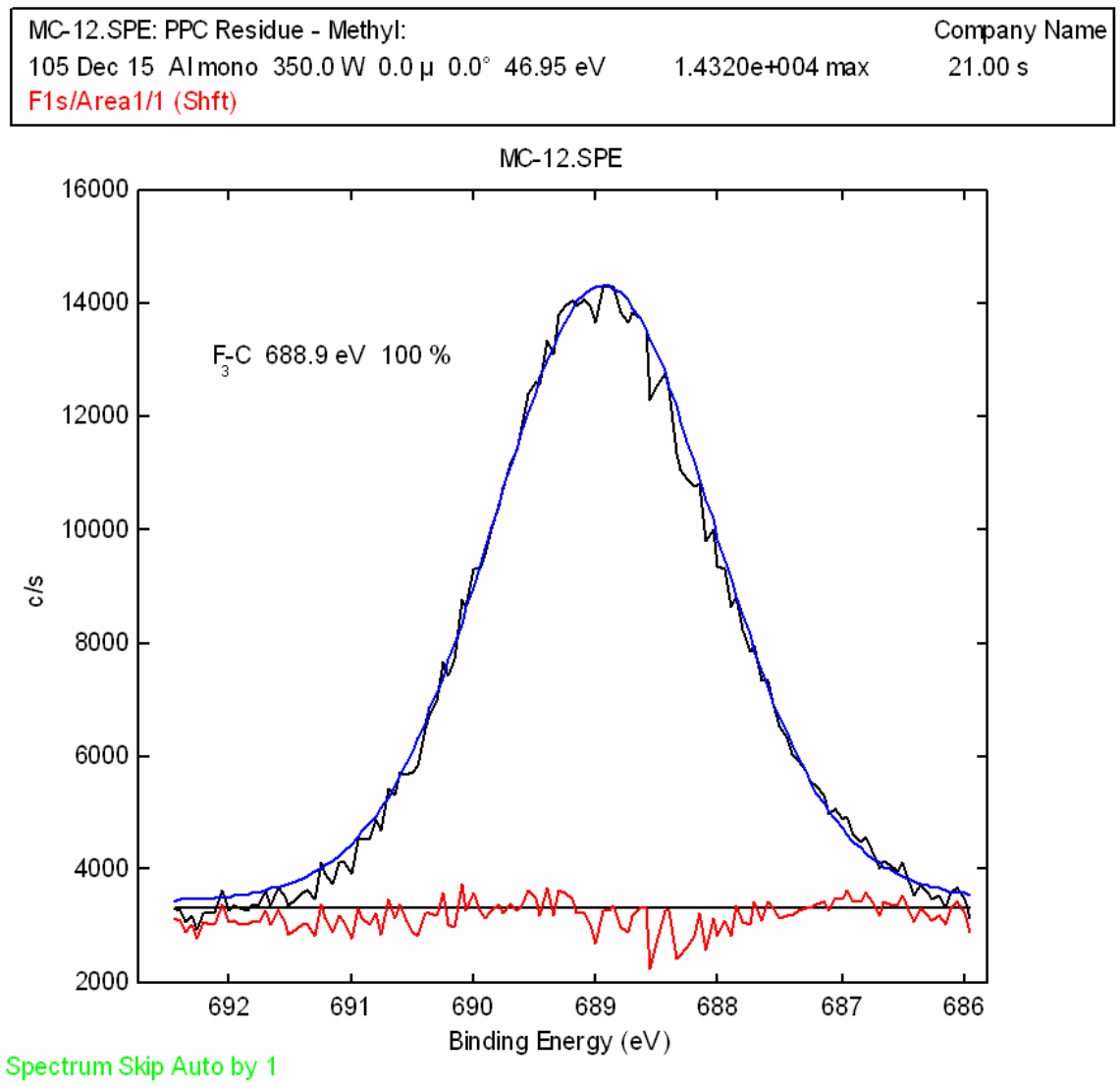

Figure 8.6: XPS analysis of BTBPI-TMM focusing on the fluorine bonding data

As expected, the above symmetrical curve shows 100% of the fluorine bonds are bonded in the form of CF_3. The presence of other carbon-fluorine bonds would suggest the anion was decomposing or there are fluorinated impurities. Conveniently, none were found.

Overall, the XPS analysis is supportive of prior conclusions formed about the perfluorinated methide based PAG. The elements present were found to be stiochiometrically viable, and the bonding groups were accurate based on the structure of

the PAG and the polymer. The low amounts of fluorine and sulfur defend the vapor pressure arguments made in previous chapters. Also, the analysis does suggest that a different cation may result in a decrease of carbon-carbon bonding. Future work on this topic may want to look into a Rhodorsil-like cation or simply a DPI group in order to create more volatile cation decomposition products.

Leaving the discussion of BTBPI-TMM, a second full XPS residue analysis was performed on the Rhodorsil-FABA based PAG. The structure of the PAG is shown below.

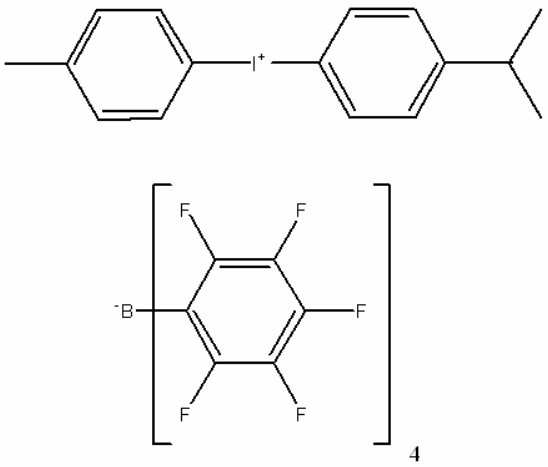

Figure 8.7: Chemical structure of the Rhodorsil-FABA PAG

The Rhodorsil-FABA contains carbon, fluorine, boron, and iodine. There is no oxygen in the acid or cation, therefore, all oxygen found in the residue is from the polymer. Figure 8.8 displays the results of the overall XPS elemental analysis that was also shown in Chapter 3.

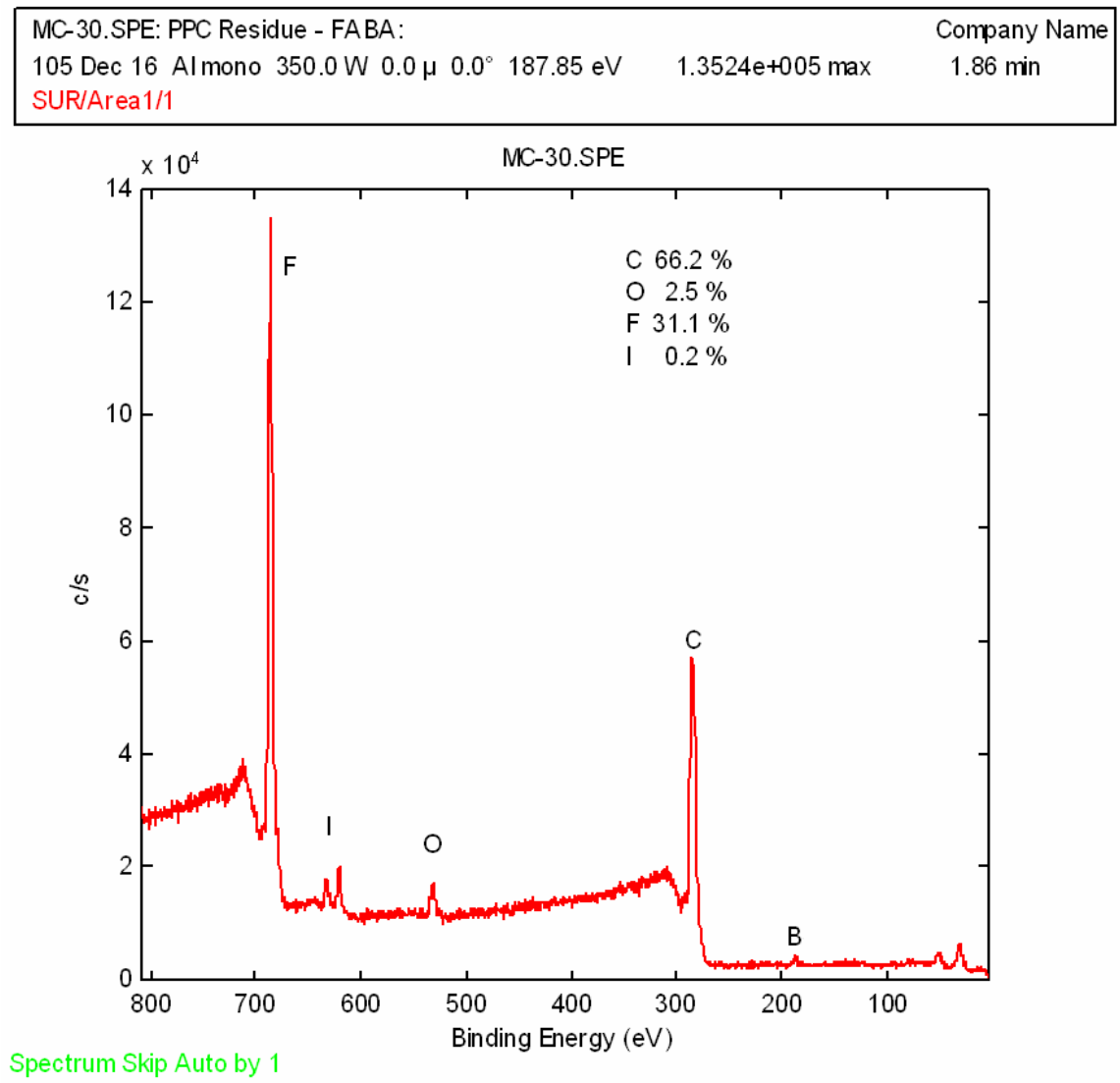

Figure 8.8: X-ray photoelectron spectroscopy (XPS) of the Rhodorsil-FABA residue

As predicted, the elements present are carbon, fluorine, oxygen, boron, and iodine, listed in order of abundance. Elemental carbon was found to consist of about 66% of the residue, with fluorine also quite high at 31%. In the FABA acid the carbon and fluorine content has a stoichiometric relationship of 6:5, which indicates that half of the carbon found is from the acid. The remaining carbon would be from the cation and polymer residues. Such high levels of fluorine signify large residual contributions from the acid

group, as expected from FABA's negligible vapor pressure. With its only contribution coming from the residual polymer, the oxygen content is fairly low at 2.5%. This result points toward a high level of polymer decomposition. In addition, the boron percentage, not shown in Figure 8.8, is approximately 1% - 2%. With 24 carbon atoms and 20 fluorine atoms associated with each boron atom, this result also agrees with the acid structure. Finally, there is a trace amount of iodine in the system from the incomplete decomposition and vaporization of the cation portion of the PAG.

Now examining each element and its bonding groups, the XPS data for carbon in the Rhodorsil-FABA residue is shown below.

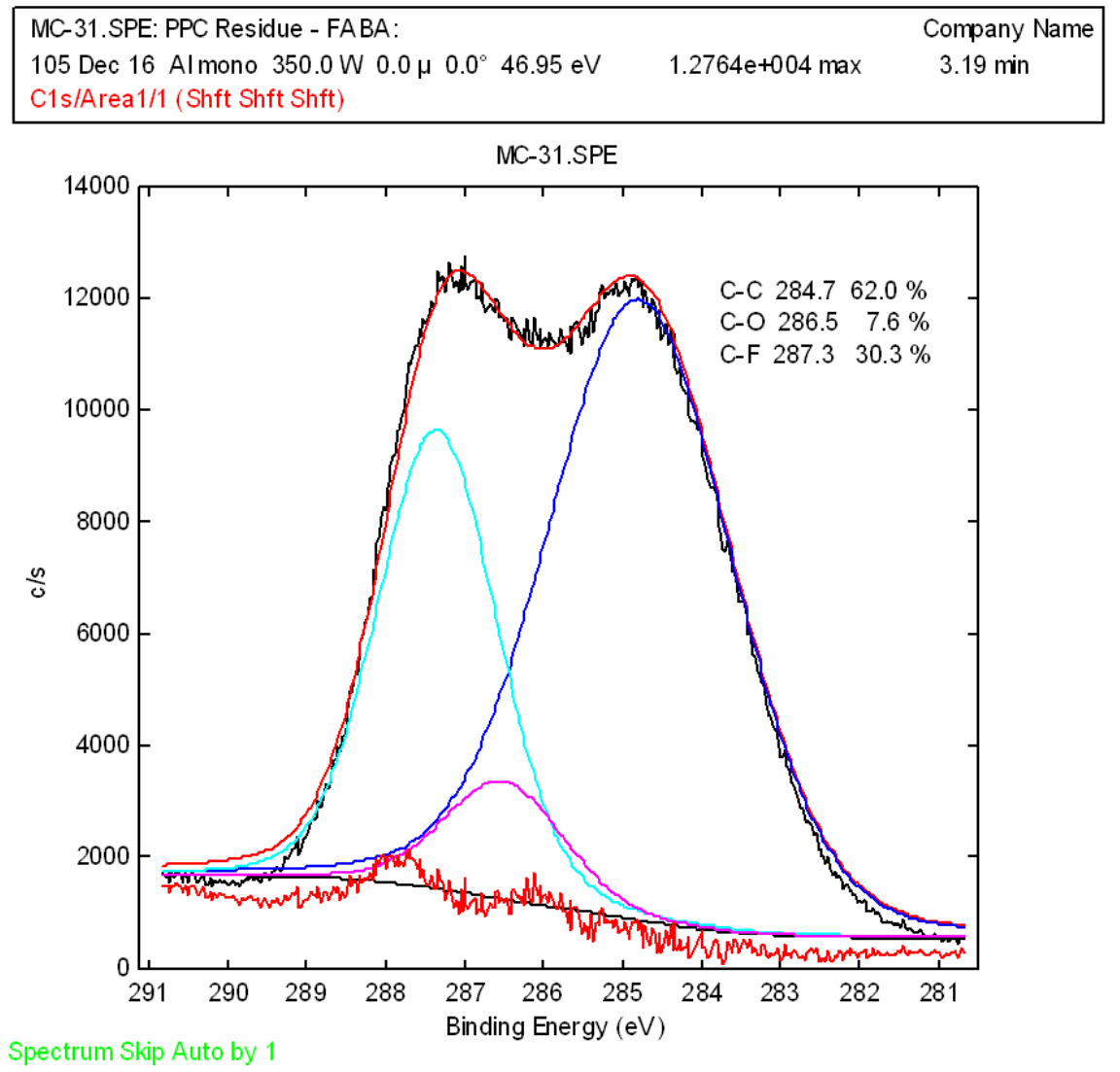

Figure 8.9: XPS analysis of Rhodorsil-FABA focusing on the carbon bonding data

The carbon analysis in Figure 8.9 shows very similar ratios to the overall elemental analysis. The carbon-fluorine bonds make up about 30% of all the residual carbon, which implies that about one third of the residual carbon is from the FABA acid. Since the original acid loading was only 4%, this result shows that the acid is not leaving the system causing it to concentrate during the decomposition. Putting aside acid contributions leaves approximately 30% of the carbon-carbon bonds as a result of the

cation and polymer. Also a result of the residual polymer is the carbon-oxygen bonds, which make up about 8% of the elemental carbon. Being the lowest percentage of all the carbon bonds suggests that the polymer is contributing the least amount to the overall residue. Since the only source of oxygen is in the polymer residue, the XPS bonding data for oxygen is one symmetrical curve, shown below.

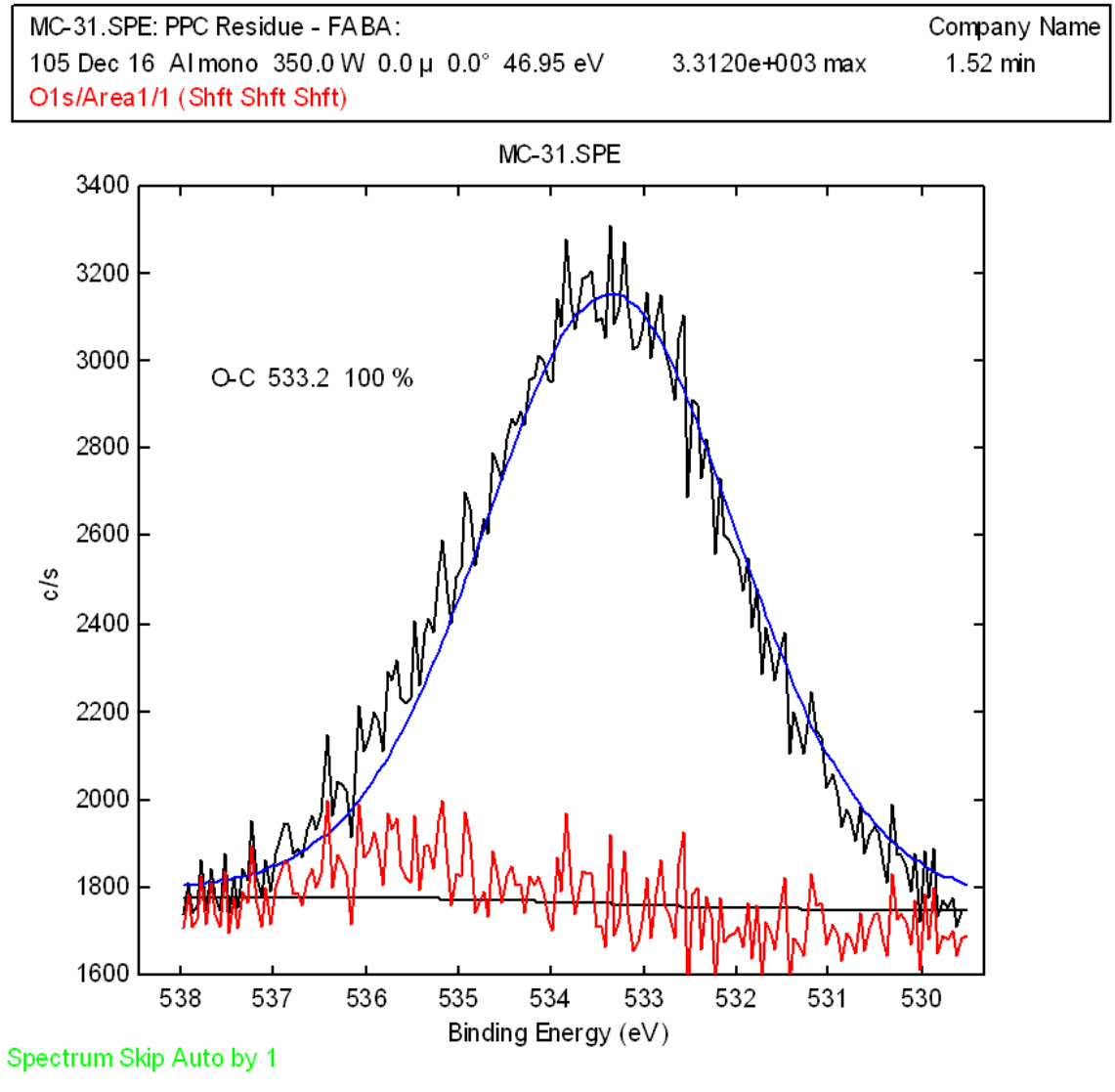

Figure 8.10: XPS analysis of Rhodorsil-FABA focusing on the oxygen bonding data

The single oxygen-carbon symmetrical bonding curve provides little insight into the overall composition of the residue, but it does support the molecular structures of the PAG components and indicate that no major side reactions involving oxygen occur. The final elemental bonding analysis is with fluorine and can be found below.

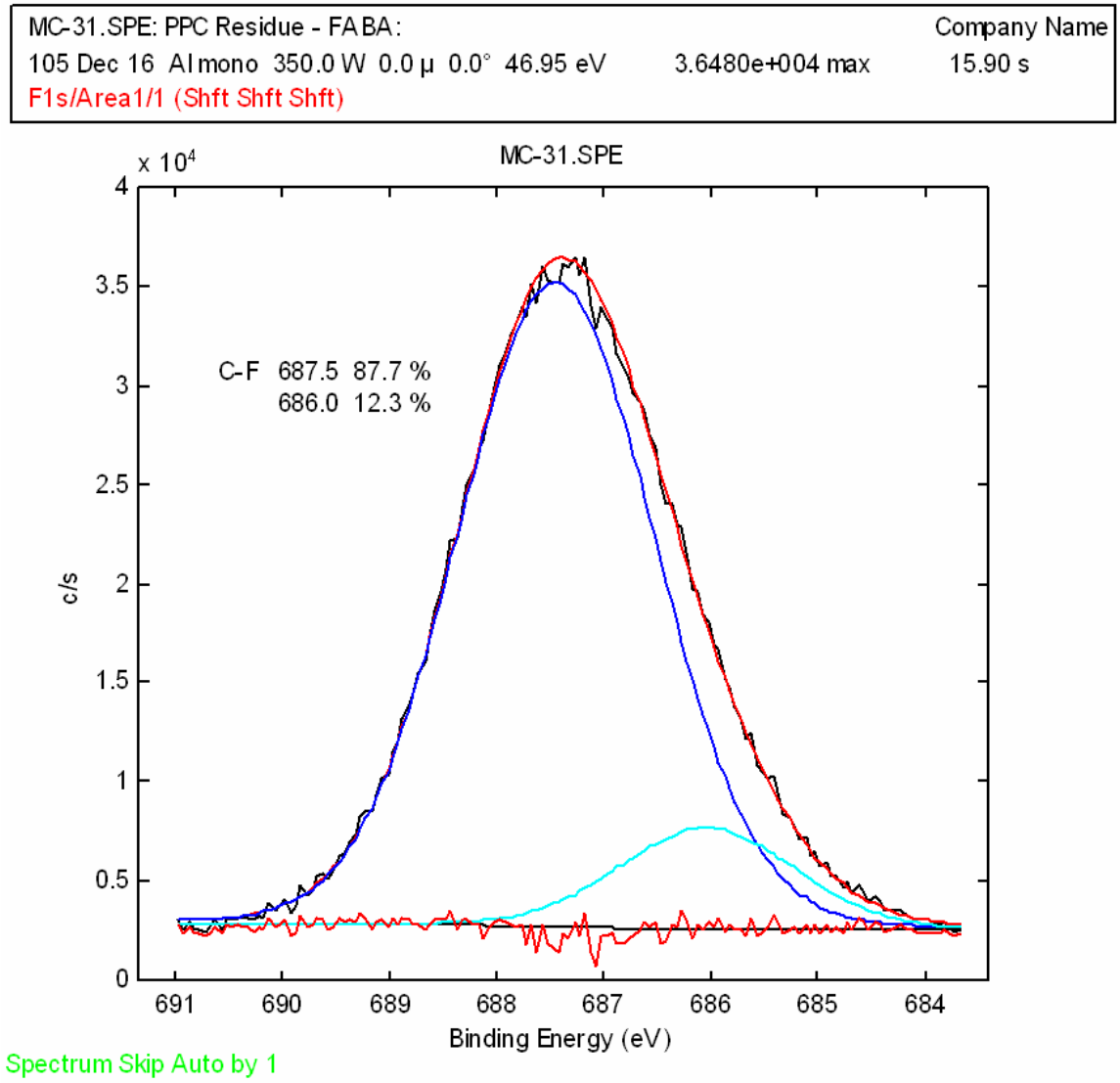

Figure 8.11: XPS analysis of Rhodorsil-FABA focusing on the fluorine bonding data

The XPS curve for fluorine in Figure 8.11 is slightly asymmetrical, which indicates that fluorine has two different bonding groups. As shown, the majority of the fluorine has a single bond with carbon. The remaining 12% is a result of the bonding environment that causes a data shift in the XPS. This shift is due to the benzene ring that the fluorine atoms are bonded. Any other groups, like CF_2 or CF_3 would not be consistent with the structure of the FABA acid, so the XPS results are satisfactory.

Due to the small amounts of iodine and boron detected by the XPS instrument, performing a bonding analysis may have lead to accurate conclusions. For this reason, those figures were omitted from this report; however, it can be said with strong confidence that based on the PAG's structure, both iodine and boron would show bonding only with carbon.

Taken as a whole, the XPS of the FABA acid PAG proceeded as expected. The elements identified along with their stoichiometric percentages and bonding associations were supported by the structure of the PAG. It was found that the acid made up a large majority, about 30%, of residue on the substrate. This result defends the low to negligible vapor pressure argument for the FABA acid. Also, the low carbon-oxygen content suggests a fairly complete decomposition of the polymer film with residuals caused mostly by the presence of polyether impurities.

Moving to the final XPS analysis, the residue from the Combination PAG sample will now be discussed. As a point of reference, the structure of both PAGs used to create this unique polymer solution are shown in Figure 8.12.

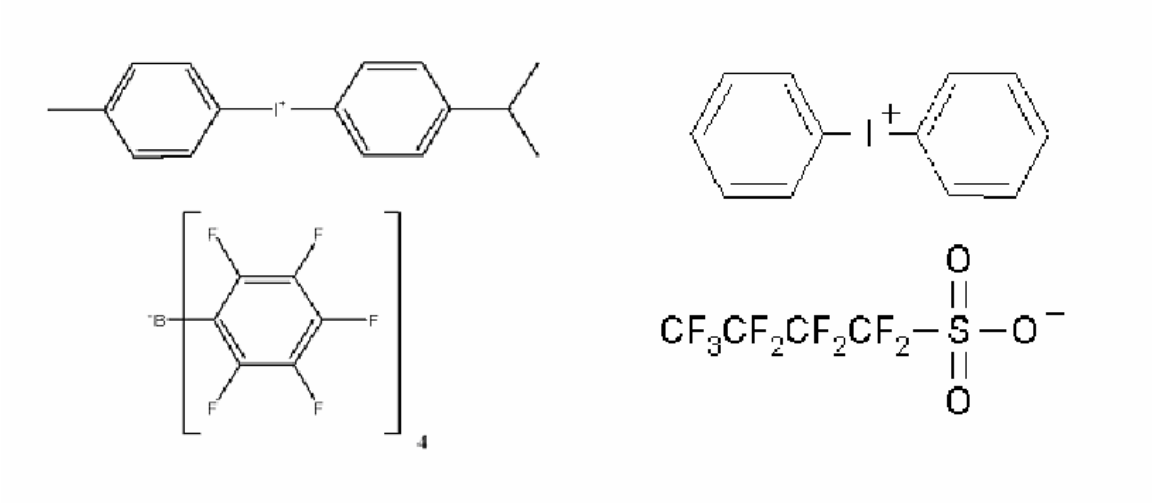

Figure 8.12: Structure of the Combination PAG with 1% Rhodorsil-FABA (left) and 3% DPI-NF (right)

With this PAG combination, there is a possibility for the presence of six different elements: carbon, oxygen, fluorine, sulfur, iodine, and boron. However, the overall XPS analysis only shows three, as shown in Figure 8.13.

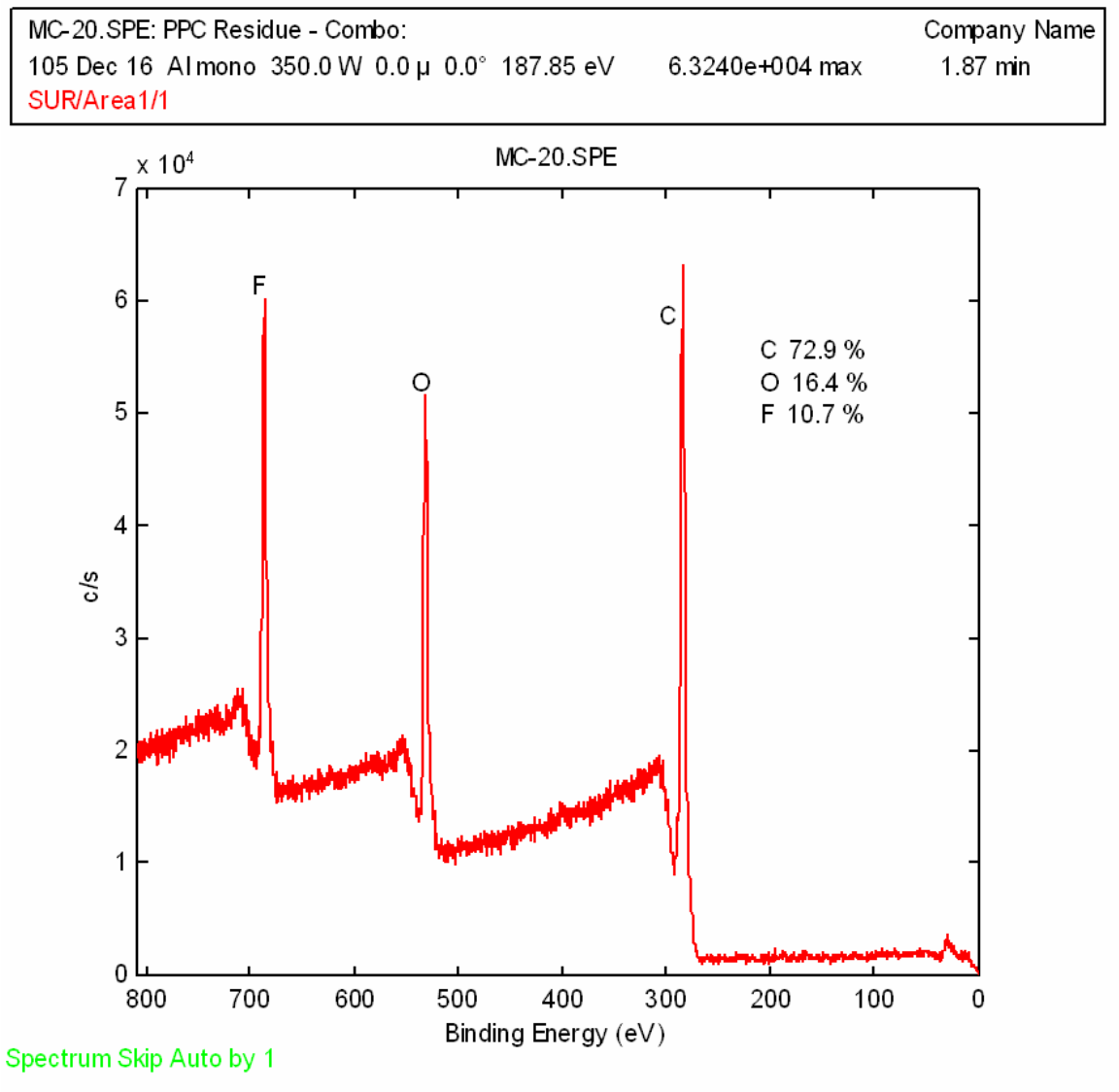

Figure 8.13: X-ray photoelectron spectroscopy (XPS) of the Combination PAG residue

The Combination PAG XPS only shows the presence of carbon, oxygen, and fluorine. It would seem that the trace amounts of iodine, boron, and sulfur have been masked by the more prevalent elements. Recalling Chapter 7, the statement was made that the residue from the Combination PAG appeared to resemble the PPC film, and it did not show many of the brown tar or oily residue characteristics of the FABA and methide PAGs. If the data in Figure 8.13 is in fact valid, then it supports the claim that the majority of the

residue in the Combination PAG samples is from the polymer. Further supporting this claim are the high levels of carbon and oxygen at 73% and 16% respectively. The fluorine content is the lowest at 11%, and the bonding analysis will be able to tell how much fluorine is coming from the FABA and nonaflic acids. Figure 8.14 shows the bonding analysis for carbon.

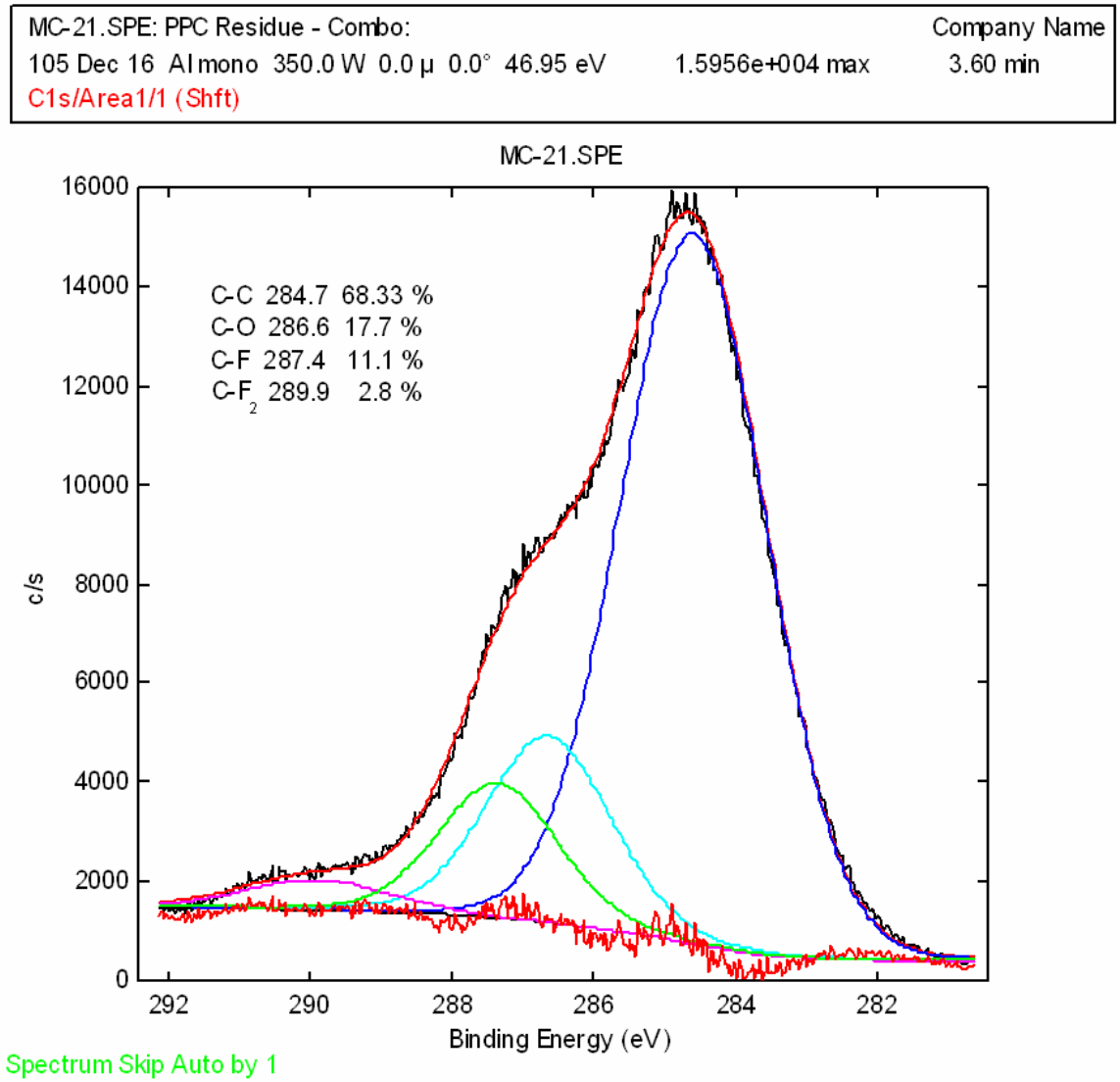

Figure 8.14: XPS analysis of Combination PAG focusing on the carbon bonding data

The largest curve in Figure 8.14 is the carbon-carbon curve at 68%, which has been typical of these analyses. More importantly is the high carbon-oxygen content at almost 18%. This indicates that a large portion of the residue is from unreacted polycarbonate or and residual polyether. The high carbon-oxygen levels support the statement that the presence of significant levels of polymer is masking the trace elements not found on the overall XPS. It also supports the visual observations made of the residue after PEB. Also quite important is the analysis of the carbon-fluorine bonds, of which there are two different types. The CF bond is associated with the FABA acid, and it is four times as prevalent as the CF_2 bond associated with the nonaflic acid (also includes CF_3). This is a very exciting result. Recall that the initial polymer solution contained only 1% Rhodorsil-FABA and 3% DPI-NF (molar equivalent). In order for the acid ratio to switch so dramatically from the initial solution to the residue, the nonaflic acid would have had to evacuate the system through vaporization, leaving behind the FABA acid in a more concentrated state. This analysis mirrors the hypothesis generated for the creation of the Combination PAG back in Chapter 7. Once again, the photo-acid vapor pressure theory has been supported.

For the sake of completeness, Figure 8.15 displays the oxygen bonding curve for the Combination PAG.

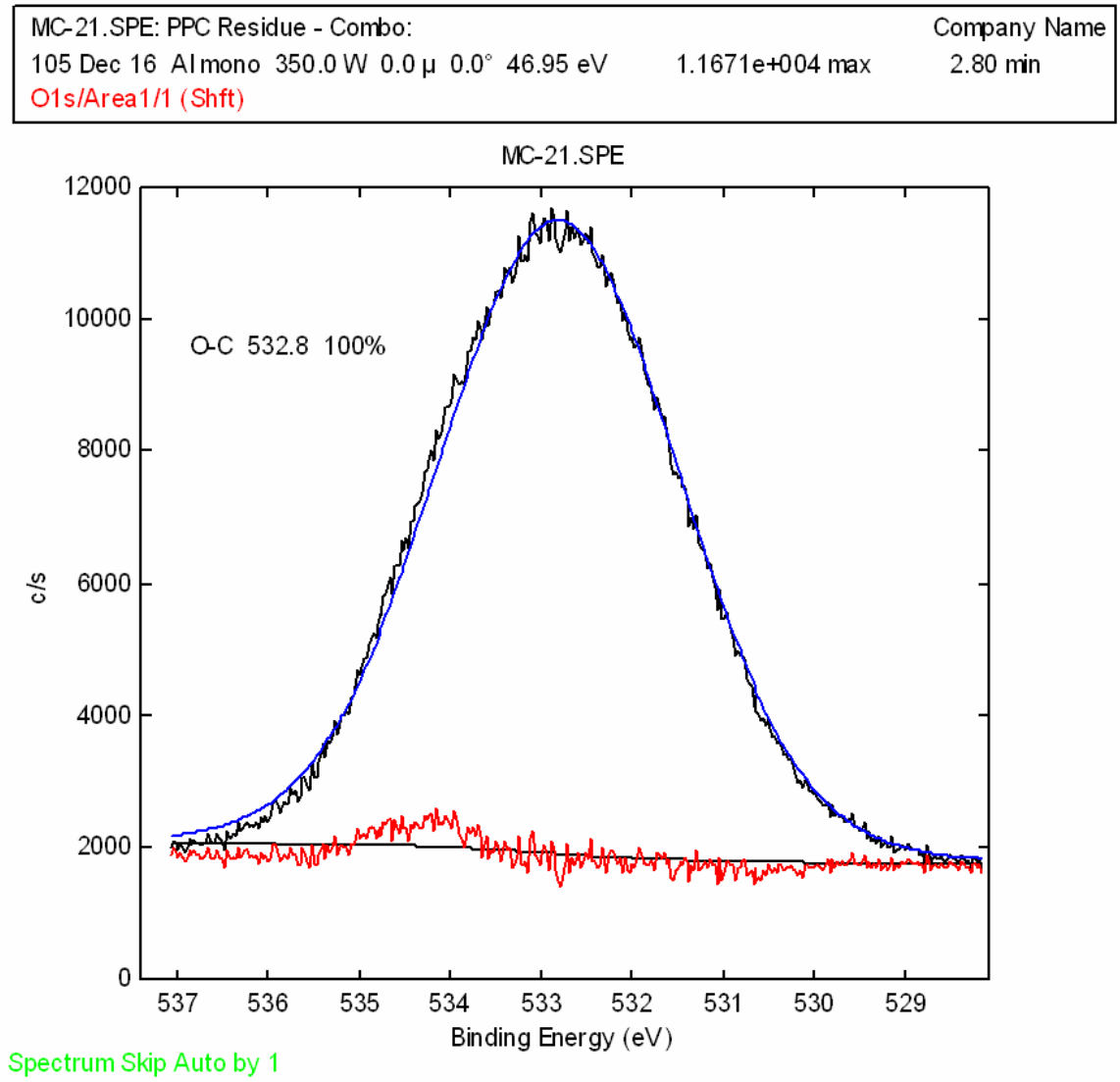

Figure 8.15: XPS analysis of Combination PAG focusing on the oxygen bonding data

The curve shows 100% bonding between oxygen and carbon and none between oxygen and sulfur. The curve appears to be quite symmetrical, so it is believable that this result is valid. Furthermore, the single curve supports the overall XPS analysis and its absence of any sulfur compounds do to the vaporization of the nonaflic acid.

Looking back at all three of the XPS residue analyses, some overall conclusions can be drawn. First, the FABA and methide based PAGs contain less residual polymer

when compared to the Combination PAG using the carbon-oxygen bonding percentage as the benchmark. Second, vapor pressure based conclusions were upheld in each PAG. The volatile perfluorinated methide PAG had smaller contributions from CF_3 compounds, which resulted in the largest observed carbon-carbon bond residue contribution observed in any of the PAGs. The non-volatile FABA acid PAG had large fluorine residue contributions from the very bulky acid. The mixed acid groups of the combination PAG had a residue in which the volatile nonaflic acid left the system while concentrating the FABA acid. Third, the visual observation that each residue appeared to be different was supported with different atomic composition in each XPS. The oily methide residue was attributed to low molecular weight hydrocarbons, the dark brown FABA residue was attributed to the remaining acid group, and the Combination PAG residue was attributed to unreacted polymer. The result of the Combination PAG suggests that further tuning of the PAG levels or the PAGs themselves needs to be done in future work. Finally, XPS was found to be a great tool for analyzing decomposition residues. In each case, stoichiometric and bonding relationships were valid based on the structure of the polymer and PAG.

One final residue analysis needs to be completed in order answer some questions about the methide based PAG residue generated in Chapter 6. Call to mind Figure 6.2, which displayed the rate of decomposition data for the BTBPI-TMM PAG. The residue for this thick film (~50um) decomposition was difficult to measure with the profilometer at and after 10 minutes due to its oily nature. The data collected from profiling the sample illustrated that the amount of residue from the methide PAG might be lower than that can be achieved from the FABA PAG. By performing a residual weight analysis

rather than a film thickness analysis, one should be able to avoid the pitfalls of an improper measurement, while still collecting valid data. To perform this test, equivalent sized pieces of silicon wafer were diced and weighed. Each wafer was spuncoat with a polymer film targeted between 45 um and 50 um. The thickness of trial samples were measured to unsure the spin recipe produced equivalent film thicknesses for both the methide and FABA based solutions. The samples were soft baked and exposed by the standards established in this report and weighed a second time. Special care was taken while moving and weighing the samples to ensure that no additional mass was added or subtracted due to errant particles or through poor/excessive handling. The samples were then decomposed at 120ºC for 30 minutes on a hotplate and weighed one final time. By subtracting the initial mass of the silicon wafer, the weight percent residue can easily be calculated. The results of this experiment are shown in Table 8.1.

Table 8.1: Weight percent residue analysis for the methide and FABA PAGs

	Bare wafer	PPC on Wafer	Residue on Wafer	Residue Alone	Residue Remaining
	(g)				(%)
DPI-FABA	1.3837	1.4641	1.3882	0.0045	**5.60%**
BTBPI-TMM	1.3961	1.4915	1.3997	0.0036	**3.77%**

The most important column in Table 8.1 is the final column which shows the weight percent of the remaining residue after decomposition. This analysis shows that the methide PAG is indeed more efficient at decomposing the thick PPC films than the FABA based PAG. As a point of note, it would not be valid to compare the weight residue percentages with the residue thickness percentages presented in the other chapters of this report. A confident recommendation can now be made to pursue fabricating

microelectronic devices using sacrificial PPC activated by a perfluorinated methide based PAG.

APPENDIX A

PAG STRUCTURES

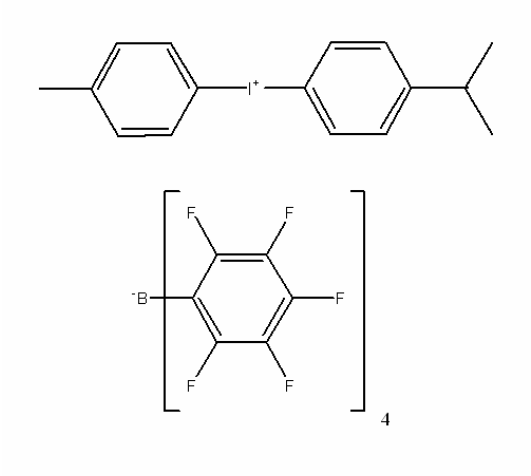

Figure A.1: Rhodorsil-FABA Structure, (tetrakis-(pentafluorophenyl)borate-4-methylphenyl[4-(1-methylethyl)phenyl]iodonium)

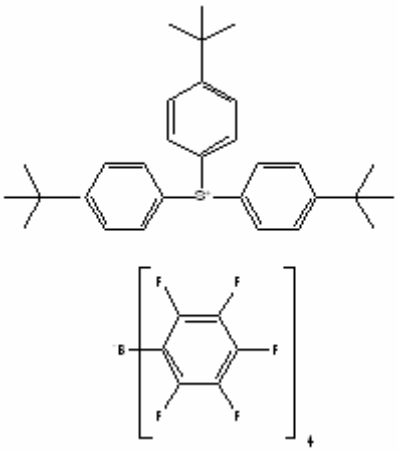

Figure A.2: TTBPS-FABA, (tris(4-tert-butylphenyl)sulfonium tetrakis-(pentafluorophenyl)borate)

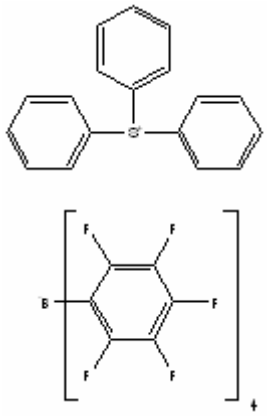

Figure A.3: TPS-FABA, (triphenylsulfonium tetrakis-(pentafluorophenyl)borate)

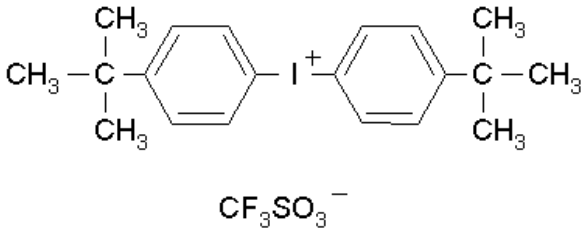

Figure A.4: BTBPI-TF, (Bis(4-tert-butylphenyl)iodonium triflate)

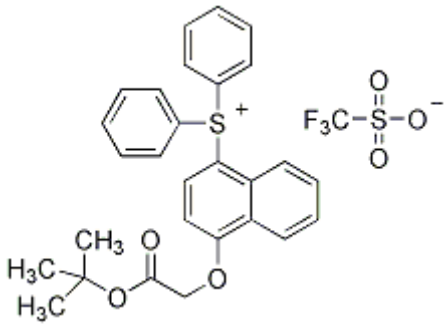

Figure A.5: TBOMDS-TF, (tert-(butoxycarbonylmethoxynaphthyl)-diphenylsulfonium triflate)

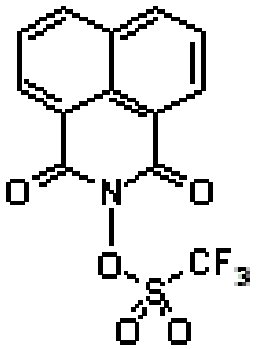

Figure A.6: NHN-TF, (N-hydroxynaphthalimide triflate)

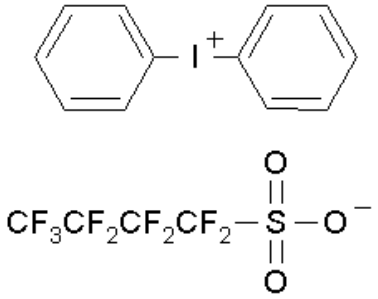

Figure A.7: DPI-NF, (Diphenyliodonium perfluoro-1-butanesulfonate)

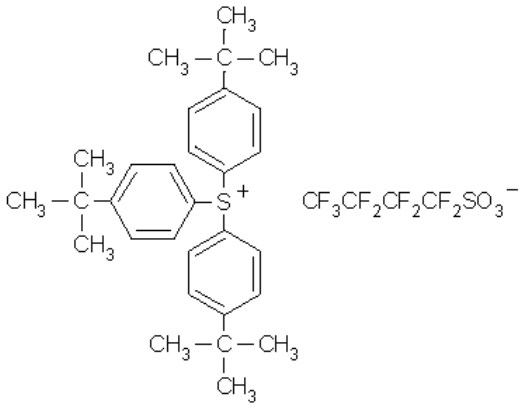

Figure A.8: TTBPS-NF, (Tris(4-tert-butylphenyl)sulfonium perfluoro-1-butanesulfonate)

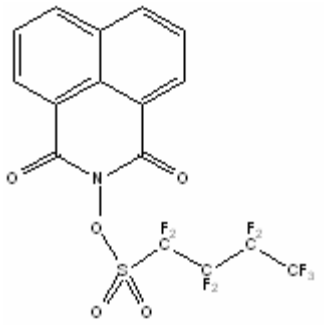

Figure A.9: NHN-NF, (N-hydroxynaphthalimide perfluoro-1-butanesulfonate)

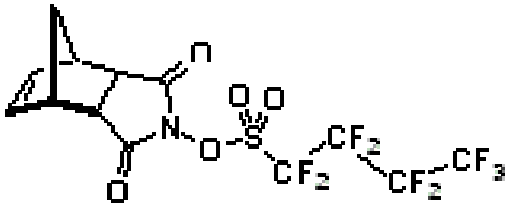

Figure A.10: NHNDC-NF, (N-hydroxy-5-norbornene-2,3-dicarboximide perfluoro-1-butanesulfonate)

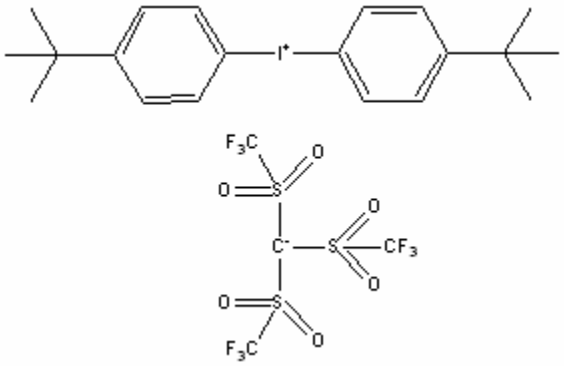

Figure A.11: BTBPI-TMM, (Bis(4-tert-butylphenyl)iodonium tris(perfluoromethanesulfonyl)methide)

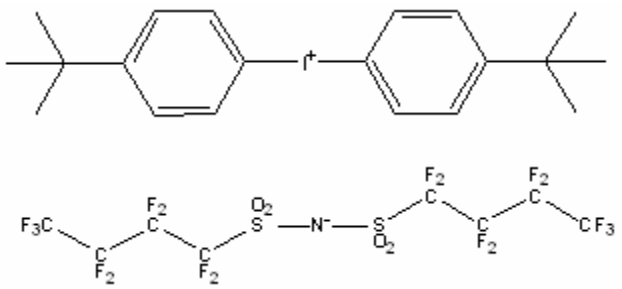

Figure A.12: BTBPI-BBI, (Bis(4-tert-butylphenyl)iodonium bis(perfluorobutanesulfonyl)imide)

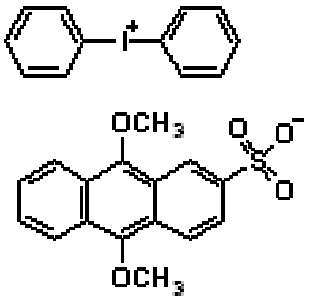

Figure A.13: DPI-DMOS, (Diphenyliodomium 9,10-dimethoxyanthracene-2-sulfonate)

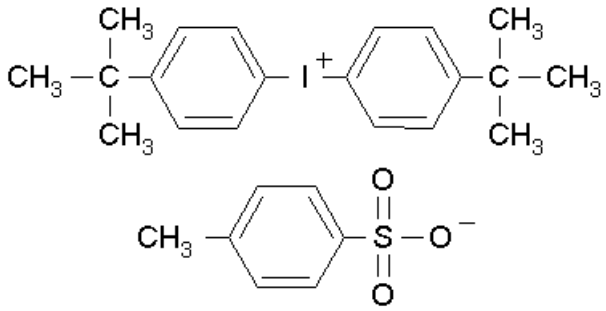

Figure A.14: BTBPI-PTS, (Bis(4-tert-butylphenyl)iodonium p-toluenesulfonate)

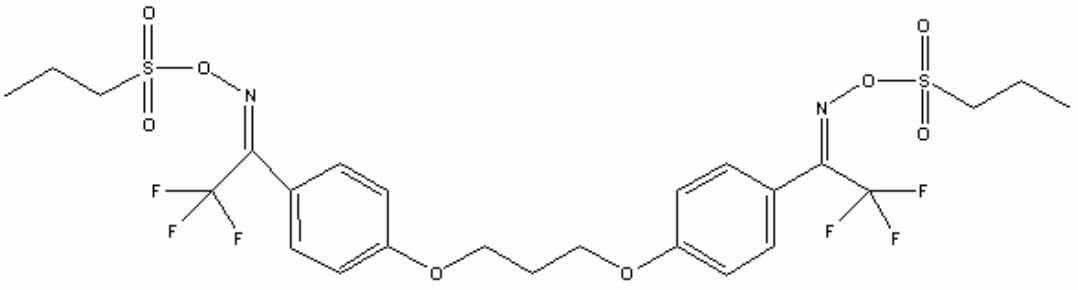

Figure A.15: Ciba 263 Non-ionic PAG

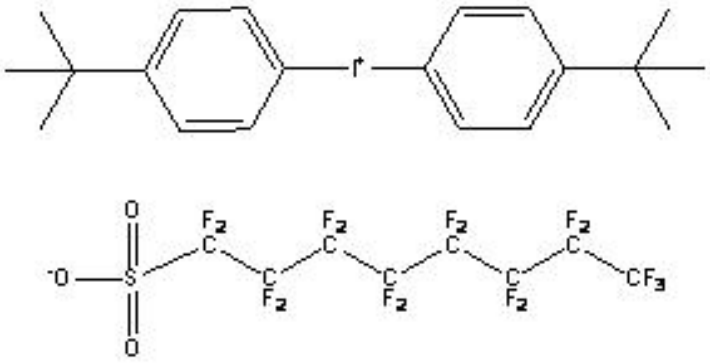

Figure A.16: BTBPI-HDF (*Bis(4-tert-butylphenyl)iodonium perfluoro-1-octanesulfonate)*

APPENDIX B

COMPLETE SET OF CATION STUDY DATA

This appendix contains the complete decomposition experimental data for PAGs listed in Chapter 4 (Cation and Non-ionic PAG Study) that were not already displayed in Chapter 3 (Photoacid Generator Anion Study).

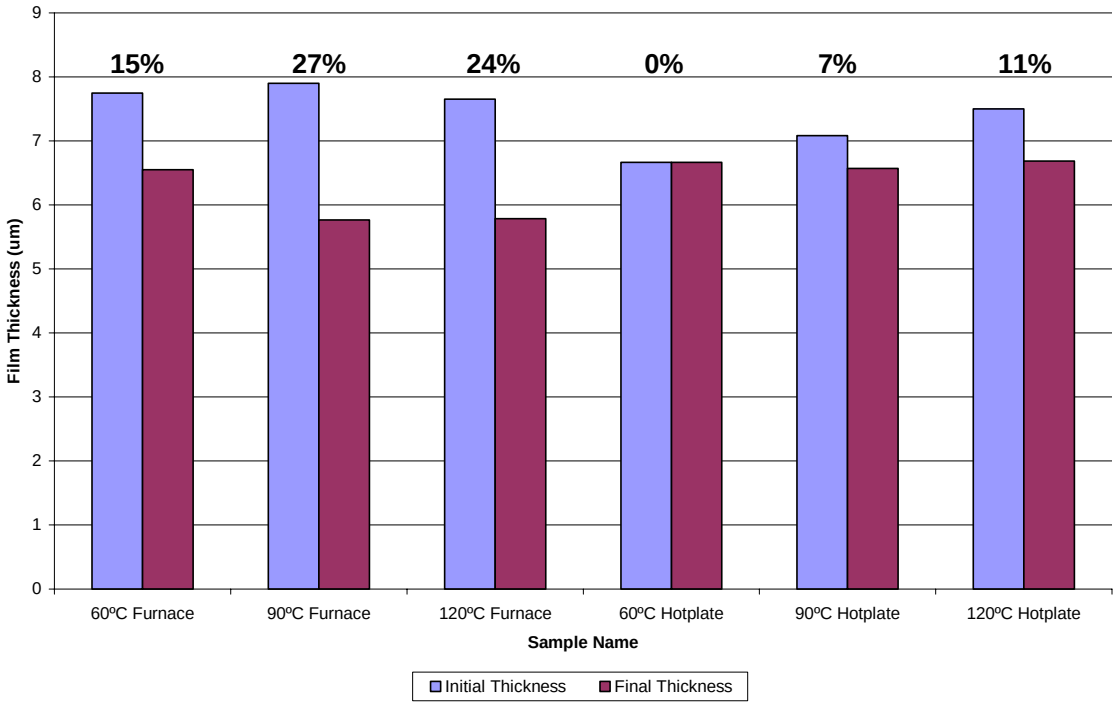

Figure B.1: TBOMDS-TF PAG decomposition levels

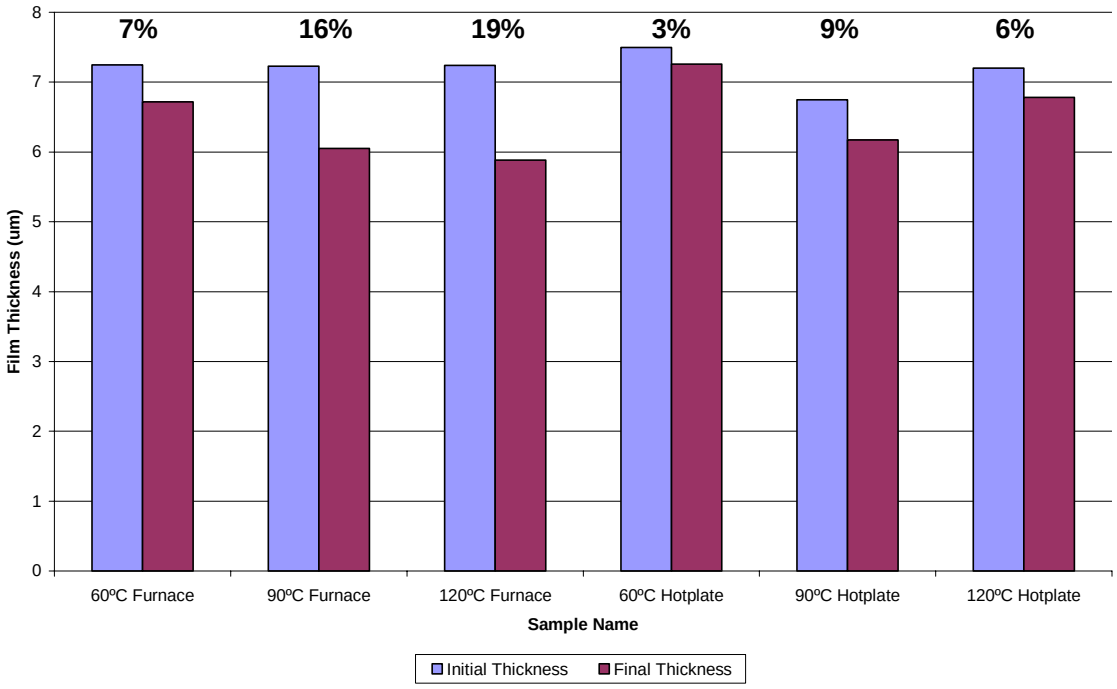

Figure B.2: NHN-TF decomposition levels

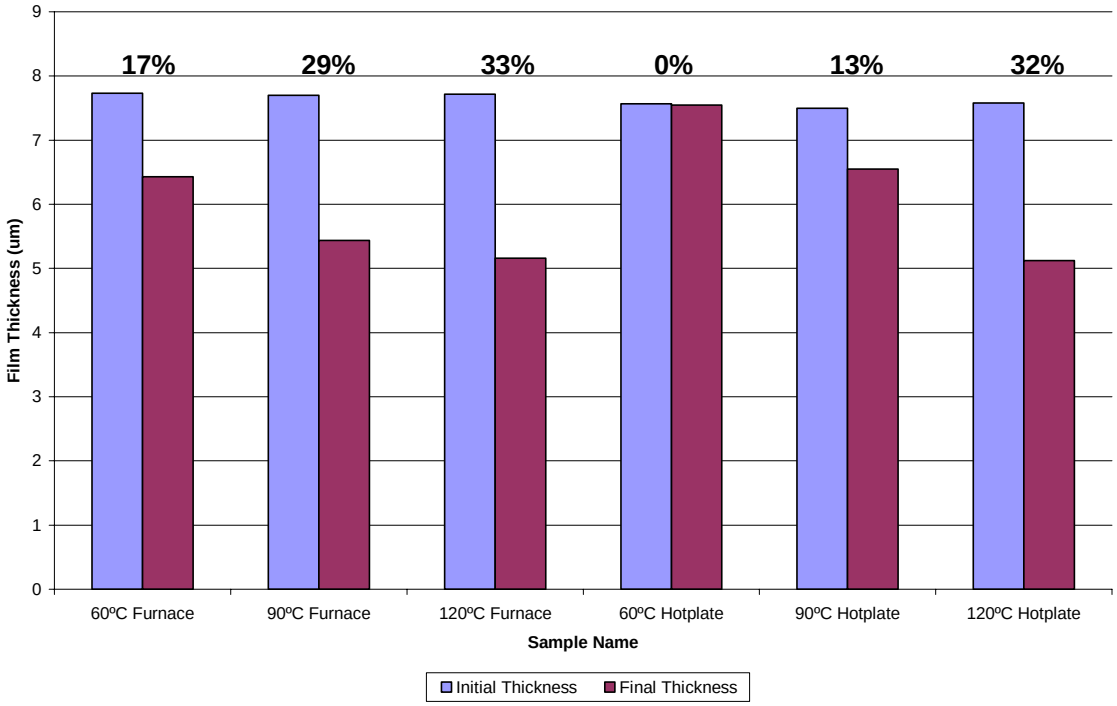

Figure B.3: TTBPS-NF decomposition levels

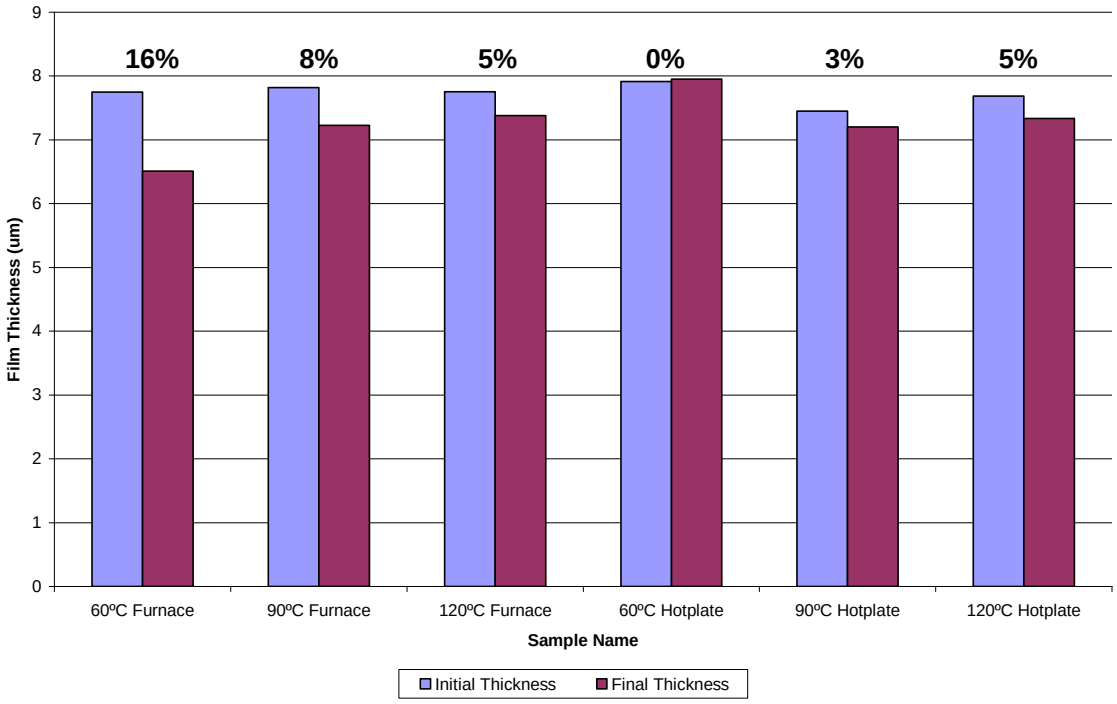

Figure B.4: NHNDC-NF decomposition levels

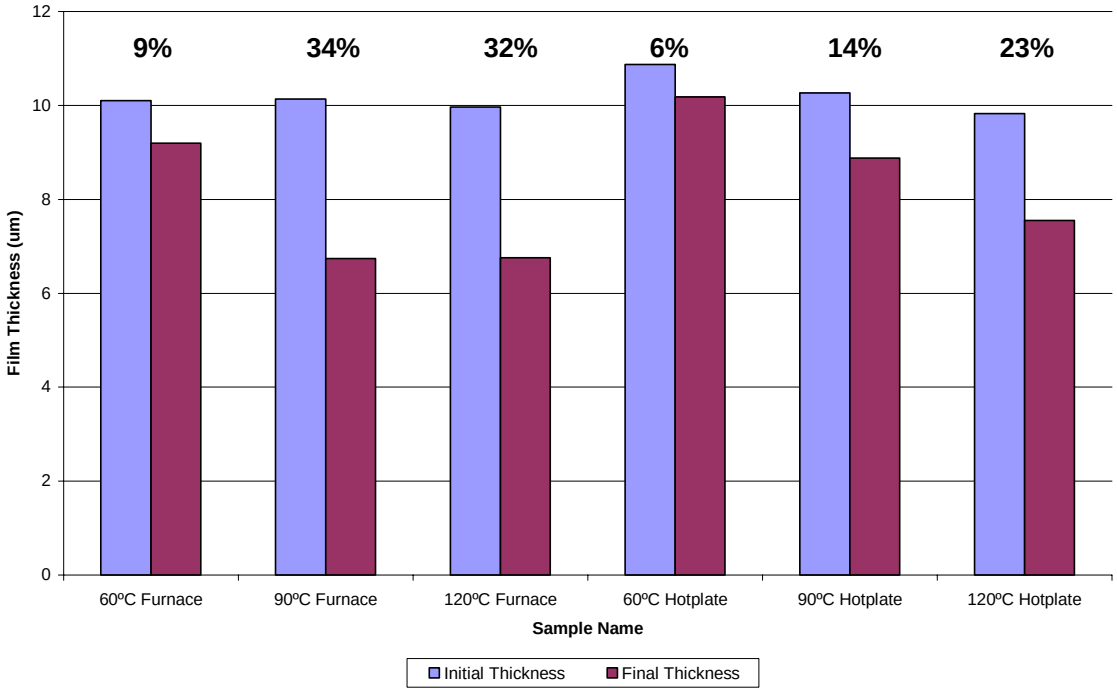

Figure B.5: NHN-NF decomposition levels

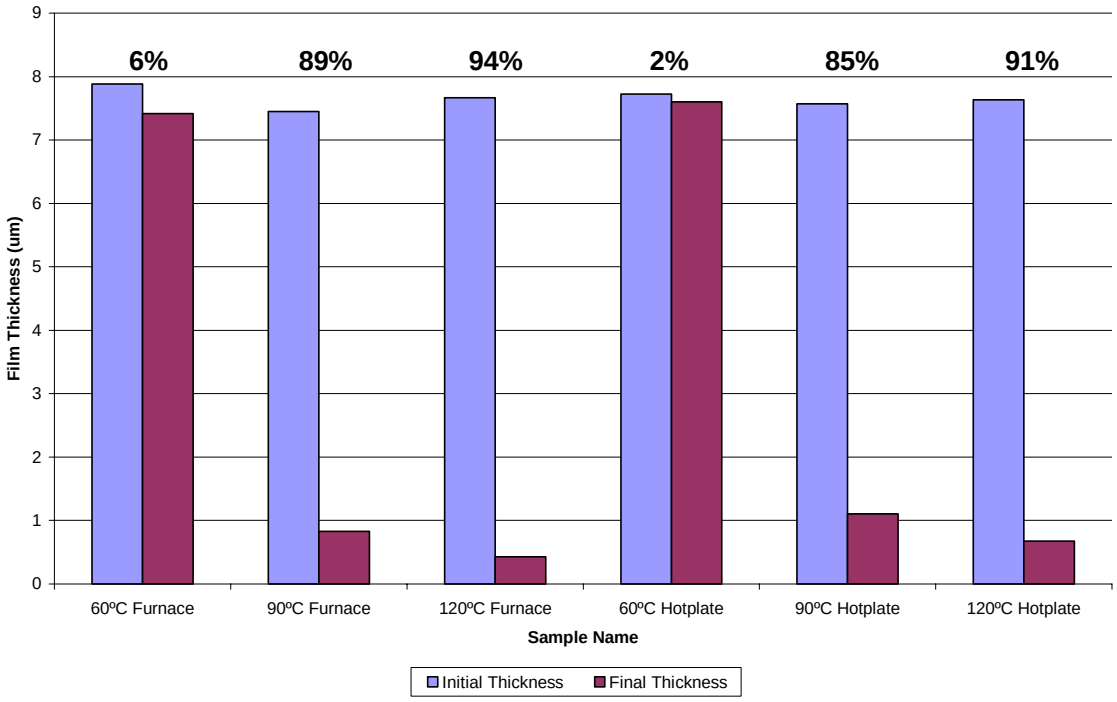

Figure B.6: TTBPS-FABA decomposition levels

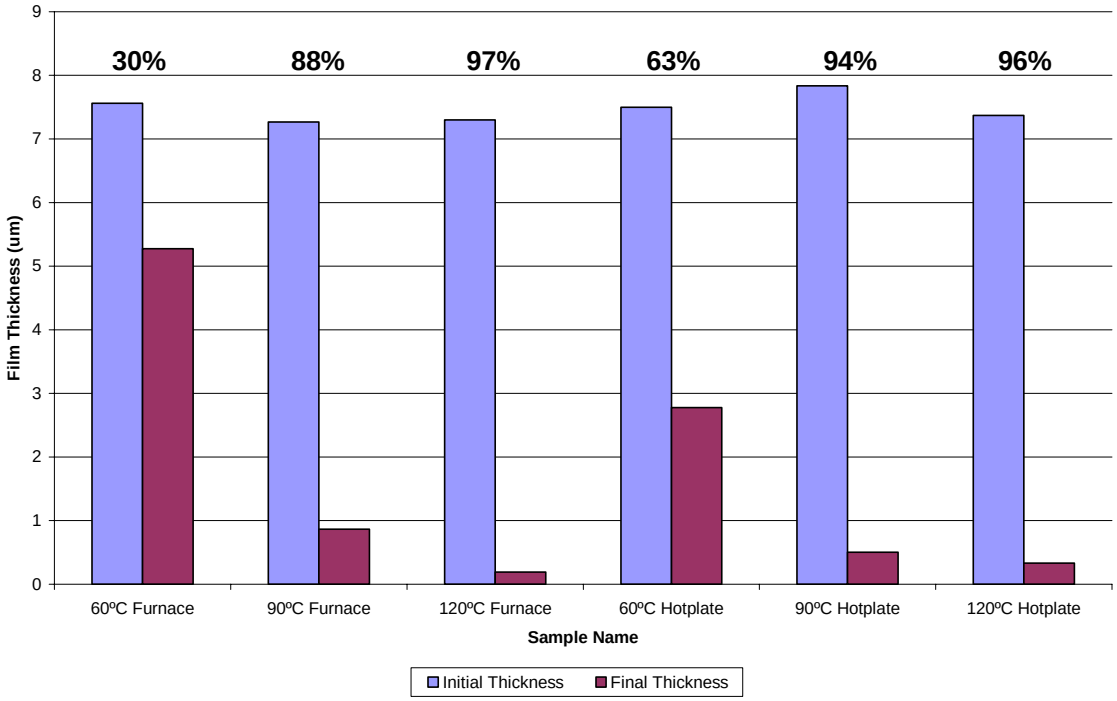

Figure B.7: TPS-FABA decomposition levels

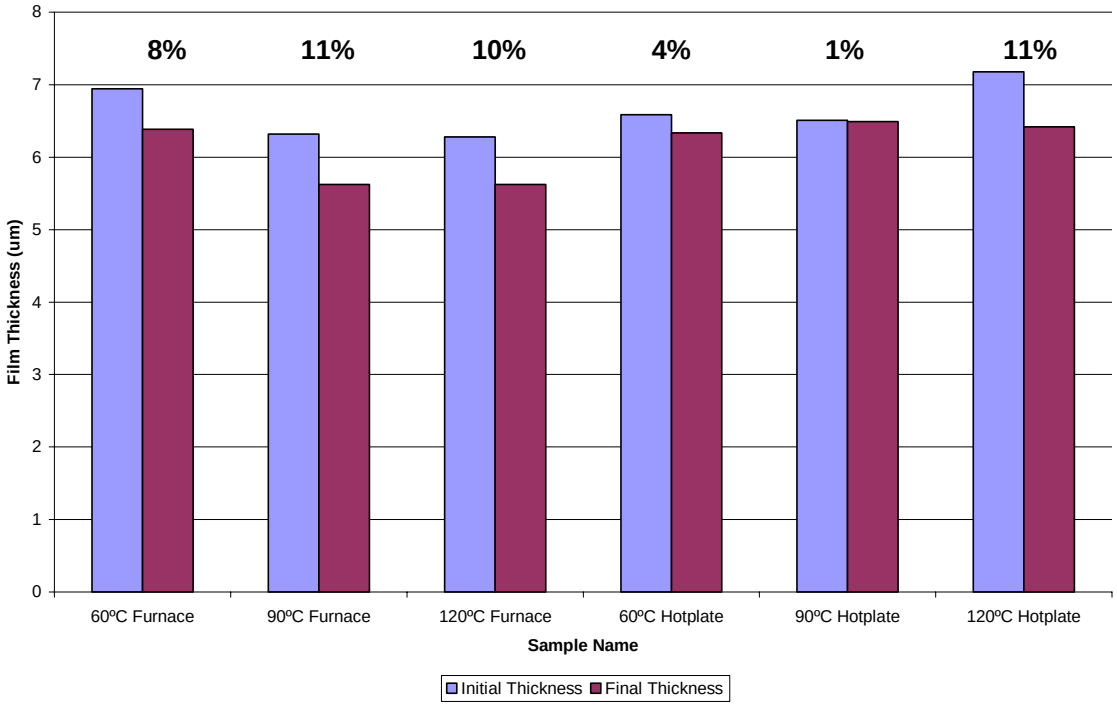

Figure B.8: Ciba-263 decomposition levels

REFERENCES

[1] P. J. Joseph, H. A. Kelleher, S. A. B. Allen, P. A. Kohl; *Journal of Micromechanics and Microengineering*. **15**, 35, 2005.

[2] J. P. Jayachandran, H. A. Reed, H. Zhen, L. F. Rhodes, C. L. Henderson, S. A. B. Allen, and P. A. Kohl; *Journal of Microelectromechanical Systems*. **12(2)**, 147, 2003.

[3] H. A. Reed, C. E. White, V. Rao, S. A. B. Allen, C. L. Henderson, P. A. Kohl; *Journal of Micromechanics and Microengineering*. **11**, 733, 2001.

[4] S. D. Burns, D. R. Medeiros, H. F. Johnson, G. M. Wallraff, W. D. Hinsberg, C. G. Willison; *Advances in Resist Technology and Processing XIX*. **4690**, 321, 2002.

[5] M. Padmanaban, R. Dammel, S. Lee, W. Kim, T. Kudo, D. Mckenzie, D. Rahman; *Advances in Resist Technology and Processing XX*. **5039**, 743, 2003.

[6] X. Wu, H. A. Reed, Y. Wang, L. F. Rhodes, E. Elce, R. Ravikiran, R. A. Shick, C. L. Henderson, S. A. B. Allen, P. A. Kohl; *Journal of The Electrochemical Society*. **150(9)**, H205, 2003.

[7] M. D. Stewart, D. J. Becker, T. B. Stachowiak, G. M. Schmid, T. B. Michaelson, H. V. Tran, C. G. Willison; *Advances in Resist Technology and Processing XIX*. **4690**, 943, 2002.

[8] T. H. Fedynyshyn, R. F. Sinta, W. A. Mowers, A. Cabral; *Advances in Resist Technology and Processing XX*, **5039**, 310, 2003.

[9] C. E. White, C. L. Henderson; *Advances in Resist Technology and Processing XXI*. **5376**, 850, 2004.

[10] C. E. White, C. L. Henderson; *Advances in Resist Technology and Processing XIX*. **4690**, 242, 2002.

[11] D. Lee, X. Ma, W. M. Lamanna, G. Pawlowski; *Advances in Resist Technology and Processing XIX*. **4690**, 169, 2002.

[12] W. M. Lamanna, C. R. Kessel, P. M. Savu, Y. Cheburkov, S. Brinduse, T. A. Kestner, G. J. Lillquist, M. J. Parent, K. S. Moorhouse, Y. Zhang, G. Birznieks, T. Kruger, M. C. Pallazzotto; *Advances in Resist Technology and Processing XIX*. **4690**, 817, 2002.

[13] G. M. Wallraff, C. E. Larson, N. Fender, B. Davis, D. Medeiros, J. Meute, W. M. Lamanna, M. J. Parent, T. Robeledo, G. Young; *Advances in Resist Technology and Processing XIX*. **4690**, 160, 2002.

[14] J. Salas, P. J. Joseph, H. A. Kelleher, S. Park, S. A. B. Allen, and P. A. Kohl; *Journal of Vacuum Science and Technology*. **B22 (3)**, 953, 2004.

[15] *Rhodia global solutions for acid catalytic systems*. (n.d). Retrieved November, 2005, from http://www.rhodia-ppa.com/media/PPA/push/Product/Acilys/acilysbrochure_final.pdf

[16] *Ciba Specialty Chemicals, Photoacid Generators for Microlithography*. (January 2003). Retrieved June, 2005, from http://www.cibasc.com/rz_photoacid_generators1.pdf

[17] *Sigma-Aldrich Electronic Catalog on Photoacid Generators*. Retrieved March, 2005, Sigma-Aldrich United States Web Site: http://www.sigmaaldrich.com/Area_of_Interest/The_Americas/United_States.htm

[18] *Midori Kagaku Co., Ltd. Electronic Catalog on Photoacid Generators.* Retrieved May 2005, Midori Kagaku Co. English Web Site: http://www.midori-kagaku.co.jp/m000908/e_index.htm